

MAY-THURNER SYNDROME
AND OTHER PELVIC VEIN COMPRESSION SYNDROMES:
EARLY DETECTION WITH DUPLEX ULTRASOUND
AND VENOGRAPHY

by

Kevin Joel Rivera

Bachelor of Arts, 2018
University of North Texas
Denton, Texas

Master of Science, 2019
University of North Texas Health Science Center
Fort Worth, Texas

Submitted to the Faculty of the
Anne Burnett Marion School of Medicine
Texas Christian University
In partial fulfillment of the requirements
For the degree of

Doctor of Medicine



**May
2023**

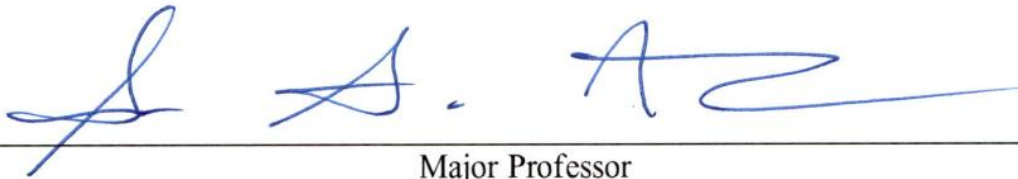
Copyright by
Kevin Joel Rivera
2023

APPROVAL

**MAY-THURNER SYNDROME
AND OTHER PELVIC VEIN COMPRESSION SYNDROMES:
EARLY DETECTION WITH DUPLEX ULTRASOUND
AND VENOGRAPHY**

by
Kevin Joel Rivera

Thesis approved:

A handwritten signature in blue ink, consisting of three distinct parts: a stylized 'S', a smaller signature, and a long horizontal stroke.

Major Professor

A handwritten signature in blue ink, appearing to read 'Michael Brown'.

For the Anne Burnett Marion School of Medicine

ACKNOWLEDGEMENT

I would like to thank my advisor and mentor, Dr. Sam Ahn, for his incredible guidance and support throughout my project. I am incredibly grateful for the balance of assistance when needed while allowing me to be creative and problem-solve. He has been vital in my development as an independent scientist.

I would also like to thank the staff and fellow colleagues in the endovascular laboratory. My comprehension and comfort of the different imaging modalities has been greatly enriched by their collective knowledge as well as their patience in teaching me.

TABLE OF CONTENTS

Acknowledgement.....	ii
List of Figures	v
List of Tables.....	vi
List of Equations	vii
Research Question.....	ix
Chapter 1: Introduction, Significance, and Rationale	1
1.1 History and Economics	1
1.2 Biofluid Mechanics	4
1.3 Cellular Biology and Pathology	13
1.4 Diagnostics	22
1.5 Physics of Sound	24
1.6 Radiation Physics	33
1.7 MTS Management.....	42
1.8 Rationale.....	44
Chapter 2: Research Materials and Methods.....	47
2.1 Research Philosophy	47
2.2 Research Design.....	49
2.3 Methodology	52

2.4 Statistical Analysis	57
2.5 Methodological Limitations	59
Chapter 3: Results	61
3.1 Descriptive Statistics	61
3.2 Inferential Statistics	72
Chapter 4: Discussion and Innovation.....	75
4.1 Investigation and Key Findings.....	75
4.2 Interpretation of Results	76
4.3 Limitations.....	80
Chapter 5: Final Analysis.....	82
5.1 Conclusions	82
5.2 Future Directions.....	83
Compliance.....	85
References	86
Vita	
Abstract	
Appendix A: R Data Output	

LIST OF FIGURES

Figure 1.1 Pelvic Vascular Anatomy	3
Figure 1.2 Vorticity of Fluid Elements	7
Figure 1.3 Laminar and Turbulent Flow	8
Figure 1.4 Vein Anatomy Cross Section.....	18
Figure 1.5A Venography Demonstrating a Vein with Stenosis.....	23
Figure 1.5B IVUS Demonstrating a Vein with Stenosis.....	23
Figure 1.6. Basic Components of a Wave.....	24
Figure 1.7 Color Flow Doppler Ultrasound of a Cardiac Chamber	28
Figure 1.8 Ultrasound of the Basilic Vein.....	30
Figure 1.9 Duplex Ultrasound of the Popliteal Vein.....	31
Figure 1.10 Ionizing Radiation Penetrability	37
Figure 1.11 X-Ray Apparatus	39
Figure 1.12 Catheter-Directed Thrombolysis.....	44
Figure 2.1 Angiography Suite	51

LIST OF TABLES

Table 2.1 Simplified Outcomes per Imaging Variable.....	55
Table 2.2 Outcomes per Imaging Variable After Transcription	56
Table 3.1 Statistical Measures of Age.....	62
Table 3.2 Risk Factors.....	64
Table 3.3 Imaging Findings for Duplex US Without Flow.....	67
Table 3.4 Imaging Findings for Duplex US Flow.....	68
Table 3.5 Imaging Findings for Venography	70
Table 3.6 Imaging Findings for IVUS.....	71
Table 3.7 Duplex Ultrasound to Venography Analyses.....	72
Table 3.8 Duplex Ultrasound to IVUS Analyses	73
Table 3.9 Venography to IVUS Analyses	74

LIST OF EQUATIONS

Force onto Surface $\mathbf{F} = \int_S (\mathbf{n}\boldsymbol{\sigma})dS$ #1	4
Pressure $P = \frac{dF_{\perp}}{dA}$ #2	4
Local Density $\rho = \lim_{\Delta V \rightarrow 0} \frac{\Delta m}{\Delta v}$ #3	5
Velocity in three Dimensions $u_p = \frac{dx_p}{dt}$, $v_p = \frac{dy_p}{dt}$, $w_p = \frac{dz_p}{dt}$ #4	5
Average Velocity $\langle \mathbf{V} \rangle = \frac{1}{A} \int_1^2 \mathbf{V} \times n dA$ #5	5
Volumetric Flow Rate $Q = \langle \mathbf{V} \rangle A = \int_1^2 \mathbf{V} \times n dA$ #6	5
Circulation $\Gamma = \oint_S \mathbf{V} \times ds$ #7	6
Shear Rate $\gamma = \frac{dv}{dz} \approx \frac{\langle v \rangle}{2R}$ #8	9
Shear Stress $\tau = \eta\gamma = \eta \frac{dv}{dz}$ #9	9
Hagen-Poiseuille $J_t = \frac{\pi\Delta P}{8l\eta} r^4$ #10	9
Reynolds Number $Re = \frac{\rho v d}{\eta}$ #11	10
Mean Transit Time $\bar{T} = \int_0^{\infty} t h(t) dt$ #12	11
Oscillatory Shear Index $OSI = \frac{\int_0^T \tau_w^* n dt}{\int_0^T \tau_w n dt}$ #13	11
Pulse Wave Velocity $\frac{Ed}{2r} = \frac{V\Delta P}{\Delta V}$ and $v_{pw} = \sqrt{\frac{V\Delta P}{\rho\Delta V}}$ #14	12

Wavelength $\lambda = \frac{v}{f}$ #15	24
Phase Velocity $v_p = \frac{\omega}{\kappa}$ #16	25
Sound Intensity $\langle I \rangle = \frac{1}{T} \int_0^T p(t)v(t)dt$ #17	25
Wave Function $y(x, t) = A \cos \left[\omega \left(\frac{x}{v} - t \right) \right] = A \cos(\kappa x - \omega t)$ #18	26
Wave Equation $\frac{\partial^2 y(x,t)}{\partial x^2} = \frac{1}{v^2} \frac{\partial^2 y(x,t)}{\partial t^2}$ #19	26
Doppler Shift $f_0 = f_s \left(\frac{v \pm v_0}{v \mp v_s} \right)$ #20	27
Radioactivity and Nuclear Decay Probability $-\frac{dN}{dt} = a = a_0 e^{-\lambda t}$ #21	35
Decay Constant $\lambda = \frac{\ln 2}{t_{1/2}} = \int_1^{W_0} N(W) dW$ #22	35
Momentum of a Photon $p = \frac{E}{c} = \frac{h}{\lambda}$ #23	36
Effective Dose $E = \sum_T W_T H_T$ #24	38
Energy Loss of Electron $\frac{dT}{dx} = N \int_0^T h\nu d\sigma_{rad}$ #25	38
Bremsstrahlung $eV_{AC} = hf_{max} = \frac{hc}{\lambda_{min}}$ #26	39

RESEARCH QUESTION

This study aims to investigate duplex ultrasound and venography imaging findings that can identify May-Thurner Syndrome and other pelvic vein compression syndromes at an earlier stage of disease for adults with lower extremity leg pain and edema.

The following research objectives facilitate the achievement of this aim:

- 1) To identify patients with lower extremity leg pain and edema and collect their demographic and imaging data.
- 2) To engage in the acquisition of the imaging modalities of interest, including duplex ultrasound, venography, and intravascular ultrasound.
- 3) To determine duplex ultrasound and venography imaging findings that predict venous compression on intravascular ultrasound.
- 4) To determine venography imaging findings that predict venous compression on intravascular ultrasound.

The following research questions facilitate the achievement of this aim:

- 1) Does reflux at the common femoral vein on duplex ultrasound predict venous compression on intravascular ultrasound?
- 2) Do abnormal flow patterns at the common femoral vein on duplex ultrasound predict venous compression on intravascular ultrasound?
- 3) Does spontaneity, phasicity, or competency on duplex ultrasound at the common femoral vein predict venous compression on intravascular ultrasound?

- 4) Does spontaneity, compressibility, or thrombosis on duplex ultrasound predict venous compression on venography?
- 5) Does compression on venography predict venous compression on intravascular ultrasound?

CHAPTER 1

INTRODUCTION, SIGNIFICANCE, AND RATIONALE

May-Thurner Syndrome (MTS) is one of many venous compression syndromes and is usually diagnosed late into the disease course given the lack of reliable non-invasive diagnostic imaging. This research aims to identify duplex ultrasound and venography findings that may be used to detect MTS and other pelvic vein compression syndromes at an earlier stage of disease. This chapter will provide an introduction to MTS including its history and economic impact, an overview of biofluid mechanics and the clinical implications of flow changes, and the cellular biology and pathology underlying venous compression syndromes. Then diagnostics are discussed including the physical foundation of ultrasound and venography, MTS management, and the rationale for this project.

1.1 History and Economics

In the 1950s, Drs. Robert May and Josef Thurner initiated an investigation as to the cause of thromboses within the pelvic veins by examination of 430 cadavers. They initially suspected a developmental etiology, and histopathologic examination revealed the presence of loose connective tissue with fibrocytes in the tunica intima. However, there was no vessel wall separation or smooth muscle fibers encircled by elastic fibers, which were unexpected findings for a developmental cause. They also found intravenous spurs, which they believed may contribute to the pathology. Interestingly, their patients had thromboses on the left side of the pelvic veins about five times more frequently than on the right side. Despite this, MTS was determined to be an anatomical variant in which the left common iliac vein is compressed by an

overriding right common iliac artery against the lumbar spine, leading to clinical sequelae. This anatomical variant need not significantly differ from normal anatomy as Figure 1.1 illustrates how the left common iliac vein can be easily compressed. This seems sensible given that subsequent studies have shown that up to 25% of the general population has more than 50% compression of the left iliac vein, although most people with this anatomical variant are asymptomatic. However, those with clinical sequelae are diagnosed with MTS, and it is estimated that 2-3% of patients with lower extremity deep vein thrombosis (DVT) have MTS.

Since its discovery, advancements in the understanding of MTS have shown that similar underlying mechanisms of disease occur in other veins. Consequently, the modern definition of MTS is inclusive of other sites of venous compression such as both common iliac veins, external iliac veins, and popliteal veins. Recent developments in vascular surgery have also expanded the understanding of venous compression syndromes, a group of diseases that includes MTS. These new sites of compression include the hypogastric artery, inguinal ligament, popliteal fossa, left renal vein, retrohepatic inferior vena cava, axillo-subclavian veins, and internal jugular veins. Over the past few decades, the knowledge of venous compression syndromes has certainly increased. At the same time, clinical outcomes for patients with this group of diseases has not kept up with these advancements to the same extent, in part because of the challenge in early detection.¹⁻⁶

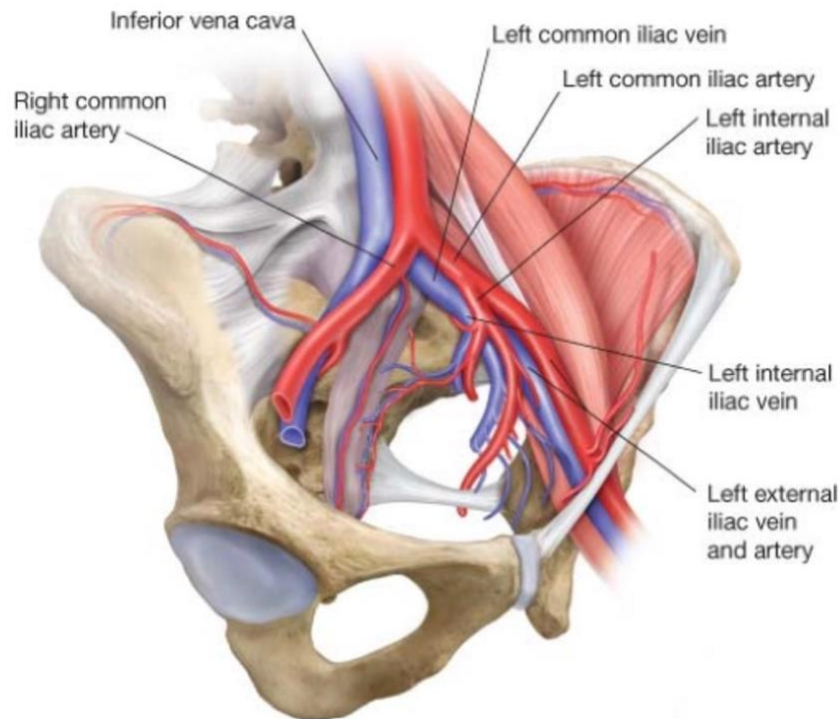


Figure 1.1. Artistic depiction of normal pelvic vascular anatomy, highlighting how the left common iliac vein can be compressed by the right common iliac artery. Acquired from Goodney & Warner.²⁰ Image accessed on December 10, 2022.

Chronic venous disease (CVD) affects a significant portion of the population and has a substantial economic impact. It is estimated that over 30 million people have CVD in the United States alone, with a prevalence of 23% for varicose veins and 1-3% for venous ulcers. The annual direct and indirect cost of CVD in the US is approximately \$5 billion, including clinician costs such as home health visits, procedures, medications, clinician time and wages, and hospitalization costs. This estimate also considers an estimated loss of productivity from 2 million days of work missed annually. CVD can also significantly reduce patients' quality of life by affecting mobility, depression, and pain. The incidence of clinical sequelae of CVD should be noted, as approximately 200,000 cases of venous thrombosis and 180,000 amputations occur in

the US each year. MTS is one type of CVD, and research that improves outcomes for these patients has the potential to both reduce its economic burden and improve the quality of life for these patients.²⁵⁻³⁴

To understand the pathological foundations of pelvic vein compression syndromes, which MTS is categorized within, it is imperative to consider how abnormal flow patterns, among other changes in intravascular fluids, can induce pathophysiologic responses which may originate or exacerbate disease. To understand the reason for this, an introduction to fluid mechanics is discussed, which is followed by its application to intravascular fluids. This is then intentionally followed by a discussion of cellular biology and pathology, which builds on the physical basis and analysis of fluids.¹¹

1.2 Biofluid Mechanics

For the discussion of fluids, the Eulerian view for the frame of reference will be used. For any fluid in a tube, a force \mathbf{F} will act onto surface S which can be calculated when given stress vector $(\mathbf{n}\boldsymbol{\sigma})$.

$$\mathbf{F} = \int_S (\mathbf{n}\boldsymbol{\sigma}) dS \quad (1)$$

The stress vector is important here as it results in deformation of the fluid. If we take the normal force originating from the fluid $d\mathbf{F}_\perp$ and divide it by an area on a point in the fluid dA , one gets pressure P .

$$P = \frac{d\mathbf{F}_\perp}{dA} \quad (2)$$

However, for fluids in motion it should be noted that pressure is calculated as the average of three normal stresses that are perpendicular to each other. Additionally, the pressure gradient determines the magnitude of the net pressure force on a given particle of interest. Intravascular fluids in motion have a density that is constantly changing. In such cases, it may be of interest to calculate the local density ρ as we approach a volume of zero given a certain change in mass m and volume v .

$$\rho = \lim_{\Delta V \rightarrow 0} \frac{\Delta m}{\Delta v} \quad (3)$$

In fluids, each individual fluid element experiences multiple forces. When studying fluids at the microfluidic scale, certain forces and energies predominate to an extent that differs when compared to fluids at the macrofluidic scale. For example, at the microfluidic scale, inertia and gravity do not affect fluids to a significant extent whereas viscoelasticity is particularly significant. The velocity for a given fluid element p is given by a change in position divided by a change in time for the x , y , and z axes, which yield velocities u , v , and w , respectively.

$$u_p = \frac{dx_p}{dt}, \quad v_p = \frac{dy_p}{dt}, \quad w_p = \frac{dz_p}{dt} \quad (4)$$

Equation 4 can be used to calculate the specific position of a fluid element of interest in the flow field given a specific point in time. The sum of these velocity components yields the net velocity vector which may also be calculated as the average velocity $\langle \mathbf{V} \rangle$ expressed as a function of cross sectional area A and n unit vector normal to A between points 1 and 2.

$$\langle \mathbf{V} \rangle = \frac{1}{A} \int_1^2 \mathbf{V} \times n dA \quad (5)$$

We can also calculate the volumetric flow rate Q with similar variables.

$$Q = \langle \mathbf{V} \rangle A = \int_1^2 \mathbf{V} \times n dA \quad (6)$$

Equations 1 to 6 ultimately allow for an adequate basic description of fluids. With this fundamental understanding, it is appropriate to superimpose other aspects of fluid mechanics that directly affect flow, which is of importance when understanding venous compression syndromes. There are many ways in which fluids may undergo translation, linear deformation, angular deformation, and rotation. The most applicable of these to intravascular flow may be rotation. Two means of measuring rotation are circulation and vorticity. Circulation measures rotation at a macroscopic, global scale. Conceptually, it is the total amount of force pushing along a path. Circulation Γ occurs around a closed curve and is mathematically defined as the line integral of the tangential component of the velocity vector \mathbf{V} around a differential length s along the curve.

$$\Gamma = \oint_s \mathbf{V} \times ds \quad (7)$$

On the other hand, vorticity measures rotation at a microscopic, local scale. Conceptually, it is a measure of the local rotation of a fluid element. The calculation for vorticity of a fluid element is relatively intricate and is not necessary to demonstrate for the purpose of this study. However, the average vorticity in a very small space can be approximated as circulation divided by the area of that space. In this manner, circulation and vorticity are directly related to each other.

Therefore, changes in intravascular fluid mechanics may affect circulation as defined in equation (7), depending on the cause. Venous compression syndromes may affect the vasculature in such a manner that a variety of factors are altered, such as rotation. Figure 1.2 aids in the visualization, and therefore conceptualization, of vorticity. The peripheral light blue dots with their corresponding arrows may be thought of as the velocity field, while the central dark blue dot is a fluid element with the corresponding arrow representing its velocity vector. The fluid element on the left has nonzero vorticity as the velocity field causes the fluid element to spin, albeit without moving along a path. The fluid element on the right also has nonzero vorticity as

the velocity field causes the fluid element to rotate as it moves along a path, given that not all vectors from the velocity field are identical. It is evident that vorticity can be present, regardless of the path taken by a fluid element.

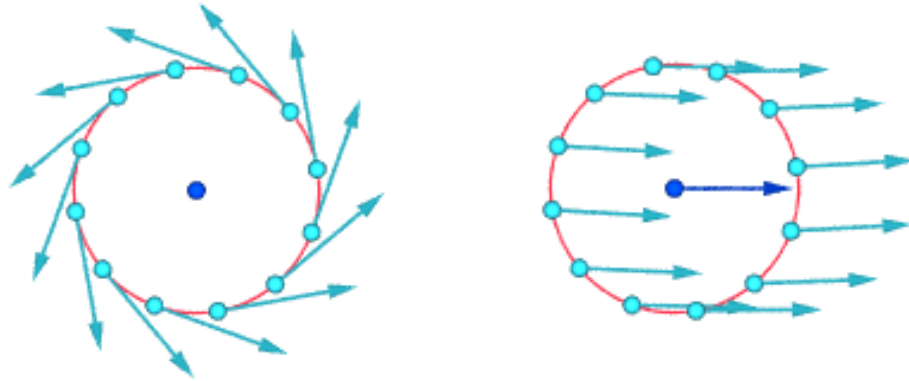


Figure 1.2. Vorticity of fluid elements. Acquired from Wikimedia Commons.¹⁰⁴⁻¹⁰⁵ Image accessed on February 21st, 2023.

When different fluid elements slide past each other, shear forces may be generated. Laminar flow may be conceptualized as the movement of fluids where there are minimal velocity fluctuations. In contrast, turbulent flow may be conceptualized as the movement of fluids where velocity fluctuations are substantial. Transitional flow, as may be expected, is a flow pattern that occurs in between laminar and turbulent flow. Figure 1.3 provides a graphical representation of flow patterns. The lines in the graphic are streamlines, which depict the direction fluid elements travel at different points in time given these lines are tangential to the net velocity vector. Altogether, streamlines represent a velocity field. Figure 1.3A depicts the velocity field for laminar flow and Figure 1.3B depicts the velocity field for turbulent flow.

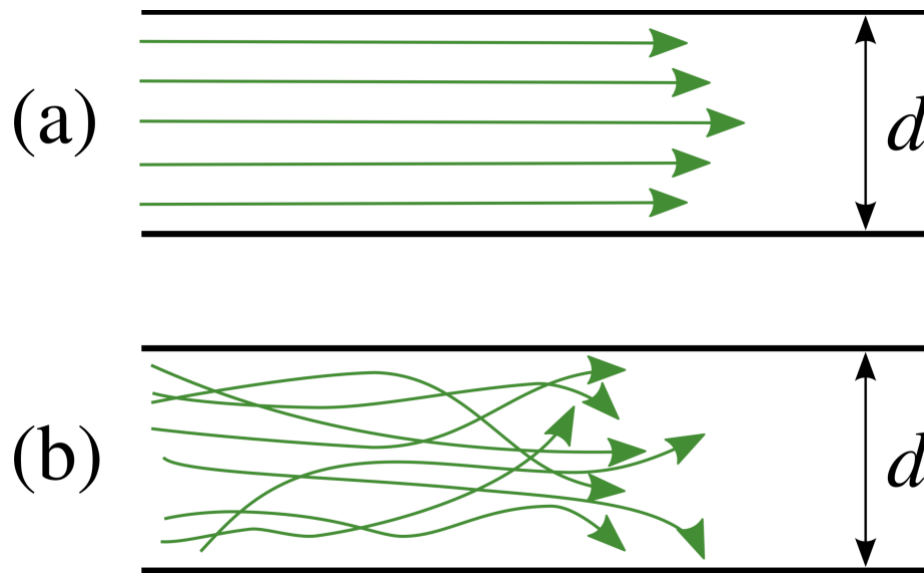


Figure 1.3. A) Laminar flow pattern. B) Turbulent flow pattern. Acquired from Wikimedia Commons.⁸⁸ Image accessed on February 13th, 2023.

In vasculature, laminar flow is associated with high shear stress, while non-laminar flow is associated with low shear stress. Shear stress τ is the product of shear rate γ and the viscosity of the fluid η . Importantly, τ is inversely proportional to the third power of the radius in a blood vessel. Therefore, a change in the radius of a blood vessel will have a greater impact on shear stress than a change of the same magnitude in either shear rate or fluid viscosity. It is worth noting that even a small amount of τ yields a pressure differential, which may be significant depending on the length of the vascular channel of interest. With that relationship in mind, it is not surprising that the forces an object immersed in a fluid experiences, such as a cell in an intravascular fluid, can be conceptualized as a pressure distribution and a shear stress distribution. The shear stress distribution is typically within the same plane as the path an object follows whereas the pressure distribution is perpendicular to the object. Tensional stress and

compressional stress may be thought of as forces that pull apart and squeeze together an object, respectively. Lift and drag are also forces that affect an immersed object. Shear rate is proportional to a change in velocity v and inversely proportional to the distance from a fixed surface z . Shear rate is also proportional to the ratio of average velocity to tube radius R given the following equation:

$$\gamma = \frac{dv}{dz} \approx \frac{\langle v \rangle}{2R} \quad (8)$$

We may substitute Equation 8 for the aforementioned product between fluid viscosity and shear rate to calculate shear stress, as it may be easier to conceptualize in this manner.

$$\tau = \eta\gamma = \eta \frac{dv}{dz} \quad (9)$$

However, the relationship between shear rate and distance from a surface is not linear. Instead, the shear rate is highest at the surface and decreases in a curvilinear manner as the distance from the surface increases. At a certain point distance, the shear rate approaches zero. At the fluid-surface interface, the velocity of fluids is zero. The Fahraeus-Lindqvist effect elucidates how this difference in shear rate affects the distribution of cellular components within the vasculature. The effect is characterized by the highest concentration of cells at the center of blood vessels and the lowest concentration at the fluid-surface interface. This emphasis on shear stress is paramount to note, as alterations in shear stress, such as those occurring during an arteriovenous shunt, can trigger physiological processes like vascular remodeling, which entails the alteration of the radius of a vessel. Laminar flow is proportional to the radius to the fourth power assuming no changes in other factors per the Hagen-Poiseuille equation given total flow J_t , driving pressure ΔP , tube length l , and fluid viscosity η .

$$J_t = \frac{\pi\Delta P}{8l\eta} r^4 \quad (10)$$

From Equation 10 it is crucial to observe that even a minute alteration in the radius of a tube, such as a blood vessel, can yield a disproportionately large change in flow. When coupled with vascular remodeling induced by shear stress, a modification in the blood vessel radius can carry significant pathological implications, such as a change in the pressure differential along a vascular structure. A notable limitation of Equation 10 is its inability to characterize fluids experiencing non-laminar flow patterns, and therefore its application should be made with caution. The likelihood of non-laminar flow, notably turbulent flow prevalent in vascular pathological processes, can be approximated using the Reynolds number Re . This dimensionless value is calculated by dividing inertial forces by viscous forces using fluid density ρ , flow velocity v , tube diameter d , and fluid viscosity η . It is important to highlight that because there are multiple factors that affect Re , there is no universal Re cutoff that determines the transition from laminar to turbulent flow. Each fluid has a distinct Re cutoff for this transition. However, it is generally accepted that fluids with $Re > 2,000$ are likely to have a turbulent flow pattern.

$$Re = \frac{\rho v d}{\eta} \quad (11)$$

Another dimensionless number worth noting is the Weissenberg number, which describes the relative strength of viscoelastic effects in a fluid. Conceptually, it is a ratio of the fluid's relaxation time to its deformation time, and it predicts whether a fluid will behave as a Newtonian or non-Newtonian fluid. A larger Weissenberg number predicts the fluid to be non-Newtonian, like blood. The drag coefficient, which contributes to drag force, is primarily determined by a combination of Reynolds number and Stokes law. This is yet another component that should be considered when understanding the flow of any fluid. Flow patterns can also be studied using radiotracers, and for a given vascular structure with the same input and output of fluid, such as an isolated blood vessel, the mean transit time \bar{T} of a radiotracer can be

determined. Under this assumption, \bar{T} can be calculated based on the transit time distribution of the outflow $h(t)$ and time t

$$\bar{T} = \int_0^{\infty} t h(t) dt \quad (12)$$

If there are multiple fluid inputs and outputs, \bar{T} can still be calculated, albeit using a more complex equation. We can also measure the ratio of the cardiac cycle where flow is reversed by calculating the oscillatory shear index (OSI) which is a function of shear stress at aortic wall τ_w , stress component τ_w^* , and time t . Higher OSI corresponds to more time in reversed flow while zero OSI corresponds to the absence of any reversed flow.

$$OSI = \frac{\int_0^T |\tau_w^* n| dt}{\int_0^T |\tau_w n| dt} \quad (13)$$

As a non-Newtonian viscoelastic fluid, blood exhibits an ever-changing viscosity due to the non-uniform distribution of cells and other blood components. This dynamic viscosity affects flow dynamics, particularly in contexts where the Reynolds number (Re) is increased, as often encountered in blood circulation. Additionally, elevated viscosity increases total peripheral resistance, which in turn increases blood pressure. These factors are critical to consider when comprehending how alterations in fluid mechanics may contribute to pathological changes within the vasculature. For example, it logically follows that stenosis which modifies the radius of a blood vessel leads to non-laminar flow, subsequently impacting the pulse velocity. The effects of stenosis on pulse velocity can be better understood with the following equations, which consider modulus of elasticity E , wall thickness d , radius r , volume V , pressure P , medium density ρ , and velocity of the pulse wave v_{pw}

$$\frac{Ed}{2r} = \frac{V\Delta P}{\Delta V} \quad (14)$$

and

$$v_{pw} = \sqrt{\frac{V\Delta P}{\rho\Delta V}} \quad (14)$$

These equations show that as wall thickness increases, pulse velocity also increases. This can lower the efficiency of nutrient and oxygen uptake to tissues near the affected vasculature and affect the uptake of metabolic waste from tissues, further exacerbating the pathological effects of a stenosed vessel on the normal function of surrounding tissue. It is also important to take into consideration the likely short length of the stenotic component of a vessel as the entirety of a vessel is rarely affected. According to the Spencer model, there is an increase in velocity in stenotic vessels to compensate for the decrease in intimal surface area available to participate in the exchange of nutrients and oxygen for metabolic waste, which preserves adequate blood flow. However, this is a nonlinear relationship and past approximately 80% stenosis, blood flow is compromised such that the velocity actually decreases and simultaneously there is less intimal surface area.

All of the mathematical relationships given up to this point provide a foundation for comprehending the fundamental principles of fluid mechanics, especially in the context of intravascular fluids. These relationships are applied to aberrant flow patterns and how they can contribute to cellular adaptations, as discussed below. ^{8,12-13,18,45-46,54-55,80-81}

1.3 Cellular Biology and Pathology

A comprehensive exploration of the pathological basis of MTS demands an interdisciplinary approach. The preceding section delved into the biophysical foundation of intravascular flow. This section starts by elucidating cellular principles that are relevant to vascular structures, with an emphasis on the cell membrane, which is intricately influenced by changes in intravascular fluid mechanics. This is followed by a discussion of MTS pathology, which considers both biophysical and cellular principles.

Molecular motion and conformations are heavily influenced by principles of thermodynamics, covalent interactions, and non-covalent interactions. Dissolution of hydrophobic molecules in water triggers an endothermic reaction, yet there is a concurrent increase in entropy. This well-known paradox occurs because the aggregation of hydrophobic molecules forms a clathrate cage, which requires fewer water molecules. This then leaves more water molecules to be mobile in the solution. The overall effect of this is a net decrease in free energy, rendering the aggregation of hydrophobic molecules in water a spontaneous process. This process is fundamental in determining the three-dimensional arrangement of cell membranes.

Covalent interactions resist breakdown from thermal motions given their high bond strength. Non-covalent interactions encompass electrostatic, hydrogen, and van der Waals forces. Although these interactions partially resist thermal perturbations, their influence is weaker compared to covalent bonds. However, the sum of all non-covalent interactions exerts a strong force that can repel or attract other molecules. The polarity of molecules adds another layer of complexity, particularly because the aqueous environment of cells causes hydrophobic groups to

cluster together. These intermolecular forces collectively dictate the extent of molecular motion. In fluid environments, vibrational, rotational, and translational motions occur. These interactions play a key role in the structure of the plasma membrane enveloping cells.

The lipids composing this bilayer are primarily fall into distinct categories: phospholipids, sphingolipids, glycolipids, and cholesterol. The amphiphilic nature of these lipids facilitates the spontaneous assembly of an energetically favorable spherical bilayer structure in aqueous environments. Thermodynamic and non-covalent interactions significantly influence the geometric arrangement of these lipids. Consequently, the hydrophobic tail groups of both lipid layers orient inward, repelled by the surrounding aqueous solution. This is in part due to the tail groups' near-uniform electron density, which results in an absence of an electrostatic charge. Conversely, the hydrophilic head groups of both layers face outward, interacting with the aqueous environment due to their hydrophilicity and non-uniform electron density. It is this orientation that yields polar groups or electrostatic charges.

Phospholipids make up the majority of the membrane structure. They are synthesized within the endoplasmic reticulum and are delivered to the plasma membrane in vesicles, organized in a specific arrangement. This ensures targeted delivery to either the exoplasmic or cytoplasmic leaflet. The persistent fluidity of many lipids in a three-dimensional manner yields an asymmetric plasma membrane. This lipid heterogeneity in both leaflets carries profound significance for life as certain proteins exclusively interact with either the extracellular or intracellular environment. This is the basis of vital cellular functions such as signal transduction.

Simultaneously, this asymmetry governs cellular responses to various stressors, intricately influencing pathophysiological outcomes.

While the preceding discussion might appear rudimentary, its purpose is to establish a strong and focused foundational understanding. This ensures a robust grasp of the fundamentals before venturing into more intricate subjects concerning the biology of the plasma membrane. Having comprehensively addressed the constituents and recognized configuration of the plasma membrane, it is now appropriate to address scenarios in which the plasma membrane faces jeopardy in the retention of its geometric integrity.

The integrity of the plasma membrane is susceptible to both chemical and biophysical stressors. When such stressors cause a breach, the lipids within the bilayer attempt to spontaneously rearrange themselves to try to seal the breach. This rearrangement attempts to counteract the energetically unfavorable interaction between water and the hydrophobic tails of the lipids in the bilayer. Chemical stressors include lipid peroxidation, enzymatic cleavage – especially by host cytotoxic enzymes or foreign phospholipases – and any factors capable of altering membrane fluidity. These fluidity-altering factors may include fluctuations in temperature or the presence of foreign amphiphilic molecules. Biophysical stressors, on the other hand, include shear stress, stretch, compression, and thermal injury. Importantly, it's worth noting that the impact of a given stressor on the plasma membrane's integrity can vary to great extents.

For instance, the Tabouillot⁹⁹ research project showed that the plasma membrane of endothelial cells exhibits a spectrum of sensitivities to shear stress, contingent on the specific membrane

microdomain affected. The process by which the plasma membrane obtains heterogeneous microdomains as discussed above, directly contributes to this varying sensitivity. No matter the mechanism of breach, various mechanisms come into play to attempt plasma membrane repair if spontaneous rearrangement is inadequate. Repair mechanisms include exocytosis or endocytosis patching or plugging, cellular contraction or constriction, and scission. Additionally, the cell actively removes any cytotoxic substances that may have infiltrated during the breach. Among the most common substances removed are calcium, eliminated by uptake in the endoplasmic reticulum and the mitochondria, and oxidative species, inactivated by antioxidants. The diverse chemical and biophysical stressors collectively contribute to pathophysiological processes as outlined below.

When a cell experiences damage from a chemical or biophysical stressor, it engages in adaptation. The response pathways a cell may follow after exposure to such a stressor are diverse, with the frequency and severity of the stressor determining whether full recovery or cellular injury follows. Atrophic adaptations may occur through the ubiquitin-proteasome pathway or autophagy. Hyperplastic and hypertrophic adaptations may occur through an increased rate of cellular proliferation. This would lead to more tissue mass or an increased rate of protein synthesis and other cellular components, respectively. When cellular stressors are frequent enough or severe enough it may alter the differentiated progeny of stem cells. This leads to metaplastic adaptations, which are often reversible, but may progress malignant transformation if the stressor persists.

Cellular stressors may cause the above adaptations, or they may injure the cell directly. This may be reversible or irreversible, and there are many mechanisms that dictate the fate of a cell upon exposure to an injurious stressor. The plasma membrane is directly affected in some of these mechanisms. One reversible mechanism of cellular injury that relates to vascular structures involves hypoxia. This initially induces the dysfunction of plasma membrane Na^+ / K^+ ATPases can lead to hydropic degeneration by increasing the intracellular concentration of Na^+ , which has the effect of increasing the total water content of a cell in addition to alterations in Ca^{2+} ATPase activity. The combined effect of hypoxia and plasma membrane ATPase dysfunction is anaerobic respiration, and the sequelae of this includes protein denaturation, decreased protein synthesis via ribosomal dysfunction, cytoskeletal disruption leading to blebbing of the plasma membrane, and other effects. Should the stressor continue, as in the case of ischemia, irreversible changes may occur that occur all components of the cell. As one example focusing on the plasma membrane, phospholipid degradation may occur which can cause cell lysis. Ischemia can also lead to the generation of free radicals. These are unpaired electrons in the outermost orbital of an atom and can damage many components of the cell such as DNA or cell membranes. Essentially, free radicals can cause the peroxidation of membrane lipids which increases their permeability. Finally, cellular stressors of sufficient magnitude or frequency may lead to apoptosis or necrosis. The former is non-inflammatory and may occur through many intrinsic or extrinsic pathways. The latter is inflammatory, primarily through liquefactive or coagulative pathways.

Endothelial cells (ECs) line the innermost layer of blood vessels and play many important roles in optimal cardiovascular function. They allow for paracellular and transcellular transport, hemostasis modulation through production of many procoagulant and anticoagulant molecules,

vasodilation through production of nitric oxide and prostacyclin, vasoconstriction through production specific endothelins and prostaglandins, thermoregulation at microcirculatory sites, leukocyte extravasation, angiogenesis through production of vascular endothelial growth factor (VEGF), and blood pressure regulation through angiotensin II production. These cells are damaged in many pathological processes, as is discussed below, and are a key component of the tunica intima. While the specific components of veins differ according to the specific vein of interest, all veins have a tunica intima, tunica media, and tunica adventitia. The tunica intima is commonly composed of ECs, basal lamina to anchor ECs, valves to prevent fluid backflow, and a subendothelial layer. The tunica media is commonly composed of connective tissue and smooth muscle cells. The tunica externa is commonly composed of smooth muscle cells and layers of collagen. Figure 1.4 presents the microanatomy of veins, and importantly the cross sectional arrangement of the tunica intima, media, and externa.

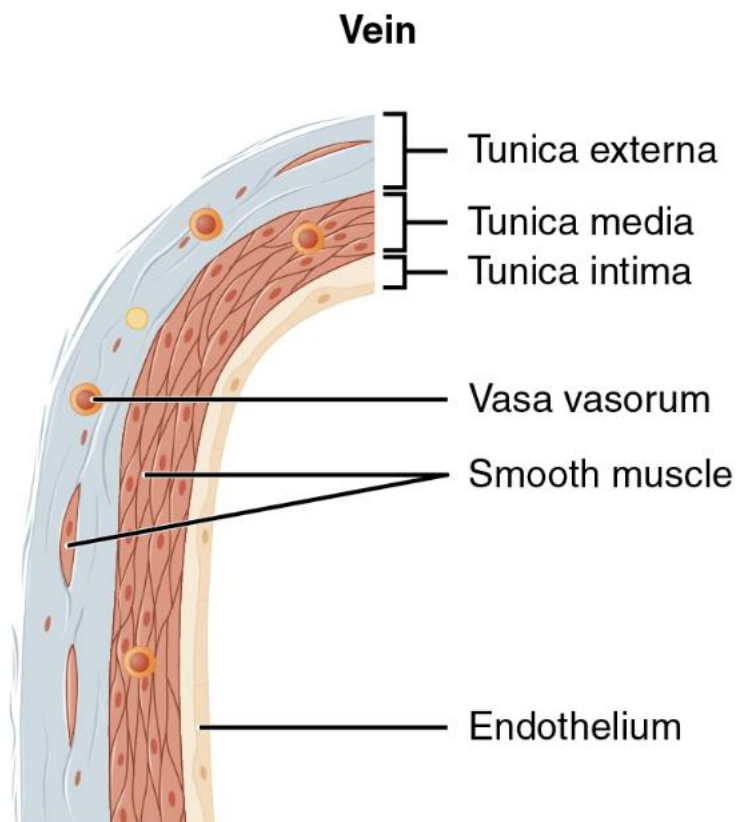


Figure 1.4. Cross sectional arrangement and composition of veins. Adapted from Betts et al.⁹¹

The vasculature is constantly subjected to an interplay of hemodynamic forces, including shear stress as outlined in Equation 9, rotational stress due to circulation as per Equation 7, hydrostatic pressure, and other fluid stressors. These forces collectively alter net velocity vectors, as described in Equation 5, consequently influencing the volumetric flow rate, as defined by Equation 6. These deviations from typical intravascular flow, coupled with factors inducing vessel wall deformation, are major contributors to vascular dysfunction. Non-laminar flow that leads to shear stress may lead to cellular injury. Other non-laminar flow patterns, such as recirculation eddies, reflux, and flow separation, can arise under specific conditions such as incompetent venous valves or outflow obstruction. These abnormal patterns contribute to pathological alterations via mechanisms like neointimal hyperplasia or thrombosis.

Neointimal hyperplasia in vasculature starts with EC injury. This prompts platelet activation and initiates the clotting cascade. At the same time, leukocytes are recruited through the inflammatory cascade. These cascades are followed by smooth muscle cell proliferation and migration from the tunica externa to the tunica intima, and this is in part facilitated by matrix metalloproteinases. EC injury along this pathway can disrupt normal valve function in the superficial and deep veins as they are pressure-dependent rather than flow dependent. More specifically, it is the hydrostatic pressure differential that is fundamental to valve closure and physiologic venous collapse. When this is disrupted by neointima hyperplasia, the changes in fluid dynamics result in venous hypertension which significantly disturbs normal pulsatile vascular flow. This vascular dysfunction is exacerbated by various disease, including chronic

venous disease. It's important to note that ECs within venous valves are already predisposed to Virchow's triad. The surrounding area typically features abnormal flow patterns characterized by reduced shear stress and potential stasis. Hypercoagulability results from differential gene expression of prothrombotic factors, alongside EC damage from leukocyte infiltration in patients with chronic venous disease.

Histopathological evidence suggests that abnormal flow patterns contribute to alterations in the geometric arrangement of endothelial cells, rendering them less elongated compared to normal ECs. Intercellular junctional protein distribution also becomes discontinuous. Additionally, low shear stress-associated abnormal flow patterns upregulate thrombogenic genes such as VEGF, whereas high laminar shear stress inhibits EC proliferation. DNA microarray studies show significant differences in gene expression profiles between valvular and vascular ECs exposed to shear stress. Valvular ECs express more anticoagulant and anti-inflammatory gene products. Exposure to abnormal flow patterns induces greater heterogeneity in gene expression compared to cells exposed to laminar flow. This accentuates the crucial role of gene expression in EC function, particularly when subjected to abnormal flow patterns. Analogous responses are observed in venous ECs exposed to reflux-driven abnormal flow patterns and arterial ECs within an atherosclerotic plaque. Both types of cells show increased leukocytes in the tunica intima and media, elevated expression of adhesion molecules, proteases, and mitogens. Collectively, these factors increase the likelihood of inflammatory damage to veins, likely contributing to the pathogenesis of chronic venous diseases.

The clinical consequences of MTS primarily stem from the hemodynamic changes induced by compression. The chronically elevated venous pressure, combined with the pulsatile overriding artery, triggers a cascade of pathophysiologic responses. The decreased vein diameter results in increased vascular resistance and the emergence of intravenous eddies due to turbulent flow prompted by velocity fluctuations. These factors likely elevate shear stress, which contribute to the development of neointimal hyperplasia through EC injury. Consequently, these altered fluid dynamics may be the underlying cause of the formation of intravenous spurs, stenosis, and venous collateral vessels, all of which are responses to decreased venous outflow.

While many patients with MTS are asymptomatic, detecting this disease is crucial to provide appropriate treatment and surveillance. This significance arises because some patients with MTS can develop clinical sequelae with an additional stressor given that their baseline risk for a DVT is greater than those without MTS. These stressors include but are not limited to medications that induce a hypercoagulable state, pregnancy, and a history of extended periods of travel. In the presence of one of these or other stressors, extravasation of intravascular fluid onto surrounding tissues can occur. The extravasated erythrocytes are consumed by macrophages as part of the normal immune response resulting in hemosiderin-laden macrophages. Over time, this culminates in venous stasis dermatitis. If left untreated, hypoxic or anoxic conditions within the affected vasculature can lead to tissue ischemia, which can lead to venous stasis ulcers.^{3,7,9-}

11,14,24,78,91,95-102

1.4 Diagnostics

The pathology discussed in the previous section serves to guide the diagnostic approach to detect these anatomic and physiologic changes. While the history and physical exam alone cannot be used to diagnose MTS or venous compression syndromes, they may be used to decrease the probability of other diseases using the familiar Bayesian approach to clinical reasoning. Then in combination with laboratory and radiographic examinations, the correct diagnosis may be obtained.

Unfortunately, given the asymptomatic nature of this disease in most patients, MTS is often diagnosed after pathological changes have occurred. Additionally, many patients with clinical sequelae of MTS have multiple DVTs before receiving a correct diagnosis. This may in part be due to the nature of the presenting DVT, as based on history and physical exam there are no known reliable indicators with an appropriate specificity for MTS. However, the astute clinician should consider this in the differential diagnosis if the patient is young with a history of DVTs, and workup for hypercoagulable factors is unremarkable.

Imaging typically starts with a duplex ultrasound, which can adequately detect iliofemoral DVTs. However, appropriate visualization of the iliac veins to the extent required to make a diagnosis of MTS is often difficult to obtain. Computed tomography and magnetic resonance venography can provide more information compared to duplex ultrasound that raises the clinical suspicion for MTS. Venography, which uses contrast dye with fluoroscopy, can visualize an entire segment of stenosis, but only from one angle which can lead to false negatives in the search for stenosis. As an example, even with multiplanar venography, iliac vein lesions can be

missed as this is merely a combination of two-dimensional images. Intravascular ultrasound (IVUS) can visualize vascular structures in three dimensions but is limited to a cross section of the vessel of interest. The gold standard for the diagnosis of MTS as of writing is a combination of venography with IVUS, as the shortcomings of one imaging modality are generally compensated for by the other modality. These two imaging modalities are shown on Figure 1.5.

3,7,9-11,14-17,19

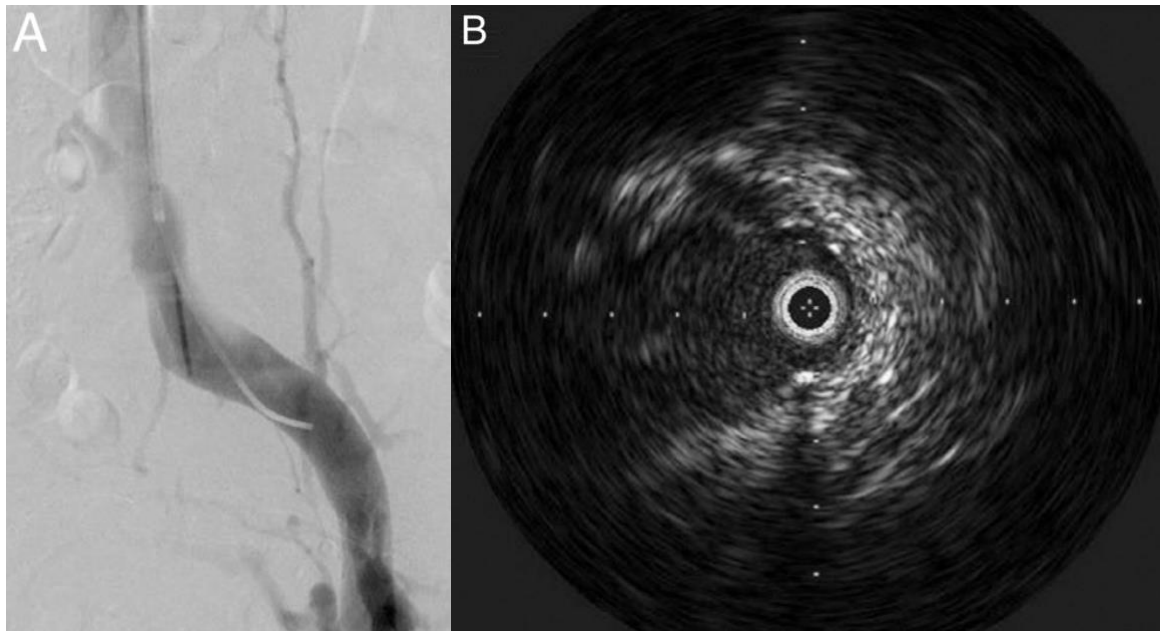


Figure 1.5. A) Venography demonstrating a stenotic left common iliac vein. B) IVUS demonstrating a portion of the same stenotic segment as A). Adapted from Birn et al.¹⁴

Given that ultrasound and venography, which uses fluoroscopy, are the imaging modalities that are key in the findings of this research project, it is beneficial to ensure adequate understanding of their physical principles and clinical applications.

1.5 Physics of Sound

Sound may be defined as energy that is transmitted as a longitudinal scalar wave through a medium by fluctuations of high and low pressure that are termed compression and rarefaction, respectively. Additionally, sound is categorized as a type of mechanical wave and longitudinal waves displace particles in a medium parallel relative to the direction in which the wave is propagated. The frequency of a wave is simply the number of cycles per second and is measured in hertz (Hz) while the wavelength is the distance between one point in a wave and the corresponding same point at the next point in that wave, such as the distance between one trough and the next trough or between one crest and the next crest. The classical equation used to obtain the wavelength λ for a given sinusoidal waveform can be calculated by dividing wave velocity v over frequency f

$$\lambda = \frac{v}{f} \quad (15)$$

The amplitude is the height of a wave from its resting position to the crest or trough. Figure 1.6 depicts these components of a wave, as its visualization is often easier to conceptualize than its description alone.

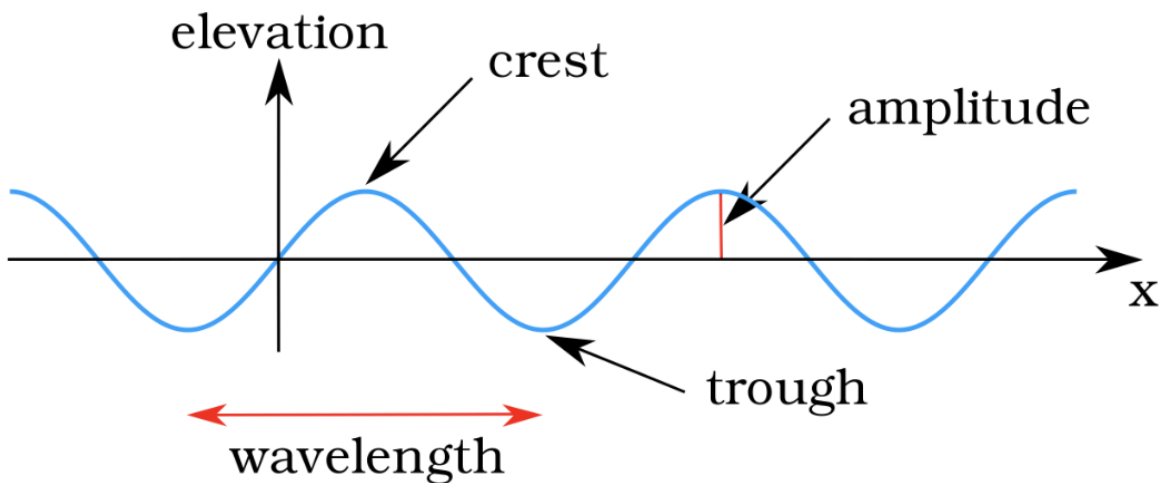


Figure 1.6. Artistic depiction of the basic components of a wave. Acquired from Wikimedia Commons.⁹² Image accessed on February 13th, 2023.

Other important characteristics include the propagation speed which is the speed of waves passing through a medium and decibels which is a logarithmic scale used to measure sound intensity. The propagation speed for a monochromatic wave may also be referred to as the phase velocity v_p which is a function of a wave's angular frequency ω over angular wavenumber κ .

$$v_p = \frac{\omega}{\kappa} \quad (16)$$

The propagation speed is essential in the use of ultrasound as the varying densities of tissues affects the speed coming back to the transducer, and that has an effect on the image output.

Sound intensity is the power delivered to a specific area by sound waves. This is related to decibels as decibels measure sound intensity on a logarithmic scale. Since decibels are usually referenced when relating sound intensity to the way people perceive sound, decibels are not the optimal unit of measurement of sound intensity for the purposes of this project. Instead, sound intensity is used alone, and the average sound intensity $\langle I \rangle$ at time T is a function of sound pressure p and particle velocity v as shown below.

$$\langle I \rangle = \frac{1}{T} \int_0^T p(t)v(t)dt \quad (17)$$

To truly understand waves, it is necessary to understand the basics of wave functions, which describe the position of a particle at any time of interest. Generally, we can think of a particle at position x along the x-axis that is also transferred distance y which is along the y axis, and the position of a particle along those two axes depends on time t. With this description in mind, y depends on x and t, which can be otherwise stated as wave function $y(x,t)$ and for a sinusoidal

wave function can be calculated given amplitude A , angular frequency ω , wave speed v , and wave number κ

$$y(x, t) = A \cos \left[\omega \left(\frac{x}{v} - t \right) \right] = A \cos(\kappa x - \omega t) \quad (18)$$

Furthermore, many waves can be described with the established wave equation

$$\frac{\partial^2 y(x, t)}{\partial x^2} = \frac{1}{v^2} \frac{\partial^2 y(x, t)}{\partial t^2} \quad (19)$$

Equations 18 and 19 provide a description of the components of sound waves and are key to reasonably understand the physical basis of ultrasound. Varying densities of tissues can affect the speed of sound waves and influence the output of images. Given that humans can generally hear between 20 Hz to 20,000 Hz, ultrasound is any frequency that is higher than the human range of hearing. Clinically relevant ultrasound waves have a wide range as changes in the frequency allow for changes in resolution and penetration. This is because frequency is directly proportional to resolution but is inversely proportional to penetration. As such, if a clinician needs to obtain an ultrasound image of deep tissues the frequency should be decreased to allow for better penetration, but the resolution will be sacrificed. The mechanism by which ultrasound imaging works is the probe emits ultrasound waves through the piezoelectric effect, then those waves traverse structures in the body and are reflected to a transducer on the probe that transforms this information into an image. Waves are emitted in a pulsatile manner to allow for the reception of reflected waves and thereafter the conversion to an electrical signal. Some ultrasound modalities, such as duplex ultrasound, may use the doppler effect to display an object of interest that is in motion. One common application of this is the directionality of intravascular fluids. In that case, the frequency that is emitted from the probe is different than the frequency received by the transducer due to intravascular fluid motion. This change in frequency is

primarily due to a doppler shift, which describes how the observed frequency f_0 is a function of the source frequency f_s , speed of sound v , observer speed v_0 , and speed of source v_s .

$$f_0 = f_s \left(\frac{v \pm v_0}{v \mp v_s} \right) \quad (20)$$

In the case of duplex ultrasound, which detects a doppler shift and outputs it as an image, v_0 is the transducer and v_s is the sound waves emitted from the probe as they reflect off tissues. The image output using this modality can be conceptualized as two images that are superimposed. One component is the normal ultrasound modality. The second component are the areas in the image in which there is a significant frequency shift due to motion. The directionality is typically indicated by a color gradient and is oftentimes red through blue for flow approaching the transducer and flow moving away from the transducer, respectively. Turbulent flow can also be depicted as a green color. While these are the standard interpretations of these colors, any color may be used for any interpretation, so care should be taken to ensure accurate interpretation. Color flow doppler ultrasound imaging findings are shown on Figure 1.7. Just as with any imaging modality, there are advantages and limitations that should be understood. Likely the biggest advantage is that this is a non-invasive diagnostic imaging modality that does not disturb the flow of intravascular fluids, which avoids the general risks of invasive procedures while providing real-time imaging. Other advantages include the absence of ionizing radiation and portability. Some limitations include those of general ultrasound use, such as the high dependence of image quality on the skill of the ultrasound tech and patient obesity or body habitus which can affect the quality of the image. General artifacts on any ultrasound modality can occur as discussed previously and it is important to note that with color flow doppler ultrasound, the penetrability can be affected to a greater extent depending on a variety of factors. Additionally, the reflecting interface or particles that the ultrasound interprets may not

necessarily have the same velocity as that of the fluid as a whole. This should be taken into account to avoid potentially oversimplifying the velocity of individual fluid components.

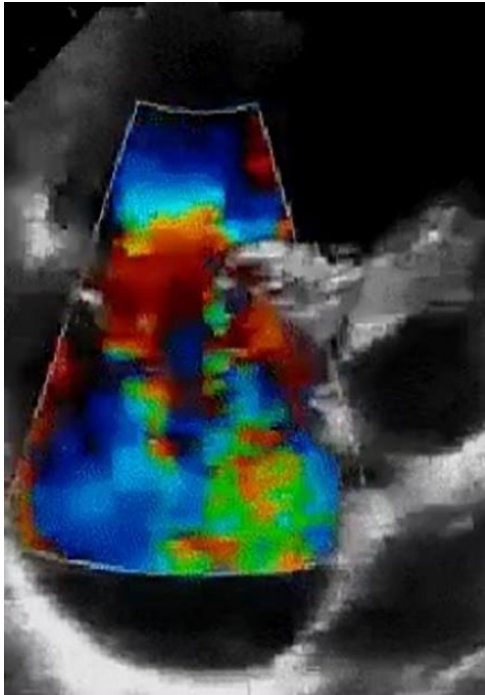


Figure 1.7. Color flow doppler ultrasound of the cardiac apical chamber. Case courtesy of David Carroll, Radiopaedia.org, rID: 64272

When ultrasound waves interact with densities in the body, they reflect back to varying extents which affects the input to the transducer and ultimately the output image. For example, when an ultrasound wave is emitted onto low density structures, such as water, few waves are reflected to the transducer, resulting in a black area on the image known as an anechoic structure. On the other hand, if an ultrasound wave is emitted onto high density structures, such as bone, most waves are reflected to the transducer, resulting in a white area on the image. This relationship is important in interpreting ultrasound images, including understanding artifacts. An ultrasound of the basilic vein is shown on Figure 1.8, which shows blood as hypoechoic relative to other structures in its immediate vicinity. For example, if an ultrasound wave interacts with bone, it is

unlikely to propagate through that material given its high resistance and as such sometimes structures behind bone can appear to be falsely anechoic. This phenomenon is known as acoustic shadowing. The angle of incidence is the angle at which the ultrasound wave approaches a structure of interest, and this can also affect image quality. For optimal ultrasound imaging, the waves that interact with a structure of interest should be perpendicular to the angle of incidence. Otherwise, less waves make it back to the transducer which creates an artifact. Another source of artifact is refraction which occurs when waves traverse through mediums of different densities as this can bend the path of the wave. This can distort the image to varying extents. Yet one other source of artifact is Rayleigh scattering which in the context of human imaging occurs when the output wavelength is larger than the structure of interest. This distorts the image as waves are not appropriately reflected to the transducer and instead undergo elastic scattering, which propagates waves in many directions. There are many other sources of artifacts, but these are some to be aware of. Transducers come in different shapes and sizes, each optimized for visualization of different body structures. Flat linear probes generate high frequency waves which is optimal for superficial imaging. Curvilinear probes generate low frequency waves which is optimal for deep imaging. Phased array probes generate waves from a single point in the probe in multiple directions which is optimal for imaging of structures that may otherwise have a superficial source of acoustic shadowing, such as visualizing structures deep to the ribs.

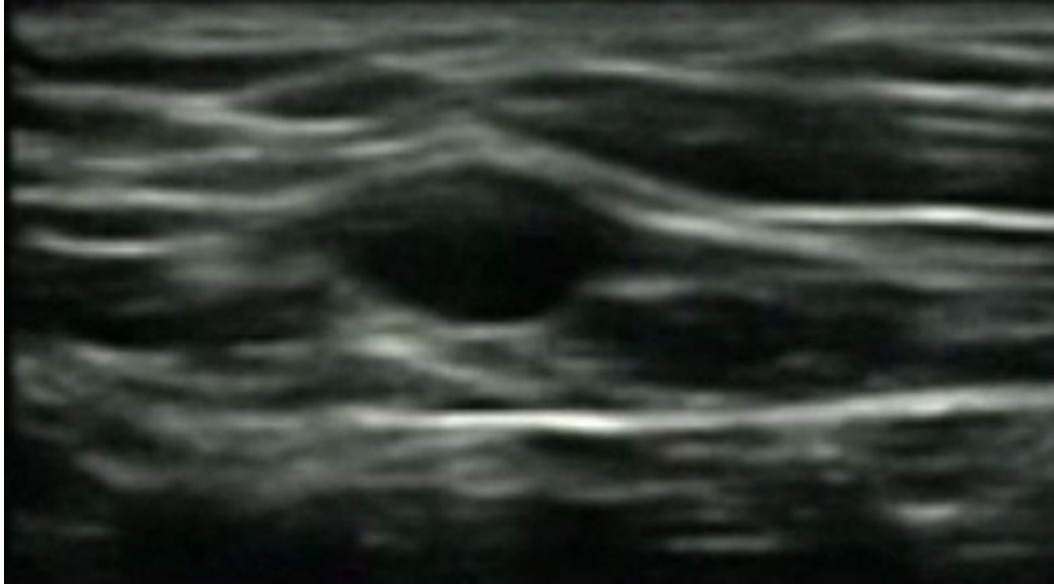


Figure 1.8. Ultrasound of the basilic vein. Case courtesy of David Carroll, Radiopaedia.org, rID: 64446.

Duplex ultrasound aids in the assessment of fluids. The mathematical relationships outlined in Equations 5 through 6 are directly applied to this ultrasound modality as velocity and flow rate are critical parameters that are evaluated within the framework of doppler shifts (Equation 20). Several physical phenomena are relevant to the image output of this modality, including shear rate (Equation 9), Reynolds number (Equation 11), mean transit time (Equation 12), pulse wave velocity (Equation 14), and phase velocity (Equation 16). These factors exert an influence on both velocity and flow rate, which consequently changes the image output. As one example, if Reynolds number is elevated, signifying a high likelihood of turbulent flow, duplex ultrasound may be unable to distinguish between incoming vs outgoing flow. In such a scenario, reflected waves may erroneously be transduced as a distinct color that is typically reserved for turbulent flow. As discussed earlier, duplex ultrasound uses data points from conventional ultrasound and color flow doppler. A third component, spectral doppler analysis, is used in addition to these two

modalities for duplex ultrasound. This technique employs Fourier analysis, which in the context of duplex ultrasound, transforms data given by multiple sound waves from a time domain to a frequency domain. Consequently, a frequency spectrum is produced which can be combined with doppler shifts to achieve a composite output of multiple frequency shifts.

Overall, these calculations for spectral analysis are automated and the output is a two-dimensional graph. Time and frequency are assigned in the x and y axes, respectively, in addition to magnitude that is represented by the waveform's brightness. One example of the output for duplex ultrasound is represented on Figure 1.9 which illustrates a normal popliteal vein on the left and an abnormal popliteal vein on the right. Note the color doppler is superimposed on a conventional ultrasound image, which shows normal unidirectional flow on the left and anomalous flow from reflux on the right. Also note the spectral analysis shows a normal triphasic waveform on the left, characteristic of laminar flow, and contrasts with the spectral analysis on the right that shows abnormal bidirectional flow, characteristic of a disturbed flow pattern.

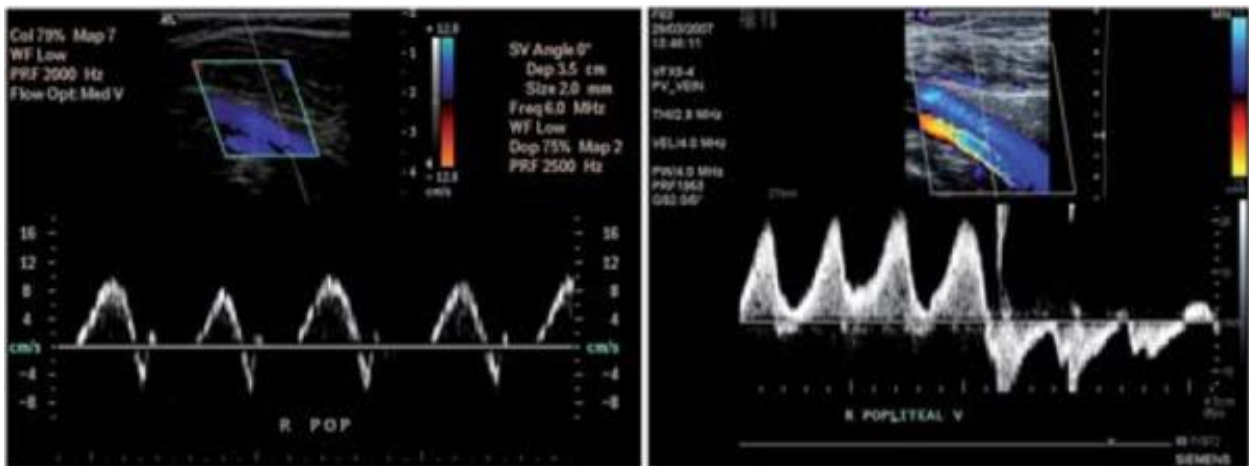


Figure 1.9. Duplex ultrasound of the popliteal vein. Left: Normal popliteal vein. Right:

Incompetent popliteal vein. Acquired from: Necas et al.⁷⁶

From a clinical standpoint, venous duplex ultrasound waveforms are described based on parameters encompassing flow direction, pattern, spontaneity, augmentation, and reflux. It should be noted that these terms are all relative to the vein under assessment and the angle from which it is being assessed. Additionally, it's important to recognize that waveform descriptors are not universal. Presented here is a common depiction of waveform attributes.

The flow direction can be described as antegrade when aligned with the normal course of flow, retrograde when flow is in the opposite direction to what is considered normal, or absent in instances of no flow. Flow patterns can be categorized as respirophasic if flow velocities vary in concordance with the respiratory cycle or diminished if variations in flow velocities are blunted. Flow patterns can be described as pulsatile when flow velocities vary in concordance with the cardiac cycle, continuous if there is an absence of respiratory or cardiac-related flow velocity variations, or regurgitant when flow velocities during the cardiac cycle exhibit heightened amplitudes in both directions relative to pulsatile flow. Spontaneous waveforms occur in veins that exhibit inherent fluid propulsion, absent of purposeful maneuvers to facilitate such movement. Conversely, nonspontaneous waveforms emerge when movement lacks intentional movement of fluids. Augmentation refers to alterations in flow velocity that comes from deliberate maneuvers and can be described as normal, reduced, or absent. Lastly, reflux is the presence of retrograde flow persisting longer than the time required for venous valves to close.

In lower extremity venous doppler ultrasound, continuous waveforms are usually due to a proximal obstruction, while pulsatile waveforms are usually due to increased central venous pressure. Reflux, often attributed to incompetent valves, involves retrograde flow as stated

earlier. This discussion of sound has been systematically structured to build upon foundational physical principles, subsequently applying them to ultrasound modalities. The progression logically introduced various ultrasound modalities, culminating in a discussion of duplex ultrasound – a pivotal imaging technique within the scope of the current study.^{36-37,45,74-77,79}

1.6 Radiation Physics

This research project uses venography, a technique used to evaluate veins using fluoroscopy. This equipment emits radiation by production of X-Rays. Therefore, it is imperative to understand the fundamentals of radiation for the purposes of being knowledgeable of the equipment used as well as patient safety. This section of the chapter starts by discussing basic atomic physics, then focuses on X-Ray phenomena, and concludes on the application of radiation to patient safety and radiation sickness.

Atoms consist of a central nucleus housing nucleons, such as uncharged neutrons and positively charged protons, alongside electrons which are elementary particles that surround the nucleus. The nucleons are composite particles that collectively contribute a net positive charge to the nucleus. Electrons form an electron cloud made of multiple orbitals, which are probability densities where specific electrons positions are likely. Certain elementary particles, such as electrons, have both particle and wave properties. This wave-particle duality can be appreciated by the de Broglie relationship, which states that a particle with a given momentum has a corresponding wavelength. Thus, electrons within orbitals are described by wavefunctions derived from the time-dependent Schrödinger equation. Although the mathematical intricacies of this equation is not pertinent to the current study, it should be noted that three quantum numbers

are required for the computation of these atomic orbitals: principal quantum number n representing electron energy and shell size, angular momentum quantum number l characterizing orbital shapes within subshells, and magnetic quantum number m_l which gives information on the number of orbitals that are allowed in a subshell along with their orientations. In addition to these quantum numbers, the radial contribution and probability function, angular contribution and probability function, and radial and angular nodes are fundamental in calculating atomic orbitals. Radial and angular wavefunctions deliver a more accurate representation of atomic orbitals. Once these orbitals are obtained, electrons can be assigned to them which requires a spin quantum number m_s , and this only has values of $+\frac{1}{2}$ or $-\frac{1}{2}$. The central idea in this brief description of quantum mechanics lies in the probabilistic nature of atomic behavior. This paves the way for nuclear phenomena that may otherwise be unexpected if approached through an absolute perspective rather than this probabilistic framework.

Subatomic particles with the same electrical charge repel per Coulomb repulsion, but the nuclear strong force overcomes this, driving protons and neutrons into close proximity within the nucleus. The relatively larger strength of the nuclear force compared to Coulomb repulsion is pivotal in maintaining atomic stability. In cases of atomic instability, radiation in the form of particles or electromagnetic radiation may be emitted. Unlike mechanical waves such as sound, electromagnetic waves do not require a medium to travel, enabling the transfer of heat via radiation. Each type of radioactive decay has varying degrees of matter penetration, which is important to note in potential radiation exposure situations. The activity of radioactive material a is defined as the number of decays per second and can be calculated as a function of number of

radioactive nuclei N , time t , and decay constant λ which is the probability for each nucleus to decay.

$$-\frac{dN}{dt} = a = a_0 e^{-\lambda t} \quad (21)$$

In turn, λ is given as a function of half-life $t_{1/2}$, total electron energy normalized to the rest mass energy W , and total energy of the transition W_0 .

$$\lambda = \frac{\ln 2}{t_{1/2}} = \int_1^{W_0} N(W) dW \quad (22)$$

In all types of radioactive decay, there are conservation laws that dictate how these processes occur. While not necessary to show their mathematical relations for the purposes of this study, it should be noted that these laws include the conservation of energy, linear momentum, angular momentum, electric charge, and nucleon number. These laws help to conceptualize the behavior of radioactive phenomena.

Alpha decay ejects a high-speed alpha particle, composed of 2 protons and 2 neutrons, from the nucleus as explained by the phenomenon of quantum tunneling. This phenomenon describes how small particles can occasionally pass through an energy barrier due to their quantum properties given a certain transmission probability, even though classical physics would predict that they are unable to do so. During this process, no energy is lost. In the context of alpha decay, alpha particles in the nucleus have less kinetic energy than the potential energy barrier that must be overcome for them to be ejected. Quantum tunneling has also been suggested as a potential explanation for various clinically relevant phenomena, such as potassium ion movement through closed membrane channels in the setting of phantom limb pain. Given its positive charge and

large mass, these alpha particles are unlikely to penetrate relatively thin materials such as paper or skin. However, the kinetic energy emitted has sufficient energy to severely damage organs if the radioactive source is internal to the body. Beta decay involves isobars and can take three forms: beta-minus decay involving electron and electron antineutrino emission, beta-plus decay involving positron and electron neutrino emission, or electron capture involving neutrino formation from the collision of an orbital electron onto a proton in the nucleus. All types of beta decay can penetrate skin, but one can be easily shielded by a layer of clothing, aluminum, or plastic. Gamma decay does not involve the emission of a particle, but rather a gamma ray photon that contains a high amount of energy. This has a relatively small mass with high energy, so it can easily damage body tissues and is difficult to be shielded from, as shielding requires inches of lead or concrete. X-Rays, similar to gamma rays, also give off high energy photons, though they have relatively lower energy. These high-energy photons can be produced via the photoelectric effect, where a photon contacts an electron in the inner shell of an atom, or Compton scattering, where a photon contacts an electron with a lower binding energy in any shell of an atom. Regardless of the mechanism by which a high-energy photon is produced, the momentum of a photon p can be easily calculated given the photon energy E divided by speed of light c or Planck's constant h divided by wavelength λ . It should be noted that mass is not considered in this calculation as photons are one of the two elementary particles that are massless.

$$p = \frac{E}{c} = \frac{h}{\lambda} \quad (23)$$

While X-rays have lower energy photons compared to gamma rays, they can still damage tissue and protective measures, such as lead shielding, are recommended. Figure 1.10 summarizes the

penetrability of different types of ionizing radiation for the purposes of radiation protection as was discussed above.

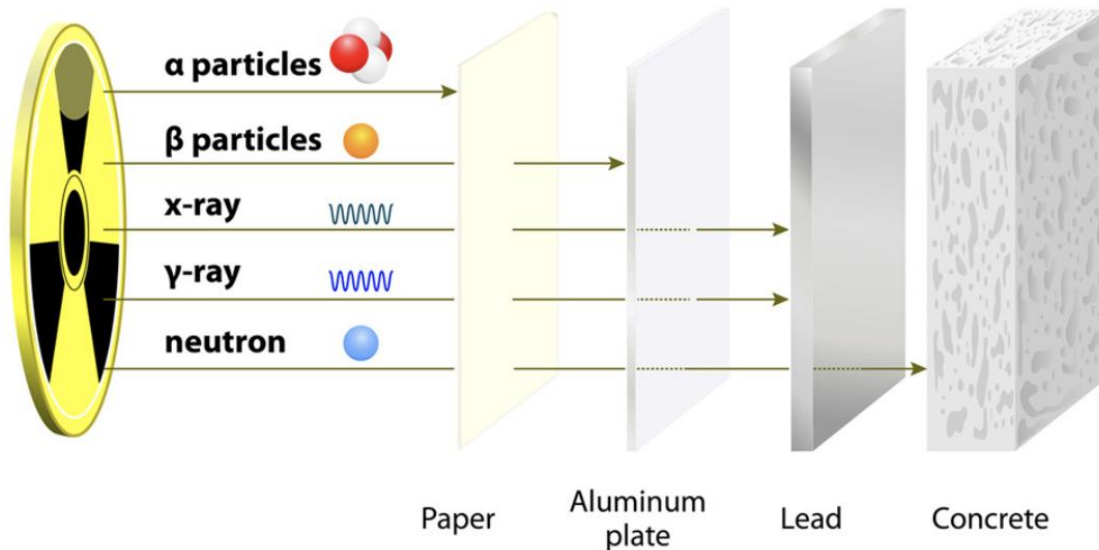


Figure 1.10. Penetrability of types of ionizing radiation. Adapted from Nuclear Safety.⁸⁹ Image accessed on February 7th, 2023.

Fluoroscopy uses X-Rays to image the body in real time as a dynamic video as opposed to a static image such as a Chest X-Ray (CXR), to give one example. Logically, it follows that fluoroscopy exposes the patient and personnel to much greater levels of radiation compared to a CXR. We can quantify the amount of energy delivered to the body as the absorbed dose in Gray (Gy) which is measured in joules per kilogram. It is important to consider the type of radiation when comparing the absorbed dose, as some energies are more damaging than others. For example, 100 Gy from alpha decay would not injure body tissues to nearly the same extent as 100 Gy from gamma decay, assuming an external source. This varying level of potential injury is considered by calculating the equivalent dose rather than the absorbed dose. The equivalent dose is the product of absorbed dose and relative biological effectiveness, which is how efficient a

radioactive source is at damaging the tissue. Additionally, different tissues have varying levels of radiosensitivity. To account for those factors, effective dose E for different tissues T can be calculated as a function of a weighting factor W_T and equivalent dose H_T which can estimate tissue damage from ionizing radiation

$$E = \sum_T W_T H_T \quad (24)$$

We can also calculate the radiative mass stopping power, the energy lost per distance traveled due to collisions with subatomic particles that result in X-Ray emission. While not necessary to show this equation, it should be noted that it is influenced by the energy lost by an electron moving through distance dT/dx given number of nuclei N , energy radiated $h\nu$, and cross section per unit solid angle to emit X Rays $d\sigma_{rad}$

$$\frac{dT}{dx} = N \int_0^T h\nu d\sigma_{rad} \quad (25)$$

Equations 21 through 25 should be appreciated in the context of radiation protection. This information has been fundamental in finding ways to decrease the probability of radiation damage, such as determining the appropriate depth for a protective lead apron during a fluoroscopy procedure.

X-Rays can be produced in an X-Ray tube by heating the cathode, which has a filament similar to that of a light bulb. When the cathode is heated, electrons are released via thermionic emission, though they aggregate at the cathode filament due to electrostatic interactions. Then a high voltage is applied which creates an electric field between the cathode and anode. Given a large enough potential difference between the anode and cathode V_{AC} , electrons are accelerated to the positively charged anode with high kinetic energy. These high energy electrons decelerate

and change direction upon contact with the target atoms. Figure 1.11 shows a typical X-Ray apparatus to visualize the process outlined above.

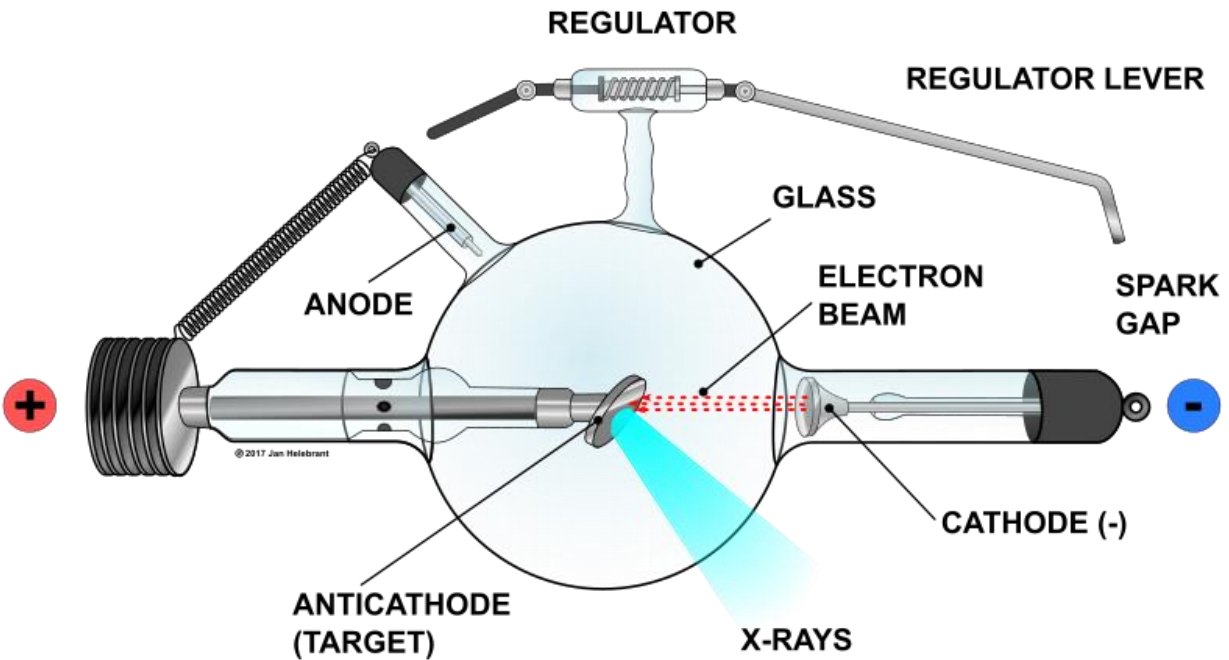


Figure 1.11. Artistic depiction of an X-Ray apparatus. Acquired from Wikimedia commons.⁹³
Image accessed on February 13th, 2023.

High energy electron deceleration and directional change as described above leads to two mechanisms by which X Rays are produced. The first mechanism involves rapid deceleration of electrons approaching target atoms which causes X-Ray photon emission, and that process is termed bremsstrahlung which releases a continuous spectrum of X-Rays. The kinetic energy lost by the electron in this process eV_{AC} can be calculated as a function of the maximum energy of an emitted photon hf_{max} or dividing the product of Planck's constant h and speed of light c by the minimum photon wavelength λ_{min}

$$eV_{AC} = hf_{max} = \frac{hc}{\lambda_{min}} \quad (26)$$

The second mechanism of X Ray production occurs when the high-energy electrons collide with a target atom. This can cause an energy transfer onto an inner shell electron causing it to be ionized, and that process is termed K-shell ionization. Thereafter, another electron from a higher energy level takes the place of the electron that was knocked out, which releases an X-Ray photon in a process called Auger electron emission. The calculation of the energy via this latter mechanism is simply the difference in energy between the initial and final electron orbitals.

As X-Rays travel and interact with the object of interest, they may either penetrate, be scattered, or be absorbed. The beams of photons that penetrate through the object then go onto the detector for the purpose of obtaining an image. The number of photons that penetrate the object is related to the density of the material it interacts with. Low density materials such as water are easily penetrable and are seen as dark areas on the image because a greater number of X-Rays pass through the material and are detected. In contrast, high density materials such as bone are not easily penetrable and are seen as white areas on the image because a greater number of X-Rays are absorbed by the material and are not detected. The benefits of image acquisition using fluoroscopy should be weighed against the risk of carcinogenesis given that X-Rays can either directly damage DNA through energy deposition or indirectly damage DNA by formation of hydroxyl free radicals which then can bombard DNA which disrupt normal DNA replication and repair mechanisms, which can lead to cancer. Other factors to be aware of when assessing the risk of carcinogenesis from radiation in general are DNA repair pathways and if a given molecule has been irradiated in the same location multiple times. Of note, there are also non-carcinogenic risks of X-Ray exposure, such as cataracts or a variety of effects to the skin. Typically, when humans are exposed to radiation, we may categorize the risk as being stochastic

or deterministic. Stochastic effects refer to the increased chance of a mutation occurring as a function of increased radiation exposure over long periods of time. Deterministic effects refer to damage that is done much more acutely by radiation, as may occur in a patient that is exposed to inappropriately high amounts of radiation during fluoroscopy.

Inappropriate radiation exposure is unlikely in the clinical environment given appropriate radiation protection takes place, though it is imperative to recognize patients' clinical presentations given its severity especially when using fluoroscopy. Additionally, the association between amount of radiation exposure and severity of sequelae follows a dose-dependent curve. Acute Radiation Syndrome (ARS) occurs in the setting of a sufficient radiation dose >0.7 Gy with a short time of exposure that originates from an outside source, has sufficient energy to penetrate the skin, and is delivered to a majority of the body. Radiation injury can still occur when only part of these criteria are met, however, patient outcomes are typically not as severe as ARS. This syndrome is progressive in stages. The prodrome typically consists of nausea, vomiting, anorexia, and diarrhea shortly after exposure. Thereafter, for a few hours to weeks the affected patient is asymptomatic. Given the patient meets the criteria for ARS, symptoms will then ensue according to the organ system(s) affected. While ARS can affect any organ system, there are three in particular that warrant discussion given their lethality. Irradiated bone marrow, which occurs at doses as low as 0.7 Gy, may induce pancytopenia which can lead to death secondary to an infectious agent or hemorrhage. Irradiated gastrointestinal tissue, which occurs at doses as low as 6 Gy, may induce pathological changes that lead to dehydration, electrolyte derangements, and infection which usually leads to death. Irradiated cardiovascular or central nervous syndrome, which occurs at doses as low as 12 Gy, leads to near certain death given

elevated intracranial pressure and vascular collapse. Cutaneous radiation syndrome may occur when the source of radiation is penetrative as is the case with ARS, though other particles or photons that do not penetrate the skin such as X-Rays can give rise to this syndrome as well. Usually, the clinical manifestation is stage dependent as is the case for ARS. Here, pruritic erythema is followed by desquamation and epilation, then blisters or ulceration, and finally healing which may take a long period of time. Permanent damage to tissue is possible, with a clinical presentation that is variable. As one example, if sudoriferous glands are affected, hypohidrosis or anhidrosis can occur. If either radiation syndrome is suspected, the clinician should follow general protection and decontamination guidelines. Decreasing absolute lymphocyte count with repeated complete blood counts should be monitored every 4-6 hours for a few days and the severity can be projected using the Andrews Lymphocyte Nomogram. Treatment is largely supportive and stage-dependent with consideration of infection prophylaxis, hematopoietic stimulation, and thrombocyte transfusions.^{37,39,42,44,46-47,49-50,52-53,94}

With this understanding of the physical principles that underlie ultrasound and fluoroscopy as well as their clinical applications, we continue our discussion of MTS.

1.7 MTS Management

The acute management of MTS with a DVT previously included open surgical thrombectomy, though research has shown that catheter-directed thrombolysis followed by placement of an endovascular stent is currently the preferred treatment of choice as the literature has demonstrated greater morbidity and poor surgical outcomes with the former treatment when compared to the latter. As with all clinical decisions, this is not an absolute preference as

individual patient risk factors may make open surgical thrombectomy more appropriate. After acute management, anticoagulation should be initiated. The current body of literature is mixed on the best anticoagulant for patients with MTS and many agents have been approved and recommended for use by different societies. As such, it is imperative to consider individual patient risk factors and medication interactions when prescribing the best anticoagulant for the individual patient. Nevertheless, the clinician may consider rivaroxaban over warfarin given noninferiority of hypercoagulable events and less drug-drug interactions for rivaroxaban. Current research has shown that the recommended management for patients with MTS and an iliofemoral DVT is a combination of catheter-directed thrombolysis and anticoagulation. Figure 1.12 shows pharmacomechanical catheter-directed thrombolysis of a DVT that encompasses the left popliteal vein to the common iliac vein. ^{9,14-17,21-23,103}

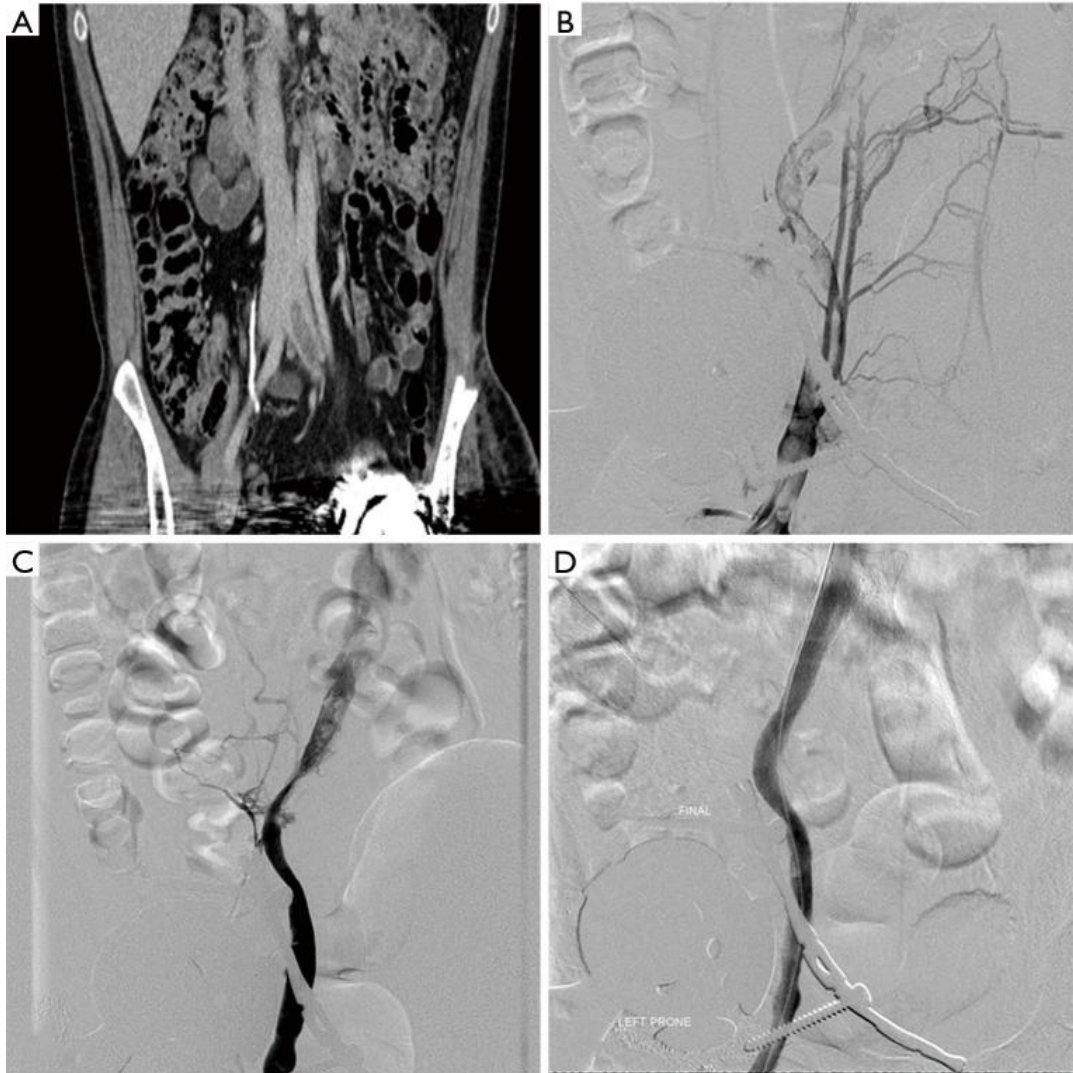


Figure 1.12 A) CT Abdomen and Pelvis demonstrating a portion of the DVT. B) Thrombolysis after placement of a temporary IVC filter. C,D) Mechanical thrombectomy followed by balloon angioplasty and stent deployment.

1.8 Rationale

Unfortunately, it is not uncommon for patients with MTS to present with lower extremity pain and edema, venous stasis dermatitis, and venous hypertension followed by a normal duplex ultrasound study. However, one study brought to attention the possibility of using duplex

ultrasound to detect MTS at an earlier stage of disease if attention is given to particular components of this imaging modality. In one study³⁵, 38 patients were identified as possibly having an MTS diagnosis due to unexplained lower extremity edema and pain who also have a normal duplex ultrasound study. Duplex ultrasound at the common femoral vein showed venous reflux in 34 of these patients, and arterial pulsatility in venous flow signals in 33 of these patients. Those patients then underwent venography and IVUS and it was found that 36 of 38 patients had pelvic vein compression syndrome. After appropriate intervention, 37 of the 38 patients showed initial improvement in lower extremity edema and pain. This study showed that the use of refined ultrasound findings may show promise in the creation of a more accurate diagnostic profile, which may allow for earlier detection of MTS.

There is variation in the definition of MTS according to sites of compression. Classical MTS only accounts for compression of the left common iliac vein, and there are a variety of ways to define modern MTS that includes other sites of compression. For that reason, the aim of this research project is to identify duplex ultrasound and venography imaging findings that may allow for earlier detection of MTS or other venous compression syndromes of the pelvic veins. This is a retrospective study that uses prospective data, as patients are first identified as having MTS or other pelvic vein compression using IVUS. Then ultrasound and venography datapoints prior to the use of IVUS is collected. The scope of this project includes imaging findings for pelvic vein compression syndromes and for patients in the Dallas-Fort Worth metroplex, as that is the patient population used in this study. Earlier detection of MTS or pelvic vein compression syndromes would likely lead to better clinical outcomes as appropriate treatment that addresses the underlying cause of disease could be achieved at an earlier stage. Additionally, earlier

detection would likely lower healthcare expenditures of CVD as less imaging would be required to arrive at the correct diagnosis. It is also possible that these research findings may be used to investigate optimal non-invasive imaging modalities for venous compression syndromes outside of the pelvic veins. Addressing the current shortage of research in this area has lasting clinical and economic implications.

The introduction chapter presents the background and context of this research project. It includes the history, physical basis, and modern context of MTS. The research aims and objectives are clearly defined, and the significance of this project has been discussed. The materials and methods chapter provides a detailed account of the research philosophy, design, and methodology used in this study. That chapter also includes information on data on statistical analyses and methodological limitations. The results chapter presents the data explicitly. The discussion and innovation chapter interprets the data in the context of existing literature within the overall limitations of this study. The final analysis chapter summarizes major findings, emphasizes their implications, and suggests logical areas for future research to further the overall understand of the diagnostics for MTS.

CHAPTER 2

MATERIALS AND METHODS

This study aims to identify duplex ultrasound and venography imaging findings that may allow for earlier detection of MTS or other pelvic vein compression syndromes. This chapter describes the research philosophy, research design, methodology, and statistical analyses in detail.

Thereafter, the methodological limitations are discussed.

2.1 Research Philosophy

The collected, retrieved, and analyzed data originates from electronic medical records and imaging reports, containing predominantly quantifiable variables. Variables that are not quantifiable are accurately categorized into distinct groups. This data is then interpreted with statistical analysis to determine its significance and the extent of its generalizability. The anticipated outcome is consistency of results, independent of the investigator, driven by the objectivity of the data which is regarded as a universal truth lacking subjective interpretation. This epistemological constitutes a foundational philosophical underpinning, shaping the assumptions guiding this study. Its significance is rooted in distinguishing the discoveries of this endeavor as empirical in nature, which is in contrast to more subjective-driven forms of knowledge. Simultaneously, this study does not intend on generating theoretical knowledge as its focus doesn't encompass extrapolating empirical relationships to unveil underlying phenomena. While empirical and theoretical frameworks are interrelated, this distinction is necessary to address the philosophical goals of this study. Each patient mandates analysis tailored to specific

findings of interest, rather than pursuing an all-encompassing analysis. Therefore, this study is constructed in a manner that generates knowledge using logical positivism.

The Combs et al.³⁵ investigation involved 38 patients and suggested that specific ultrasound findings may be used to detect MTS. This study builds on the premise of that investigation and both encompasses a larger patient population and additional imaging modalities and variables. The goal is to ascertain if ultrasound or venography can effectively identify not only MTS, but also other pelvic vein compression syndromes. Therefore, the study is guided by the framework of inductive generalization.

The fundamental principles of modern scientific cognition are embraced in this study.

Determinism forms the basis for linking causal phenomena to their effects, while accommodating probabilistic outcomes. The principle of correspondence mandates that current discoveries are rooted in preceding scientific knowledge. Complementarity ensures the recognition of interdisciplinary insights, as different fields like physics and medicine converge in this study. Embracing the standards of medical inquiry, a code of professional ethics are followed throughout the study. Universalism prevails, regardless of an investigator's level of experience. Disinterestedness drives the pursuit of truth independent of any potential accolades. Organized skepticism ensures any data acquired upholds validity and accuracy at the highest possible level. The deontological, consequentialist, pragmatic, and empirical perspectives are the basis for the research design and execution of this study. With the intersection of these perspectives, complex biophysical phenomena can be applied to medicine to fulfill the goals of this study. ^{58,59,82,86}

2.2 Research Design

This study identified patients in a non-random manner that presented to the clinical environment with lower extremity pain and edema who were then diagnosed with venous compression, which is defined here as $\geq 50\%$ stenosis on IVUS. This purposive sampling technique is appropriate for this study given that the patients of interest must have venous compression. Then data prior to this diagnosis was abstracted from the electronic medical record (EMR), software for endovascular procedures, and an imaging database. This study began in 2019 and includes patient data ranging from 2015 to 2022. This is because patients were enrolled from 2019 to 2022. Therefore, this is a longitudinal retrospective cohort study that uses prospective data. This study design is appropriate for this study as this allows for an adequate number of patients and therefore an adequate amount of data to answer the questions of interest. Given that this is a type of observational study, no control groups are needed to answer the desired research question. This approach is appropriate for the investigation as the goal is to identify components of duplex ultrasound and venography that may predict the diagnosis of compression on IVUS; there is no independent variable that need be manipulated. With this approach, loss to follow-up and withdrawal from the study are avoided. The four-year period between the diagnosis of venous compression for patients in 2015 and the beginning of this study in 2019 minimizes the cost to undertake a research study and reduces the amount of time required to enroll a large amount of patients. At the same time, the three-year period between the beginning of this study in 2019 and the last patient enrolled in 2022 allows for more patient enrollment. Given the selection criteria of diagnosis with venous compression for patients that presented with lower extremity pain and edema, the results of this study can be generalized to the clinical environment within the context of this patient population.

All patients enrolled presented to the DFW Vascular Group in Dallas, TX with lower extremity pain and edema. This outpatient facility executes high-quality patient care and teaching for vascular surgeries and procedures. High-quality research has been performed there for many years and there is robust support and staff for research activities. All patients enrolled in this study have been evaluated by a vascular surgeon at this facility. As part of the evaluation process, all patients have signed consent forms for both medical management and research. GE-Centricity was used as the EMR to collect and retrieve data for patient demographic and risk factors though during the study the group switched to athenaPractice. Venography and IVUS data was collected and retrieved using Vascunote, a web-based software used to document and code endovascular procedures. Duplex ultrasound data was collected and retrieved using Corelab, a database that stores a variety of imaging modalities. The data is a combination of quantitative and qualitative data. Variables from both types of data were translated into a specific number outlined in Table 1 to allow for appropriate statistical analysis. The collected data was input on a secure excel workbook that is on a remote server throughout the duration of the study.

Given the use of ionizing radiation in this study with venography, radiation safety is of utmost importance for all patients and personnel. The ACR appropriateness criteria was followed, as all patients were imaged initially with duplex ultrasound before imaging using venography.

Venography was performed at the endovascular angiography suite within the facility, and Figure 2.1 below provides an artistic depiction of an angiography suite. The orientation of the C-arm is such that the X-Ray tube is under the patient, the image intensifier is above the patient, and the collimator is as close as possible to the patient to decrease the surface area of radiation outside of

the area of interest while also lowering scatter radiation for both the patient and personnel. All personnel in the suite wear a lead apron and thyroid shield in addition to minimizing close distances to the X-Ray source during its use. The lead apron and thyroid shield are also stored hanging. Ceiling mounted shields are used and rollaway shields are available. The lowest possible exposure to radiation is used both in terms of cumulative dose in Gray (Gy) and dose rate in Gy/minute. These measures reduce, but do not eliminate the probability of carcinogenesis from venography.^{39-43,46,48,56-57,85-86}



Figure 2.1. Artistic depiction of an angiography suite.⁹⁰ Image accessed February 8th 2023.

2.3 Methodology

The vessels of interest for this study overall include the bilateral common femoral veins (CFV), common iliac veins (CIV), external iliac veins (EIV), and internal iliac veins (IIV). The data abstracted from duplex ultrasound reports included the following variables: venous reflux, respiratory variance, flow, compressibility, thrombosis, spontaneity, phasicity, augmentation, competency, and presence of DVT. Duplex ultrasound data was only obtained for the bilateral CFV. The rationale for only using this vessel for duplex ultrasound pertains to its proximity to the pelvis, as it is the most proximal vessel that is easily imaged with this modality. Additionally, there was insufficient data on duplex ultrasound for veins distal to the CFV. The data abstracted from venography included the following variables: compression, vessel patency, and percent stenosis. Venography data was obtained for the bilateral CFV, CIV, EIV, and IIV. The data abstracted from IVUS included the following variables: percent stenosis and presence of DVT. IVUS data was obtained for the bilateral CFV, CIV, EIV, and IIV. There were many patients that had multiple duplex ultrasound, venography, and IVUS studies. Only one of each type of study were used per patient. The first IVUS was identified and the venography and duplex ultrasound results immediately preceding the time of that IVUS study were identified and used in this study. This approach is justified as patients with stenotic segments on IVUS may be treated depending on the severity; post-treatment duplex ultrasound and venography measurements would introduce a significant confounding variable.

The excel workbook used for this study is composed of four spreadsheets. Given that the workbook includes sensitive and identifiable patient data, multiple security measures were implemented. The workbook was stored on a remote server throughout the study that required a

username and password that was generated for the specific research personnel. The workbook also required two strong passwords. Given that there are multiple ongoing research investigations, all research personnel had access to the same remote server. However, only immediate research personnel that needed to access the data for this study were given the two strong passwords for the workbook. The imaging data was input on the first spreadsheet. Each row corresponds to a specific patient identified by the Medical Record Number (MRN) and each imaging variable was input on a different column. Given MRNs are sensitive and identifiable data, once imaging findings were input, random subject ID numbers were generated which replaced the MRN data. For duplex ultrasound in particular, a variable was added and titled “overall”, which indicated whether the ultrasound study was completely normal or if it had any abnormality. No variables in addition to the previous paragraph were added for venography or IVUS. The imaging modalities with the corresponding variables as mentioned previously are on spreadsheet one in the following order: MRN, right duplex ultrasound, right venography, right IVUS, left duplex ultrasound, left venography, and left IVUS. Some variables initially had several outcomes that would make it difficult to find statistical significance given the number of patients. For this reason, some raw outcomes were grouped together into one simplified outcome. The raw outcomes for the corresponding variables were simplified in the following manner: Duplex ultrasound reflux had raw outcomes of yes or no that were simplified into abnormal or normal, respectively. Duplex ultrasound decreased respiratory variance had raw outcomes of yes or no that were simplified into abnormal or normal, respectively. Duplex ultrasound flow had a large number of raw outcomes that were technologist-dependent and as such these were interpreted and thereafter simplified into normal, pulsatile flow, continuous flow, decreased flow, or no flow. Duplex ultrasound compressibility had raw outcomes of normal, reduced, or

absent; these outcomes were not simplified. Duplex ultrasound thrombosis had raw outcomes of normal, acute, chronic, and acute on chronic; outcomes that were not normal were grouped into thrombosis while the outcome, normal was not simplified. Duplex ultrasound spontaneity had raw outcomes normal, reduced, absent, and pulsatile; no outcomes were simplified. Duplex ultrasound phasicity had raw outcomes of normal, reduced, absent, pulsatile, and continuous; no outcomes were simplified. Duplex ultrasound augmentation had raw outcomes of normal, reduced, absent; no outcomes were simplified. Duplex ultrasound competency had raw outcomes of normal, mildly reduced, moderately reduced, severely reduced, or absent. Outcomes that were not normal were grouped into abnormal while the outcome, normal was not simplified. Duplex ultrasound presence of a DVT had raw outcomes of yes or no that were simplified into abnormal or normal, respectively. Of note, variables duplex ultrasound thrombosis and duplex ultrasound DVT differ in that the former is specific to the vessel of interest, while the latter is nonspecific and refers to the entire lower extremity. Venography compression had raw outcomes of yes or no that were simplified into normal or abnormal, respectively. Venography vessel patency had raw outcomes of patent or occluded that were simplified into normal or abnormal, respectively. Venography percent stenosis had raw outcomes ranging from 0% to 100% and were categorized into two groups, one ranging from 0-49.99% and the other for 50-100%. IVUS percent stenosis also had raw outcomes ranging from 0% to 100% and were categorized into two groups, one ranging from 0-49.99% and the other for 50-100%. The limits for these two categories are based on the diagnosis of compression on IVUS if the vessel is at least 50% stenosed. IVUS presence of DVT had raw outcomes of yes or no that were simplified into abnormal or normal, respectively. Below is Table 2.1 with the outcomes for each variable after the outcomes were

simplified. Note that each variable is used twice, once for the left vessels and again for the right vessels. This is outlined in Table 2.1.

Table 2.1: Simplified Outcomes per Imaging Variable

Variable	Outcomes				
Duplex Ultrasound: Reflux	Normal	Abnormal	-	-	-
Duplex Ultrasound: Decreased Respiratory Variance	Normal	Abnormal	-	-	-
Duplex Ultrasound: Flow	Normal	Pulsatile Flow	Continuous Flow	Decreased Flow	No Flow
Duplex Ultrasound: Compressibility	Normal	Reduced	Absent	-	-
Duplex Ultrasound: Thrombosis	Normal	Thrombosis	-	-	-
Duplex Ultrasound: Spontaneity	Normal	Reduced	Absent	Pulsatile	-
Duplex Ultrasound: Phasicity	Normal	Reduced	Absent	Pulsatile	Continuous
Duplex Ultrasound: Augmentation	Normal	Reduced	Absent	-	-
Duplex Ultrasound: Competency	Normal	Reduced	-	-	-
Duplex Ultrasound: Overall	Normal	Abnormal	-	-	-
Duplex Ultrasound: Presence of DVT	Normal	Abnormal	-	-	-
Venography: Compression	Normal	Abnormal	-	-	-
Venography: Vessel Patency	Normal	Abnormal	-	-	-
Venography: Percent Stenosis	0 – 49.99%	50-100%	-	-	-
IVUS: Percent Stenosis	0 – 49.99%	50-100%	-	-	-
IVUS: Presence of DVT	Normal	Abnormal	-	-	-

After data entry with the above simplified outcomes, the outcomes for each variable were transcribed into numbers to allow for optimal statistical analysis in the following manner: “normal” was transcribed into “1”, “abnormal” was transcribed into “2”, “pulsatile flow” was transcribed into “3”, “continuous flow” was transcribed into “4”, “decreased flow” was transcribed into “5”, “no flow” was transcribed into “6”, “reduced” was transcribed into “7”, “absent” was transcribed into “8”, “thrombosis” was transcribed into “9”, “pulsatile” was transcribed into “10”, “continuous” was transcribed into “11”, percent stenosis ranging from 0 – 49.99% on either venography or IVUS was transcribed into “12”, and percent stenosis ranging

from 50 – 100% on either venography or IVUS was transcribed into “13”. This is outlined in Table 2.2.

Table 2.2: Outcomes per Imaging Variable After Transcription

Variable	Outcomes				
Duplex Ultrasound: Reflux	1	2	-	-	-
Duplex Ultrasound: Decreased Respiratory Variance	1	2	-	-	-
Duplex Ultrasound: Flow	1	3	4	5	6
Duplex Ultrasound: Compressibility	1	7	8	-	-
Duplex Ultrasound: Thrombosis	1	9	-	-	-
Duplex Ultrasound: Spontaneity	1	7	8	10	-
Duplex Ultrasound: Phasicity	1	7	8	10	11
Duplex Ultrasound: Augmentation	1	7	8	-	-
Duplex Ultrasound: Competency	1	7	-	-	-
Duplex Ultrasound: Overall	1	2	-	-	-
Duplex Ultrasound: Presence of DVT	1	2	-	-	-
Venography: Compression	1	2	-	-	-
Venography: Vessel Patency	1	2	-	-	-
Venography: Percent Stenosis	12	13	-	-	-
IVUS: Percent Stenosis	12	13	-	-	-
IVUS: Presence of DVT	1	2	-	-	-

During transcription of the simplified outcomes to numbers, care was taken to ensure that every outcome was accurately transcribed by making a pre-transcription copy of this spreadsheet and comparing it to the post-transcription version of the spreadsheet. The second spreadsheet contained all ICD-10 codes for each patient and the corresponding diagnoses. The third spreadsheet contained every patient MRN, date of birth (dob), age, and sex. The fourth spreadsheet contained every patient MRN, age, sex, and all risk factors of interest. As stated previously, MRNs were replaced with a random subject ID number given this is sensitive identifiable data. Additionally, the dob column was eliminated once patient ages were calculated from the date of birth data given that dob is sensitive identifiable data. Age and sex were necessary sensitive data to retain on the workbook to analyze age and sex data. This analysis is necessary to ensure a balanced patient population in terms of their age and sex. The risk factors of interest include: Unspecified obesity, Morbid obesity due to excess calories, Type 2 Diabetes

Mellitus (T2DM) with unspecified complications, T2DM without complications, DVT, Acute venous embolism, chronic embolism, hyperlipidemia, Essential hypertension (HTN), cardiac arrhythmias, atherosclerosis, phlebitis/thrombophlebitis, varicose veins, chronic venous HTN, localized edema, long term use anticoagulants, personal history of pulmonary embolism (PE), personal history of transient ischemic attack (TIA), presence of cardiac pacemaker, compression of vein, and chronic venous insufficiency. The outcomes for each risk factor were transcribed into one of two numbers for data analysis: “normal”, indicating the absence of the risk factor, was transcribed into “1” whereas “abnormal”, indicating the presence of the risk factor, was transcribed into “2”. Just as with the first spreadsheet, to ensure accurate transcription of simplified outcomes to numbers, pre-transcriptional and post-transcriptional versions of this spreadsheet were compared.

2.4 Statistical Analysis

The descriptive data for patient demographics, patient risk factors, duplex ultrasound, venography, and IVUS was acquired using Microsoft Excel after the MRNs were replaced with a random subject ID number and dob was eliminated to minimize the risk of identifiable and sensitive data exposure. Given that most variables are categorical, computations were performed to obtain the frequency, relative frequency, and proportion of all risk factors as well as all imaging findings per variable of interest. The statistical measures for age that were calculated include mean, median, SD, minimum, maximum, IQR, skewness, kurtosis, and standard error. Sex-adjusted data for these statistical measures were also computed.

The inferential data for duplex ultrasound, venography, and IVUS were analyzed using logistic regression on the R statistical software. This software was used as it is a well-known, powerful statistical tool. It also has a constantly growing library of packages that make statistical analyses more feasible for the specific research questions given that it is an open-source tool. Logistic regression analysis is justified as much of the data is qualitative, and the data that is quantitative was simplified into qualitative data by means of categorization for the purposes of statistical analysis. Therefore, this is an analysis of categorical data. Additionally, much of the data on analysis is binary and in all analyses one variable is fixed. Linear regression was not performed given the absence of continuous data. Chi-squared tests were not performed as some data was transformed into categories, which caused a loss of information. Fisher exact test would also be inappropriate for this same reason, and in addition the sample size would have led to suboptimal results. Nonparametric tests were not performed as the absence of ranked variables disqualified the use of Spearman correlation coefficient, absence of ordinal variables disqualified the use of Mann-Whitney U or Kruskal-Wallis H tests, and the absence of rank sum and signed rank disqualified the use of the Wilcoxon test. The absence of means for all imaging variables of interest excluded the use of T-tests and ANOVAs. The criteria to reject the null hypotheses was set to an alpha level of $p < 0.05$. It should be noted that since the vessels of interest are bilateral, statistical tests were performed on the ipsilateral vessel to eliminate the possibility of data from one vessel from affecting data on the contralateral vessel.

More specifically, the following analyses using logistic regression were performed: duplex ultrasound CFV compressibility to venography percent stenosis, duplex ultrasound CFV thrombosis to venography percent stenosis, duplex ultrasound CFV spontaneity to venography

percent stenosis, duplex ultrasound CFV reflux to IVUS percent stenosis, duplex ultrasound CFV ultrasound pulsatile flow to IVUS percent stenosis, duplex ultrasound CFV ultrasound continuous flow to IVUS percent stenosis, duplex ultrasound CFV ultrasound decreased flow to IVUS percent stenosis, duplex ultrasound CFV ultrasound no flow to IVUS percent stenosis, duplex ultrasound CFV competency to IVUS percent stenosis, duplex ultrasound CFV spontaneity to IVUS percent stenosis, duplex ultrasound CFV phasicity to IVUS percent stenosis, and venography compression to IVUS percent stenosis.^{56-57,61-63,83-85,87}

2.5 Methodological Limitations

This study design is primarily retrospective, and this is a single center study in the Dallas-Fort Worth metroplex. Therefore, selection bias is likely with these parameters and the generalizability is currently limited to patients in this specific population. The imaging reports that contain the data of interest were not designed for a research study as it is part of the medical record, so there may be confounding factors that were not taken into account. While many risk factors as potential confounders are taken into account, by the nature of this project being primarily retrospective, it is possible that there are other confounders that were not taken into account during the design of the study. Time constraints were minimized as patient data spans seven years and this study took place over three years. However, since this study has a hard deadline, time was still a limiting factor in patient enrollment. It is possible that with more patient enrollment, the number of statistically significant findings may change. Ultrasound is an imaging modality that is highly dependent on the skills and experiences of the technologist. Although all vascular ultrasound technologists involved in this study are adequately trained to provide high-quality images, it is possible that suboptimal inter-rater reliability may skew the

data. Not all patients had data from all three imaging modalities of interest, which may skew results, though to minimize this effect patients who did not have data for the imaging modalities of interest were excluded. Within all variables pertaining to the imaging modalities, not every datapoint of interest was documented which is expected given that this study partially uses retrospective data that was already collected before the start of the study. Given that this is a quantitative study that sorts this data into many variables, it is possible that the conclusion is oversimplified.⁵⁶⁻⁵⁷

CHAPTER 3

RESULTS

The variables of interest used in each imaging modality were analyzed as described in the previous chapter. This chapter begins by presenting the descriptive statistics for demographic and imaging data to understand the compositions thereof. Subsequently, the inferential statistics relating to the hypotheses are provided.

3.1 Descriptive Statistics

A total of 237 patients were used for this study with 98 (41%) being male and 139 (59%) being female. The age data for all patients in this study include a mean of 65.9 years, median of 68.0 years, standard deviation (SD) of 14.4 years, minimum of 27 years, maximum of 95 years, interquartile range (IQR) of 20.0, skewness of -0.408, kurtosis of -0.402, and standard error (SE) of 0.937. The age data for male patients in this study include a mean of 66.6 years, median of 67.0 years, SD of 13.2, minimum of 30, maximum of 92, skewness of -0.271, kurtosis of -0.253, and SE of 1.337. The age data for female patients in this study include a mean of 65.2 years, median of 68.0 years, SD of 15.2, minimum of 27, maximum of 95, skewness of -0.449, kurtosis of -0.539, and SE of 1.291. These statistical measures of age are summarized in Table 3.1.

Table 3.1: Statistical Measures of Age

Statistical Measures	All Patients	Male	Female
Mean	65.9	66.6	65.2
Median	68.0	67.0	68.0
SD	14.4	13.2	15.2
Minimum	27	30	27
Maximum	95	92	95
IQR	20.0	-	-
Skewness	-0.408	-0.271	-0.449
Kurtosis	-0.402	-0.253	-0.539
SE	0.937	1.337	1.291

The statistical measures of age when comparing males and females as listed in Table 3.1 show absolute differences of: means = 1.4, median = 1.0, SD = 2.0, minimum = 3, maximum = 3, skewness = 0.178, kurtosis = 0.286, and SE = 0.046.

The risk factors data for all patients are given as the sample size and relative frequency converted into a percentage: Unspecified obesity (n=33, 14%), Morbid obesity due to excess calories (n=8, 3%), T2DM with unspecified complications (n=3, 1%), T2DM without complications (n=54, 23%), DVT (n=2, 1%), Acute venous embolism (n=10, 4%), chronic embolism (n=66, 28%), hyperlipidemia (n=67, 29%), Essential HTN (n=137, 59%), cardiac arrhythmias (n=2, 1%), atherosclerosis (n=20, 9%), phlebitis/thrombophlebitis (n=30, 13%), varicose veins (n=44, 19%), chronic venous HTN (n=59, 25%), localized edema (n=9, 4%), long term use anticoagulants (n=9, 4%), personal history of PE (n=8, 3%), personal history of TIA (n=2, 1%), presence of cardiac pacemaker (n=13, 6%), compression of vein (n=175, 75%), and chronic venous insufficiency (n=39, 17%). The risk factors data for male patients are given as the sample size and relative frequency converted into a percentage: Unspecified obesity (n=10, 4%), Morbid obesity due to excess calories (n=4, 2%), T2DM with unspecified complications (n=2, 1%), T2DM without complications (n=20, 9%), DVT (n=1, 1%), Acute venous embolism (n=7, 3%),

chronic embolism (n=35, 15%), hyperlipidemia (n=26, 11%), Essential HTN (n=61, 26%), cardiac arrhythmias (n=0, 0%), atherosclerosis (n=8, 3%), phlebitis/thrombophlebitis (n=12, 5%), varicose veins (n=21, 9%), chronic venous HTN (n=23, 10%), localized edema (n=0, 0%), long term use anticoagulants (n=4, 2%), personal history of PE (n=5, 2%), personal history of TIA (n=1, 1%), presence of cardiac pacemaker (n=6, 3%), compression of vein (n=73, 31%), and chronic venous insufficiency (n=13, 6%). The risk factors data for female patients are given as the sample size and relative frequency converted into a percentage: Unspecified obesity (n=23, 10%), Morbid obesity due to excess calories (n=4, 2%), T2DM with unspecified complications (n=1, 1%), T2DM without complications (n=34, 15%), DVT (n=1, 1%), Acute venous embolism (n=3, 1%), chronic embolism (n=31, 13%), hyperlipidemia (n=41, 18%), Essential HTN (n=76, 32%), cardiac arrhythmias (n=2, 1%), atherosclerosis (n=12, 5%), phlebitis/thrombophlebitis (n=18, 8%), varicose veins (n=23, 10%), chronic venous HTN (n=36, 15%), localized edema (n=9, 4%), long term use anticoagulants (n=5, 2%), personal history of PE (n=3, 1%), personal history of TIA (n=1, 1%), presence of cardiac pacemaker (n=7, 3%), compression of vein (n=102, 44%), and chronic venous insufficiency (n=26, 11%). The ratio of males with the risk factor to females with the risk factor is as follows: Unspecified Obesity = 0.44, Morbid Obesity = 1.00, T2DM with unspecified complications = 2.00, T2DM without complications = 0.59, DVT = 1.00, Acute Venous Embolism = 2.33, Chronic Embolism = 1.13, Hyperlipidemia = 0.63, Essential HTN = 0.80, Cardiac Arrhythmias = 0.00, Atherosclerosis = 0.67, Phlebitis/Thrombophlebitis = 0.67, Varicose Veins = 0.91, Chronic Venous HTN = 0.64, Localized Edema = 0.00, Long Term Use Anticoagulants = 0.80, Personal History of PE = 1.67, Personal History of TIA = 1.00, Presence of Cardiac Pacemaker = 0.86, Compression of Vein = 0.72, Chronic Venous Insufficiency = 0.50. The ratio of females with the risk factor to males

with the risk factor is as follows: Unspecified Obesity = 2.30, Morbid Obesity = 1.00, T2DM with unspecified complications = 0.50, T2DM without complications = 1.70, DVT = 1.00, Acute Venous Embolism = 0.43, Chronic Embolism = 0.89, Hyperlipidemia = 1.58, Essential HTN = 1.25, Cardiac Arrhythmias = 0.00, Atherosclerosis = 1.50, Phlebitis/Thrombophlebitis = 1.50, Varicose Veins = 1.10, Chronic Venous HTN = 1.57, Localized Edema = 0.00, Long Term Use Anticoagulants = 1.25, Personal History of PE = 0.60, Personal History of TIA = 1.00, Presence of Cardiac Pacemaker = 1.17, Compression of Vein = 1.40, Chronic Venous Insufficiency = 2.00. These risk factors are summarized in Table 3.2 as the sample size and relative frequency in parenthesis.

Table 3.2: Risk Factors

Risk Factors	All Patients	Male	Female
Unspecified Obesity	33 (0.14)	10 (0.04)	23 (0.10)
Morbid Obesity	8 (0.03)	4 (0.02)	4 (0.02)
T2DM with unspecified complications	3 (0.01)	2 (0.01)	1 (0.01)
T2DM without complications	54 (0.23)	20 (0.09)	34 (0.15)
DVT	2 (0.01)	1 (0.01)	1 (0.01)
Acute Venous Embolism	10 (0.04)	7 (0.03)	3 (0.01)
Chronic Embolism	66 (0.28)	35 (0.15)	31 (0.13)
Hyperlipidemia	67 (0.29)	26 (0.11)	41 (0.18)
Essential HTN	137 (0.59)	61 (0.26)	76 (0.32)
Cardiac Arrhythmias	2 (0.01)	0 (0.00)	2 (0.01)
Atherosclerosis	20 (0.09)	8 (0.03)	12 (0.05)
Phlebitis/Thrombophlebitis	30 (0.13)	12 (0.05)	18 (0.08)
Varicose Veins	44 (0.19)	21 (0.09)	23 (0.10)
Chronic Venous HTN	59 (0.25)	23 (0.10)	36 (0.15)
Localized Edema	9 (0.04)	0 (0.00)	9 (0.04)
Long Term Use Anticoagulants	9 (0.04)	4 (0.02)	5 (0.02)
Personal History of PE	8 (0.03)	5 (0.02)	3 (0.01)
Personal History of TIA	2 (0.01)	1 (0.01)	1 (0.01)
Presence of Cardiac Pacemaker	13 (0.06)	6 (0.03)	7 (0.03)
Compression of Vein	175 (0.75)	73 (0.31)	102 (0.44)
Chronic Venous Insufficiency	39 (0.17)	13 (0.06)	26 (0.11)

The risk factors shown in Table 3.2 indicate that for the 237 patients in this study, there is a relative frequency >0.50 for essential HTN and vein compression. The presence of the following

risk factors with a relative frequency between 0.20 and 0.50 should be noted: T2DM without complications, chronic embolism, hyperlipidemia, and chronic venous HTN. The ratio of the presence of a given risk factor for males to females is ≥ 2 for T2DM with unspecified complications and acute venous embolism. The ratio of the presence of a given risk factor x for males to females is $2 > x > 1$ for chronic embolism and personal history of PE. The ratio of the presence of a given risk factor for females to males is ≥ 2 for unspecified obesity and chronic venous insufficiency. The ratio of the presence of a given risk factor for females to males is $2 > x > 1$ for T2DM without complications, hyperlipidemia, essential HTN, atherosclerosis, phlebitis/thrombophlebitis, varicose veins, chronic venous HTN, long term use anticoagulants, presence of cardiac pacemaker, and compression of vein. Summation of all risk factors for males is 332 and summation of all risk factors for females is 458. Altogether, there are a total of 790 risk factors in the patients for this study.

The statistical measures of each imaging finding below are given as the frequency followed by the proportion as a percentage and relative frequency as a decimal in parenthesis.

Right Duplex Ultrasound CFV Reflux: normal = 155 (71.4%, 0.65) and abnormal = 62 (28.6%, 0.26). Right Duplex Ultrasound CFV Decreased Respiratory Variance: normal = 49 (80.3%, 0.21) and abnormal = 12 (19.7%, 0.05). Right Duplex Ultrasound CFV Compressibility: normal = 203 (94.9%, 0.86), reduced = 9 (4.2%, 0.04), absent = 2 (0.9%, 0.01). Right Duplex Ultrasound CFV Thrombosis: normal = 202 (94.4%, 0.85), thrombosis = 12 (5.6%, 0.05). Right Duplex Ultrasound CFV Spontaneity: normal = 164 (76.6%, 0.69), reduced = 46 (21.5%, 0.19), absent = 3 (1.4%, 0.01), pulsatile = 1 (0.4%, 0.01). Right Duplex Ultrasound CFV Phasicity:

normal = 122 (57.0%, 0.51), reduced = 13 (6.1%, 0.05), absent = 2 (0.9%, 0.01), pulsatile = 52 (24.3%, 0.22), continuous = 25 (11.7%, 0.11). Right Duplex Ultrasound CFV Augmentation: normal = 209 (98.1%, 0.88), reduced = 3 (1.4%, 0.01), absent = 1 (0.4%, 0.01). Right Duplex Ultrasound CFV Competency: normal = 150 (70.4%, 0.63), reduced = 63 (29.6%, 0.27). Right Duplex Ultrasound CFV Overall: normal = 92 (43.0%, 0.39), abnormal = 122 (57.0%, 0.51). Right Duplex Ultrasound DVT: normal = 140 (67.3%, 0.59), abnormal = 68 (32.7%, 0.29). Left Duplex Ultrasound CFV Reflux: normal = 151 (70.6%, 0.64), abnormal = 63 (29.4%, 0.27). Left Duplex Ultrasound CFV Decreased Respiratory Variance: normal = 44 (75.9%, 0.186), abnormal = 14 (24.1%, 0.06). Left Duplex Ultrasound CFV Compressibility: normal = 201 (93.5%, 0.84), reduced = 13 (6.0%, 0.05), absent = 1 (0.5%, 0.01). Left Duplex Ultrasound CFV Thrombosis: normal = 200 (92.6%, 0.84), thrombosis = 16 (7.4%, 0.07). Left Duplex Ultrasound CFV Spontaneity: normal = 160 (74.1%, 0.68), reduced = 50 (23.1%, 0.21), absent = 4 (1.8%, 0.02), pulsatile = 2 (0.9%, 0.01). Left Duplex Ultrasound CFV Phasicity: normal = 114 (52.8%, 0.48), reduced = 15 (6.9%, 0.06), absent = 1 (0.5%, 0.01), pulsatile = 57 (26.4%, 0.24), continuous = 29 (13.4%, 0.12). Left Duplex Ultrasound CFV Augmentation: normal = 207 (96.3%, 0.87), reduced = 6 (2.8%, 0.03), absent = 2 (0.9%, 0.01). Left Duplex Ultrasound CFV Competency: normal = 152 (70.7%, 0.64), reduced = 62 (28.8%, 0.26), absent = 1 (0.4%, 0.01). Left Duplex Ultrasound CFV Overall: normal = 88 (40.7%, 0.37), abnormal = 128 (59.3%, 0.54). Left Duplex Ultrasound DVT: normal = 131 (60.9%, 0.55), abnormal = 84 (39.1%, 0.35). These imaging findings for duplex US without consideration for the variable of flow are outlined in Table 3.3 as the sample size and relative frequency in parenthesis.

Table 3.3: Imaging Findings for Duplex US Without Flow

Imaging Finding	Normal	Abnormal	Reduced	Absent	Thrombosis	Pulsatile	Continuous
Right Duplex US CFV Reflux	155 (0.65)	62 (0.26)	-	-	-	-	-
Right Duplex US CFV Decreased Respiratory Variance	49 (0.21)	12 (0.05)	-	-	-	-	-
Right Duplex US CFV Compressibility	203 (0.86)	-	9 (0.04)	2 (0.01)	-	-	-
Right Duplex US CFV Thrombosis	202 (0.85)	-	-	-	12 (0.05)	-	-
Right Duplex US CFV Spontaneity	164 (0.69)	-	46 (0.19)	3 (0.01)	-	1 (0.01)	-
Right Duplex US CFV Phasicity	122 (0.51)	-	13 (0.05)	2 (0.01)	-	52 (0.22)	25 (0.11)
Right Duplex US CFV Augmentation	209 (0.88)	-	3 (0.01)	1 (0.01)	-	-	-
Right Duplex US CFV Competency	150 (0.63)	-	63 (0.27)	-	-	-	-
Right Duplex US CFV Overall	92 (0.39)	122 (0.51)	-	-	-	-	-
Right Duplex US CFV DVT	140 (0.59)	68 (0.29)	-	-	-	-	-
Left Duplex US CFV Reflux	151 (0.64)	63 (0.27)	-	-	-	-	-
Left Duplex US CFV Decreased Respiratory Variance	44 (0.19)	14 (0.06)	-	-	-	-	-
Left Duplex US CFV Compressibility	201 (0.84)	-	13 (0.05)	1 (0.01)	-	-	-
Left Duplex US CFV Thrombosis	200 (0.84)	-	-	-	16 (0.07)	-	-
Left Duplex US CFV Spontaneity	160 (0.68)	-	50 (0.21)	4 (0.02)	-	2 (0.01)	-
Left Duplex US CFV Phasicity	114 (0.48)	-	15 (0.06)	1 (0.01)	-	57 (0.24)	29 (0.12)
Left Duplex US CFV Augmentation	207 (0.87)	-	6 (0.03)	2 (0.01)	-	-	-
Left Duplex US CFV Competency	152 (0.64)	-	62 (0.26)	1 (0.01)	-	-	-
Left Duplex US CFV Overall	88 (0.37)	128 (0.54)	-	-	-	-	-
Left Duplex US CFV DVT	131 (0.55)	84 (0.35)	-	-	-	-	-

The imaging findings in Table 3.3 indicate that most variables have normal relative frequencies of at least 0.50, the exceptions being duplex US CFV overall for both the right and left CFV. There are relative frequencies between 0.20 – 0.50 for abnormal US CFV reflux bilaterally, abnormal US CFV decreased respiratory variance on the left, reduced US CFV spontaneity bilaterally, pulsatile for US CFV phasicity bilaterally, reduced US CFV competency bilaterally, abnormal right US CFV DVT bilaterally.

Right Duplex Ultrasound CFV Flow: normal flow = 120 (56.9%, 0.51), pulsatile flow = 50 (23.7%, 0.21), continuous flow = 21 (10.0%, 0.09), decreased flow = 17 (8.1%, 0.07), no flow = 3 (1.4%, 0.01). Left Duplex Ultrasound CFV Flow: normal flow = 114 (53.0%, 0.48), pulsatile flow = 55 (25.6%, 0.23), continuous flow = 20 (9.3%, 0.08), decreased flow = 23 (10.7%, 0.10), no flow = 3 (1.4%, 0.01). These imaging findings for duplex ultrasound for the variable of flow are outlined in Table 3.4 as the sample size and relative frequency in parenthesis.

Table 3.4: Imaging Findings for Duplex US Flow

Imaging Finding	Normal	Pulsatile Flow	Continuous Flow	Decreased Flow	No Flow
Right Duplex US CFV Flow	120 (0.51)	50 (0.21)	21 (0.09)	17 (0.07)	3 (0.01)
Left Duplex US CFV Flow	114 (0.48)	55 (0.23)	20 (0.08)	23 (0.10)	3 (0.01)

The imaging findings in Table 3.4 indicate relative frequencies ~0.50 for normal flow. There are relative frequencies > 0.20 for pulsatile flow bilaterally.

Right Venography CFV Compression: normal = 5 (3.4%, 0.02), abnormal = 143 (96.7%, 0.60). Right Venography CFV Patency: normal = 144 (97.3%, 0.61), abnormal = 4 (2.7%, 0.02). Right

Venography CFV Percent Stenosis: 0 – 49.99% = 88 (58.7%, 0.37), 50 – 100% = 62 (41.3%, 0.26). Right Venography CIV Compression: normal = 32 (17.8%, 0.14), abnormal = 148 (82.2%, 0.62). Right Venography CIV Patency: normal = 174 (97.2%, 0.73), abnormal = 5 (2.8%, 0.02). Right Venography CIV Percent Stenosis: 0 – 49.99 % = 86 (47.8%, 0.36), 50-100% = 94 (52.2%, 0.40). Right Venography EIV Compression: normal = 17 (9.8%, 0.07), abnormal = 157 (90.2%, 0.66). Right Venography EIV Patency: normal = 168 (97.1%, 0.71), abnormal = 5 (2.9%, 0.02). Right Venography EIV Percent Stenosis: 0 – 49.99% = 79 (45.4%, 0.33), 50 – 100% = 95 (54.6%, 0.40). Right Venography IIV Compression: normal = 0 (0%, 0.00), abnormal = 4 (100%, 0.02). Right Venography IIV Patency: normal = 4 (100%, 0.02), abnormal = 0 (0%, 0.00). Right Venography IIV Percent Stenosis: 0 – 49.99% = 4 (100%, 0.02), abnormal = 0 (0%, 0.00). Left Venography CFV Compression: normal = 11 (6.0%, 0.05), abnormal = 171 (94.0%, 0.72). Left Venography CFV Patency: normal = 179 (98.4%, 0.76), abnormal = 3 (1.6%, 0.01). Left Venography CFV Percent Stenosis: 0 – 49.99% = 113 (62.4%, 0.48), 50 – 100% = 68 (37.6%, 0.29). Left Venography CIV Compression: normal = 45 (23.6%, 0.19), abnormal = 146 (76.4%, 0.62). Left Venography CIV Patency: normal = 179 (94.7%, 0.76), abnormal = 10 (5.3%, 0.04). Left Venography CIV Percent Stenosis: 0 – 49.99% = 67 (35.6%, 0.28), 50 – 100% = 121 (64.4%, 0.51). Left Venography EIV Compression: normal = 22 (12.0%, 0.09), abnormal = 162 (88.0%, 0.68). Left Venography EIV Patency: normal = 180 (97.8%, 0.76), abnormal = 4 (2.2%, 0.02). Left Venography EIV Percent Stenosis: 0 – 49.99% = 79 (43.2%, 0.33), 50 – 100% = 104 (56.8%, 0.44). Left Venography IIV Compression: normal = 0 (0.0%, 0.00), abnormal = 11 (100%, 0.05). Left Venography IIV Patency: normal = 11 (100%, 0.05), abnormal = 0 (0.0%, 0.00). Left Venography IIV Percent Stenosis: 0 – 49.99% = 9 (90.0%, 0.04), 50 –

100% = 1 (10.0%, 0.01). These imaging findings for venography are outlined in Table 3.5 as the sample size and relative frequency in parenthesis.

Table 3.5: Imaging Findings for Venography

Imaging Finding	Normal	Abnormal	0.00 – 49.99%	50.00 – 100%
Right Venography CFV Compression	5 (0.02)	143 (0.60)	-	-
Right Venography CFV Patency	144 (0.61)	4 (0.02)	-	-
Right Venography CFV Percent Stenosis	-	-	88 (0.37)	62 (0.26)
Right Venography CIV Compression	32 (0.14)	148 (0.62)	-	-
Right Venography CIV Patency	174 (0.73)	5 (0.02)	-	-
Right Venography CIV Percent Stenosis	-	-	86 (0.36)	94 (0.40)
Right Venography EIV Compression	17 (0.07)	157 (0.66)	-	-
Right Venography EIV Patency	168 (0.71)	5 (0.02)	-	-
Right Venography EIV Percent Stenosis	-	-	79 (0.33)	95 (0.40)
Right Venography IIV Compression	0 (0.00)	4 (0.02)	-	-
Right Venography IIV Patency	4 (0.02)	0 (0.00)	-	-
Right Venography IIV Percent Stenosis	-	-	4 (0.02)	0 (0.00)
Left Venography CFV Compression	11 (0.05)	171 (0.72)	-	-
Left Venography CFV Patency	179 (0.76)	3 (0.01)	-	-
Left Venography CFV Percent Stenosis	-	-	113 (0.48)	68 (0.29)
Left Venography CIV Compression	45 (0.19)	146 (0.62)	-	-
Left Venography CIV Patency	179 (0.76)	10 (0.04)	-	-
Left Venography CIV Percent Stenosis	-	-	67 (0.28)	121 (0.51)
Left Venography EIV Compression	22 (0.09)	162 (0.68)	-	-
Left Venography EIV Patency	180 (0.76)	4 (0.02)	-	-
Left Venography EIV Percent Stenosis	-	-	79 (0.33)	104 (0.44)
Left Venography IIV Compression	0 (0.00)	11 (0.05)	-	-
Left Venography IIV Patency	11 (0.05)	0 (0.00)	-	-
Left Venography IIV Percent Stenosis	-	-	9 (0.04)	1 (0.01)

The imaging findings in Table 3.5 indicate relative frequencies greater than 0.50 for abnormal venography compression of the CFV bilaterally, CIV bilaterally, and EIV bilaterally. There is a relative frequency greater than 0.50 for $\geq 50\%$ stenosis on venography of the left CIV. There are also relative frequencies between 0.20 – 0.50 for $\geq 50\%$ stenosis on venography of the CFV bilaterally, right CIV, and EIV bilaterally.

Right IVUS CFV Percent Stenosis: 0 – 49.99% = 43 (32.9%, 0.18), 50 – 100% = 92 (68.1%, 0.39). Right IVUS CIV Percent Stenosis: 0 – 49.99% = 33 (20.0%, 0.14), 50 – 100% = 132

(80.0%, 0.56). Right IVUS EIV Percent Stenosis: 0 – 49.99% = 41 (25.9%, 0.17), 50 – 100% = 117 (74.0%, 0.49). Right IVUS IIV Percent Stenosis: 0 – 49.99% = 0 (0%, 0.00), 50 – 100% = 0 (0%, 0.00). Right IVUS DVT: normal = 117 (73.1%, 0.49), abnormal = 43 (26.9%, 0.18). Left IVUS CFV Percent Stenosis: 0 – 49.99% = 68 (44.2%, 0.29), 50 – 100% = 86 (55.8%, 0.36). Left IVUS CIV Percent Stenosis: 0 – 49.99% = 19 (11.4%, 0.08), 50 – 100% = 148 (88.6%, 0.62). Left IVUS EIV Percent Stenosis: 0 – 49.99% = 50 (30.5%, 0.21), 50 – 100% = 114 (69.5%, 0.48). Left IVUS IIV Percent Stenosis: 0 – 49.99% = 0 (0%, 0.00), 50 – 100% = 0 (0%, 0.00). Left IVUS DVT: normal = 110 (67.1%, 0.46), abnormal = 54 (32.9%, 0.23). These imaging findings for IVUS are outlined in Table 3.6 as the sample size and relative frequency in parenthesis.

Table 3.6: Imaging Findings for IVUS

Imaging Finding	Normal	Abnormal	0.00 – 49.99%	50.00 – 100%
Right IVUS CFV Percent Stenosis	-	-	43 (0.18)	92 (0.39)
Right IVUS CIV Percent Stenosis	-	-	33 (0.14)	132 (0.56)
Right IVUS EIV Percent Stenosis	-	-	41 (0.17)	117 (0.49)
Right IVUS IIV Percent Stenosis	-	-	0 (0.00)	0 (0.00)
Right IVUS DVT	117 (0.49)	43 (0.18)	-	-
Left IVUS CFV Percent Stenosis	-	-	68 (0.29)	86 (0.36)
Left IVUS CIV Percent Stenosis	-	-	19 (0.08)	148 (0.62)
Left IVUS EIV Percent Stenosis	-	-	50 (0.21)	114 (0.48)
Left IVUS IIV Percent Stenosis	-	-	0 (0.00)	0 (0.00)
Left IVUS DVT	110 (0.46)	54 (0.23)	-	-

The imaging findings in Table 3.6 indicate relative frequencies greater than 0.50 for $\geq 50\%$ stenosis on IVUS of the CIV bilaterally. There are also relative frequencies between 0.20 – 0.50 for $\geq 50\%$ stenosis on IVUS of the CFV bilaterally and the EIV bilaterally.

There are also relative frequencies of 0.49 for $\geq 50\%$ stenosis on IVUS of the right EIV and 0.48 for $\geq 50\%$ stenosis on IVUS of the left CIV.

3.2 Inferential Statistics

The following results are an outcome of logistic regression analyses on R statistical software.

Table 3.7: Duplex Ultrasound to Venography Analyses

Left p-value = 0.0245*		CFV Ultrasound Compressibility		Right p-value = 0.0135*		CFV Ultrasound Compressibility	
		Normal	Reduced			Normal	Reduced or Absent
Venography	<50% Stenosis	101	2	Venography	<50% Stenosis	81	1
	≥50% Stenosis	56	7		≥50% Stenosis	52	9

Left p-value = 0.0145*		CFV Ultrasound Thrombosis		Right p-value = 0.0093**		CFV Ultrasound Thrombosis	
		Normal	Thrombosis			Normal	Thrombosis
Venography	<50% Stenosis	101	2	Venography	<50% Stenosis	81	1
	≥50% Stenosis	56	8		≥50% Stenosis	51	10

		CFV Ultrasound Spontaneity	
		Normal	Reduced, Absent, or Pulsatile
Venography	<50% Stenosis	69	13
	≥50% Stenosis	42	19

The analyses on Table 3.7 show a variety of relationships between findings on duplex ultrasound and venography. Reduced compressibility on duplex ultrasound of the left CFV is a statistically significant predictor of ≥50% stenosis on venography. Reduced or absent compressibility on duplex ultrasound of the right CFV is a statistically significant predictor of ≥50% stenosis on venography. Thrombosis on duplex ultrasound of either the left or the right CFV is a statistically significant predictor of ≥50% stenosis on venography. Reduced, absent, or pulsatile spontaneity on duplex ultrasound of the right CFV is a statistically significant predictor of ≥50% stenosis on venography.

Table 3.8: Duplex Ultrasound to IVUS Analyses

Left p-value = 0.008**		CFV Ultrasound Reflux	
		Normal	Abnormal
IVUS	<50% Stenosis	33	28
	≥50% Stenosis	62	20

Right p-value = 0.731		CFV Ultrasound Reflux	
		Normal	Abnormal
IVUS	<50% Stenosis	25	13
	≥50% Stenosis	62	28

Left p-value = 0.036*		CFV Ultrasound Phasicity	
		Not Continuous	Continuous
IVUS	<50% Stenosis	48	14
	≥50% Stenosis	85	8

Left p-value = 0.008**		CFV Ultrasound Competency	
		Normal	Reduced
IVUS	<50% Stenosis	34	28
	≥50% Stenosis	63	20

Left p-value = 0.035*		CFV Ultrasound Flow	
		Not Continuous Flow	Continuous Flow
IVUS	<50% Stenosis	41	11
	≥50% Stenosis	77	5

The analyses on Table 3.8 show a variety of relationships between findings on duplex ultrasound and IVUS. “Normal reflux” (the absence of reflux) on duplex ultrasound of the left CFV is a statistically significant predictor of ≥50% stenosis on IVUS. “Normal reflux” (the absence of reflux) on duplex ultrasound of the right CFV is not a statistically significant predictor of ≥50% stenosis on IVUS. Continuous phasicity on duplex ultrasound of the left CFV is a statistically significant predictor of <50% stenosis on IVUS. Normal competency on duplex ultrasound of the left CFV is a statistically significant predictor of ≥50% stenosis on IVUS. Continuous flow on duplex ultrasound of the left CFV is a statistically significant predictor of <50% stenosis on IVUS.

Table 3.9: Venography to IVUS Analyses

Left p-value = 0.264		Venography Compression	
		Normal	Abnormal
IVUS	<50% Stenosis	3	63
	≥50% Stenosis	8	77

Right p-value = 0.991		Venography Compression	
		Normal	Abnormal
IVUS	<50% Stenosis	0	37
	≥50% Stenosis	3	86

The analysis on Table 3.9 shows that compression on venography is not a statistically significant predictor of $\geq 50\%$ stenosis on IVUS.

CHAPTER 4

DISCUSSION AND INNOVATION

This chapter contains the analysis and interpretation of the results from the previous chapter. A reminder as to the questions and purpose of the research project as well as key findings are discussed initially. This is followed by a detailed discussion of the results of interest, and in particular their interpretation. Thereafter, the limitations of this study are stated and recommendations for further research are explored.

Investigation and Key Findings

The aim of this study is to discover imaging findings on duplex ultrasound and venography that can be used in the identification of MTS and other pelvic vein compression syndromes for adults with lower extremity leg pain and edema, particularly earlier in the disease course than is currently possible. The objectives are to identify these patients, acquire data from the imaging modalities of interest including duplex ultrasound, venography, and IVUS, and determine findings on duplex ultrasound and venography that can predict venous compression on IVUS.

This investigation examines if the findings of reflux or abnormal flow patterns as seen on duplex ultrasound at the CFV predicts venous compression on IVUS. There is also an investigation as to whether the findings of spontaneity, phasicity, or competency as seen on duplex ultrasound at the CFV predicts venous compression on IVUS. Spontaneity, compressibility, and thrombosis on duplex ultrasound is assessed for its predictability of venous compression on venography.

Finally, compression on venography was assessed for its predictability of venous compression on IVUS.

Males and females in this study are similar in terms of their statistical measures of age and most risk factors with the exception of males, who are disproportionately affected by T2DM with unspecified complications and acute venous embolism and females, who are disproportionately affected by unspecified obesity and chronic venous insufficiency. Venography demonstrated high relative frequencies of abnormal compression on the bilateral CFVs, CIVs, and EIVs. Venography also demonstrated high relative frequency of $\geq 50\%$ stenosis on the left CIV. IVUS demonstrated high relative frequencies of $\geq 50\%$ stenosis on the bilateral CIVs.

Logistic regression analyses identified duplex ultrasound findings on the CFV that are statistically significant predictors of $\geq 50\%$ stenosis on venography and IVUS. The predictors for $\geq 50\%$ stenosis on venography include reduced compressibility, thrombosis, and spontaneity that is reduced, absent, or pulsatile. The predictors for $\geq 50\%$ stenosis on IVUS include the absence of reflux and normal competency. The analysis also identified that compression on venography is not a statistically significant predictor of $\geq 50\%$ stenosis on IVUS.

Interpretation of Results

The statistical measures of age for the 237 patients in this study are similar overall when comparing males ($n = 98$) and females ($n = 139$). This is shown by male and female medians of 67.0 and 68.0 and SD of 13.2 and 15.2, respectively. Additionally, they have low absolute differences of median = 1.0, and SD = 2.0. Both distributions have negative skewness between 0.0 and -0.5 and kurtosis < 3 . Therefore, these distributions are nearly symmetric and platykurtic which makes them appropriate sample populations for further statistical analysis, from the perspective of age distributions.

There are some risk factors that are warrant discussion. Most patients in this study have essential HTN and vein compression given relative frequencies $rf > 0.50$ and a notable amount have T2DM without complications, chronic embolism, hyperlipidemia, and chronic venous HTN given relative frequencies $0.50 > rf > 0.20$. Comparing the prevalence of some of these risk factors as a percentage between patients in this study and the general population: essential HTN is greater in this study (57.8%) than the general population (47%), diabetes is greater in this study (24.1%; summation of T2DM with complications and T2DM without complications) than the general population (11.3%), and hyperlipidemia is higher in this study (28.3%) than the general population (12%). However, obesity is lower in this study (17.3%; summation of unspecified obesity and morbid obesity) than the general population (41.9%). Since the patients for this study were selected in a non-random manner, particularly those that sought healthcare who had lower extremity pain and edema, it is not surprising that patients in this study have a higher prevalence of essential HTN, diabetes, and hyperlipidemia. However, it is interesting that patients in this study have a lower prevalence of obesity than the general population. Risk factors were also stratified by sex. The ratio of the presence of a given risk factor for males to females is ≥ 2 for T2DM with unspecified complications and acute venous embolism. The estimated number of adults in the US in 2020 with diabetes broken down by sex is 17.9 million and 16.2 million for males and females, respectively. Therefore, the ratio of adult males with diabetes for this study seems to be higher than adult males in the US. While there is data for venous thromboembolism broken by sex, the data for adults in the US with acute venous embolism broken down by sex is not readily available. Therefore, a comparison to relate sex-adjusted data of this risk factor in this study to the general US population is not done. The ratio of the

presence of a given risk factor for females to males is ≥ 2 for unspecified obesity and chronic venous insufficiency. From 2017 – 2018, 43.0% of adult males in the US were obese and 41.9% of adult females in the US were obese. Therefore, the ratio of adult females with obesity for this study seems to be higher than adult females in the US. Even when adjusted for sample sizes, more women are affected by venous disease than men. Therefore, it is not surprising that 75% of chronic venous insufficiency in this study is seen in women.

Duplex ultrasound had relative frequencies > 0.50 classified as normal for most imaging findings, and all imaging findings for this modality are for the CFVs. There are relative frequencies between 0.20 – 0.50 for the presence of reflux bilaterally and pulsatile phasicity bilaterally. Interestingly the Combs et al.³⁵ 2019 study reported venous reflux in 34/38 patients and pulsatility in 33/38 patients, and 36/38 patients were found to have pelvic vein compression syndrome. There are also relative frequencies between 0.20 – 0.50 for decreased respiratory variance on the left, reduced spontaneity bilaterally, reduced competency bilaterally, and the presence of a DVT bilaterally. Some of these findings may be explained as there is an association between differences in phasicity and obstruction of the pelvic veins. As for the flow studies, the relative frequency of pulsatile waveforms was > 0.20 bilaterally. Pulsatile waveforms in the venous system of the lower extremity are generally highly suggestive of pathology. Therefore, it is not surprising that this waveform has a moderately high relative frequency bilaterally in these patients. Venography had relative frequencies > 0.50 for abnormal venography compression of the CFV bilaterally, CIV bilaterally, and EIV bilaterally. Given that venous obstructions are resistant to compression, these high relative frequencies are not surprising. Venography also had relative frequencies > 0.50 for $\geq 50\%$ stenosis of the left CIV,

0.20 – 0.50 for $\geq 50\%$ stenosis of the CFV bilaterally, right CIV, and EIV bilaterally. IVUS had relative frequencies > 0.50 for $\geq 50\%$ stenosis of the CIV as well as 0.20 – 0.50 for $\geq 50\%$ stenosis of the CFV bilaterally and EIV bilaterally. The highest relative frequency for $< 50\%$ stenosis on venography is < 0.50 and on IVUS is < 0.30 . Looking at the relative frequencies for percent stenosis of venography and IVUS, the data is suggestive that IVUS identifies vessels with $> 50\%$ stenosis to a greater extent than venography with $> 50\%$ stenosis. This is congruent with the literature that supports the superiority of IVUS over venography for assessment of stenosis of vessels.

The logistic regression analyses were notable for several relationships. The analyses found that on duplex ultrasound, reduced compressibility of the left CFV; reduced or absent compressibility of the right CFV; thrombosis on the bilateral CFVs; and reduced, absent, or pulsatile spontaneity are statistically significant predictors for $\geq 50\%$ stenosis on venography. On duplex ultrasound, the absence of reflux on the left CFV is a highly statistically significant predictor of $\geq 50\%$ stenosis on IVUS. However, there was no statistically significant relationship for reflux of the right CFV. Normal competency on duplex ultrasound of the left CFV is a statistically significant predictor of $\geq 50\%$ stenosis on IVUS. Additionally, continuous phasicity and continuous flow on duplex ultrasound of the left CFV are each statistically significant predictors of $< 50\%$ stenosis on IVUS. This is an interesting contrast to the literature, as continuous waveforms in venous systems are indicative of obstructions that are proximal relative to the location of measurement, probably due to less changes in flow velocity as a function of respiratory variation. Lastly, compression on venography is not a statistically significant predictor of $\geq 50\%$ stenosis on

IVUS. This is plausible since if a vessel on IVUS shows substantial stenosis, it should not be compressible.^{9,15,64-74}

Limitations

The limitations for this study should be noted. The scope of this study in terms of the pathology under investigation is focused on compression of the pelvic veins. This study assessed imaging techniques not usually applied for the diagnosis of interest, so there was limited prior research focused for the questions of the study. This is a single center study which restricts the extent to which findings in this study may be generalized to the population of interest. The sampling technique was not random and very purposive to obtain enough patients with the clinical presentation of interest. This is a study that is primarily retrospective which can introduce confounding variables that were not thought of during the design phase. The quality of data obtained from ultrasound is highly dependent on the technologist, and it is possible that sub-optimal inter-rater reliability skewed the data since multiple technologists took the images of interest. The focus on imaging studies prior to intervention limits the clinical significance of the imaging findings in their applicability to exclude their use in post-intervention imaging. The analyses relating to duplex ultrasound only assessed the CFV as there was less data available overall for veins distal to the CFV. Since this study takes some quantitative data that is sorted into categories, it is possible that the findings are oversimplified and that more elegant statistical analysis techniques may have identified different statistically significant findings.

Despite these limitations, this study identified many patients over a 7-year period given the delimitations of both the clinical presentation and venous compression for patient enrollment.

The design excluded loss to follow-up and withdrawal from the study as possible biases. It also excluded confounding imaging findings had post-intervention images been included for analysis. Though research studies for the specific questions were limited, this study partially relied on the application of established physical principles of fluids and sound to form its theoretical basis.

CHAPTER 5

FINAL ANALYSIS

This chapter features the key findings of this study and relates them to the research aim and questions. The contribution and impact of this study for the understanding of May-Thurner Syndrome and other pelvic vein compression syndromes is discussed and this is followed by stating the limitations. This chapter concludes by declaring the opportunities for logical directions of future research.

Conclusions

This study aimed to investigate imaging findings on duplex ultrasound and venography that can identify May-Thurner Syndrome and other pelvic vein compression syndromes at an earlier stage of disease for adults with lower extremity leg pain and edema. The results indicate that spontaneity that is either reduced, absent, or pulsatile, compressibility that is reduced, and the presence of thrombosis predict compression on venography. They also indicate that the absence of reflux and normal competency on duplex ultrasound predict compression on intravascular ultrasound.

The lack of reliable non-invasive diagnostic imaging for May-Thurner Syndrome and other pelvic vein compression syndromes leads to a delay in their diagnosis. The consequences of delayed diagnosis are poor clinical outcomes, as severe as limb amputation, and increased healthcare expenditures as these patients undergo more diagnostic studies. This study suggests that the non-invasive imaging findings on duplex ultrasound stated above could lead to the

diagnosis of pelvic vein compression syndromes. Since this is one of the first imaging modalities used with patients that present with lower extremity leg pain and edema, use of these findings may identify this group of compression syndromes at an earlier stage of disease. This study is limited in its generalizability given it is a partially retrospective single center study that used non-random sampling techniques to identify patients presenting with lower extremity pain and edema.

Future Directions

Given that this is partially a retrospective study that also used prospective data, a prospective study should be performed with the same imaging findings on duplex ultrasound, venography, and IVUS. A confirmatory study designed in that manner may be able to indicate with greater confidence whether the predictors in this study are accurate with respect to the diagnosis of pelvic venous compression. A multicenter study should be performed in order to increase the generalizability by including other patient populations. A national study in particular could allow for generalizability to patients in the United States that have the clinical presentation of interest. While these findings are intended for use of assessment of the pelvic veins, it may be possible to apply these findings to venous compression syndromes outside of the pelvis given a similar underlying mechanism leading to pathology is probable. One surprising finding in this study is that continuous phasicity and continuous flow were both statistically significant predictors of < 50% stenosis on IVUS, which should be further researched as this contrasts the current understanding of continuous flow in the venous system. Clinical outcomes such as lower extremity pain or edema after intervention for patients diagnosed with venous compression syndrome using the findings in this study should also be investigated and compared to clinical

outcomes for patients diagnosed with venous compression syndrome using standard findings. Investigations that apply these predictors of venous compression syndromes to those clinical outcomes would give insight as to the extent to which these predictors may decrease the burden of this group of diseases for both the individual patient from a treatment and outcomes perspective, and society from an economic perspective.

COMPLIANCE

This study has IRB approval through the Western and Aspire Methodist Hospital System. This study did not require any consideration or approval from IACUC. All required CITI training has been completed at the time of this study.

REFERENCES

1. MAY R, THURNER J. The cause of the predominantly sinistral occurrence of thrombosis of the pelvic veins. *Angiology*. 1957;8(5):419-427. doi:10.1177/000331975700800505
2. Raju S, Neglen P. High prevalence of nonthrombotic iliac vein lesions in chronic venous disease: a permissive role in pathogenicity. *J Vasc Surg*. 2006;44(1):136-144. doi:10.1016/j.jvs.2006.02.065
3. Garrie A., et al: New Vein Compression Entities in Patients with Unexplained Leg Swelling. *Journal of Vascular Surgery* 2017; 45: pp. 173-178. DOI: <https://doi.org/10.1016/j.avsg.2017.06.044>
4. Butros SR, Liu R, Oliveira GR, Ganguli S, Kalva S. Venous compression syndromes: clinical features, imaging findings and management. *Br J Radiol*. 2013;86(1030):20130284. doi:10.1259/bjr.20130284
5. Kibbe MR, Ujiki M, Goodwin AL, Eskandari M, Yao J, Matsumura J. Iliac vein compression in an asymptomatic patient population. *Journal of Vascular Surgery*. 2004;39(5):937-943. doi:10.1016/j.jvs.2003.12.032
6. O'Sullivan GJ, Semba CP, Bittner CA, et al. Endovascular management of iliac vein compression (May-Thurner) syndrome. *J Vasc Interv Radiol*. 2000;11(7):823-836. doi:10.1016/s1051-0443(07)61796-5
7. Marder V, Aird W, Bennett J, Schulman S, White II G. *Hemostasis and Thrombosis: Basic Principles and Clinical Practice*. 6th ed. Philadelphia: Wolters Kluwer health - Lippincott Williams & Wilkins; 2012.
8. Pontiga F, Gaytán SP. An experimental approach to the fundamental principles of Hemodynamics. *Advances in Physiology Education*. 2005;29(3):165-171. doi:10.1152/advan.00009.2005
9. Mangla A, Hamad H. May-Thurner Syndrome. [Updated 2022 May 14]. In: StatPearls [Internet]. Treasure Island (FL): StatPearls Publishing; 2022 Jan-. Available from: <https://www.ncbi.nlm.nih.gov/books/NBK554377/>
10. Peters M, Syed RK, Katz M, et al. May-Thurner syndrome: a not so uncommon cause of a common condition. *Proc (Bayl Univ Med Cent)*. 2012;25(3):231-233. doi:10.1080/08998280.2012.11928834
11. Chiu JJ, Chien S. Effects of disturbed flow on vascular endothelium: pathophysiological basis and clinical perspectives. *Physiol Rev*. 2011;91(1):327-387. doi:10.1152/physrev.00047.2009

12. Dillon PF. Chapter 7: Fluid and air flow. In: *Biophysics: A Physiological Approach*. Cambridge, New York: Cambridge University Press; 2012:144-164.
13. Spencer MP, Reid JM. Quantitation of carotid stenosis with continuous-wave (C-W) Doppler ultrasound. *Stroke*. 1979;10(3):326-330. doi:10.1161/01.str.10.3.326
14. Birn J, Vedantham S. May-Thurner syndrome and other obstructive iliac vein lesions: meaning, myth, and mystery. *Vasc Med*. 2015;20(1):74-83. doi:10.1177/1358863X14560429
15. Zucker EJ, Ganguli S, Ghoshhajra BB, Gupta R, Prabhakar AM. Imaging of venous compression syndromes. *Cardiovasc Diagn Ther*. 2016;6(6):519-532. doi:10.21037/cdt.2016.11.19
16. Enden T, Haig Y, Kløw NE, et al. Long-term outcome after additional catheter-directed thrombolysis versus standard treatment for acute iliofemoral deep vein thrombosis (the CaVenT study): a randomised controlled trial. *Lancet*. 2012;379(9810):31-38. doi:10.1016/S0140-6736(11)61753-4
17. Comerota AJ, Kearon C, Gu CS, et al. Endovascular Thrombus Removal for Acute Iliofemoral Deep Vein Thrombosis. *Circulation*. 2019;139(9):1162-1173. doi:10.1161/CIRCULATIONAHA.118.037425
18. Phillips RB, Kondev J, Theriot J, et al. Chapter 12: The Mathematics of Water. In: *Physical Biology of the Cell*. 1st ed. New York, New York: Garland Science;2010:457-466.
19. Cohen B. Intravascular Ultrasound (IVUS). Intravascular ultrasound (IVUS). <http://www.ptca.org/ivus/ivus.html>. Published 2013. Accessed December 10, 2022.
20. Goodney P, Warner C. Endovascular treatment for May–thurner syndrome. *Endovascular Treatment for May–Thurner Syndrome*. <https://thoracickey.com/endovascular-treatment-for-may-thurner-syndrome/>. Published June 15, 2016. Accessed December 10, 2022.
21. Fernandez S, Lenoir C, Samer C, Rollason V. Drug interactions with apixaban: A systematic review of the literature and an analysis of VigiBase, the World Health Organization database of spontaneous safety reports. *Pharmacol Res Perspect*. 2020;8(5):e00647. doi:10.1002/prp2.647
22. Crader MF, Johns T, Arnold JK. Warfarin Drug Interactions. In: *StatPearls*. Treasure Island (FL): StatPearls Publishing; May 8, 2022.
23. Kang JM, Park KH, Ahn S, et al. Rivaroxaban after Thrombolysis in Acute Iliofemoral Venous Thrombosis: A Randomized, Open-labeled, Multicenter Trial. *Sci Rep*. 2019;9(1):20356. Published 2019 Dec 30. doi:10.1038/s41598-019-56887-w

24. Kumar V, Aster JC, Perkins JA, Cotran RS, Abbas AK, Turner JR. Chapters 2,3,4,14. In: *Robbins and COTRAN Pathologic Basis of Disease*. 10th ed. Philadelphia, PA: Elsevier; 2021:33-66, 73-84, 110, 115-127, 133, 638
25. McGuckin M, Waterman R, Brooks J, et al. Validation of venous leg ulcer guidelines in the United States and United Kingdom. *Am J Surg*. 2002;183(2):132-137. doi:10.1016/s0002-9610(01)00856-x
26. Van den Oever R, Hepp B, Debbaut B, Simon I. Socio-economic impact of chronic venous insufficiency. An underestimated public health problem. *Int Angiol*. 1998;17(3):161-167.
27. Kolluri R, Lugli M, Villalba L, et al. An estimate of the economic burden of venous leg ulcers associated with deep venous disease [published correction appears in *Vasc Med*. 2021 Sep 22;:1358863X211048020]. *Vasc Med*. 2022;27(1):63-72. doi:10.1177/1358863X211028298
28. Bergan JJ, Schmid-Schönbein GW, Smith PD, Nicolaidis AN, Boisseau MR, Eklof B. Chronic venous disease. *N Engl J Med*. 2006;355(5):488-498. doi:10.1056/NEJMra055289
29. McArdle M, Hernandez-Vila EA. Management of Chronic Venous Disease. *Tex Heart Inst J*. 2017;44(5):347-349. Published 2017 Oct 1. doi:10.14503/THIJ-17-6357
30. Bonkemeyer Millan S, Gan R, Townsend PE. Venous Ulcers: Diagnosis and Treatment. *Am Fam Physician*. 2019;100(5):298-305.
31. Piazza G. Varicose veins. *Circulation*. 2014;130(7):582-587. doi:10.1161/CIRCULATIONAHA.113.008331
32. van Korlaar I, Vossen C, Rosendaal F, Cameron L, Bovill E, Kaptein A. Quality of life in venous disease. *Thromb Haemost*. 2003;90(1):27-35.
33. Waheed, S., Kudaravalli, P., & Hotwagner, D. (2021). *Deep Vein Thrombosis*. NCBI Bookshelf. Retrieved December 12, 2022, from <https://www.ncbi.nlm.nih.gov/books/NBK507708/>
34. Sanguily III, J., Martinsen, B., Igyarto, Z., & Pham, M. K. (2016). *Reducing Amputation Rates in Critical Limb Ischemia Patients Via a Limb Salvage Program: A Retrospective Analysis*. CardioVascular Learning Network. Retrieved December 11, 2022, from <https://www.hmpgloballearningnetwork.com/site/vdm/content/reducing-amputation-rates-critical-limb-ischemia-patients-limb-salvage-program>
35. Combs A., Richmond J., Feldtman R., Peper B., Ahn S. New Description of Unique Sonographic Findings in Patients with May Thurner Syndrome. *Society for clinical vascular surgery 47th annual symposium*. 2019. DOI:

<https://scvs.org/symposium/abstracts/2019/MP48.cgi>

36. Grogan, S., & Mount, C. (2022). *Ultrasound physics and Instrumentation*. NCBI Bookshelf. Retrieved December 12, 2022, from <https://www.ncbi.nlm.nih.gov/books/NBK570593/>
37. Young, H. D., Freedman, R. A., & Ford, A. L. (2007). Chapters 15, 16, 33, 38, 40, 41, 43, 44. In *University physics*. 12th ed. Addison-Wesley. pp 488-491, 527-557, 1121-1128, 1307-1312, 1319-1326, 1330-1334, 1375-1387, 1401-1408, 1468-1484, 1489-1492, 1509-1514
38. Carroll D, Basilic vein cannulation (ultrasound). Case study, Radiopaedia.org (Accessed on 12 Dec 2022) <https://doi.org/10.53347/rID-64446>
39. Johnson MM. Radiation protection education in fluoroscopy. *Radiol Technol*. 2015;86(5):511-532.
40. Expert Panel on Vascular Imaging: Hanley M, Steigner ML, et al. ACR Appropriateness Criteria® Suspected Lower Extremity Deep Vein Thrombosis. *J Am Coll Radiol*. 2018;15(11S):S413-S417. doi:10.1016/j.jacr.2018.09.028
41. Radiation Safety. Yale Environmental Health & Safety. <https://ehs.yale.edu/radiation>. Accessed December 15, 2022.
42. Penetration Abilities of Different Types of Radiation. <https://www.cdc.gov/training/products/RN/page4976.html>. Accessed December 15, 2022.
43. PowerPoint Presentation. <https://yale.cloud-cme.com/assets/YALE/Presentations/8920/8920.pdf>. Published July 25, 2019. Accessed December 15, 2022.
44. Geleijns J, Wondergem J. X-ray imaging and the skin: radiation biology, patient dosimetry and observed effects. *Radiat Prot Dosimetry*. 2005;114(1-3):121-125. doi:10.1093/rpd/nch544
45. Thorne, K, Blandford, R. *Modern Classical Physics: Optics, Fluids, Plasmas, Elasticity, Relativity, and Statistical Physics*. (2017). Chapters 13, 15, 16. 1st ed., Princeton University Press. pp 716-718, 787-789, 862-863.
46. Smith, F. *A Primer In Applied Radiation Physics*. (2000). Chapters 1, 2, 3, 10, 11. 1st ed., World Scientific Publishing. pp 3-9, 80-82, 95-96, 370-389, 411-423.
47. Tintinalli, J. *Emergency Medicine: A Comprehensive Study Guide*. Chapter 10. 9th ed., McGraw-Hill Education; 2020: 47-52.

48. Frane N, Bitterman A. Radiation Safety and Protection. In: StatPearls. Treasure Island (FL): StatPearls Publishing; May 23, 2022.
49. CDC. (2018, April 4). *CDC radiation emergencies*. Acute Radiation Syndrome: A Fact Sheet for Clinicians. Retrieved December 23, 2022, from <https://www.cdc.gov/nceh/radiation/emergencies/arsphysicianfactsheet.htm>
50. CDC. (2018, April 4). *Cutaneous radiation injury (CRI)/CDC radiation emergencies*. Cutaneous Radiation Injury (CRI): A Fact Sheet for Clinicians. Retrieved December 23, 2022, from <https://www.cdc.gov/nceh/radiation/emergencies/crphysicianfactsheet.htm>
51. Nakashima J, Duong H. Radiation Physics. In: StatPearls. Treasure Island (FL): StatPearls Publishing; May 8, 2022.
52. Krane, K. S. (2012). Chapters 3, 12, 14. In *Modern physics* (pp. 69-93, 369–401, 441-447). essay, Wiley.
53. Alrabayah M, Qaswal AB, Suleiman A, Khreesha L. Role of Potassium Ions Quantum Tunneling in the Pathophysiology of Phantom Limb Pain. *Brain Sci.* 2020;10(4):241. Published 2020 Apr 18. doi:10.3390/brainsci10040241
54. Truskey, G. A., Yuan, F., & Katz, D. F. (2010). Chapters 2,3,4,5. In *Transport phenomena in biological systems* (pp. 55–251). essay, Pearson.
55. Alexandrou A. Chapter 4. In: *Principles of Fluid Mechanics*. Upper Saddle River, New Jersey: Prentice Hall; 2001:139-166.
56. Pagano M, Gauvreau K, Mattie H. Chapters 2, 7, 8, 9, 10, 16, 17, 18, 21, 22. In: *Principles of Biostatistics*. Boca Raton, FL: CRC Press, Taylor & Francis Group; 2022:470-484.
57. Hammond F, Malec JF, Nick T, Buschbacher RM. *Handbook for Clinical Research: Design, Statistics, and Implementation*. Demos Medical; 2015.
58. Ryan G. Introduction to positivism, interpretivism and critical theory. *Nurse Res.* 2018;25(4):14-20. doi:10.7748/nr.2018.e1466
59. Serrelli E. Philosophy of Biology. Internet encyclopedia of philosophy. <https://iep.utm.edu/philosophy-of-biology/>. Published 2016. Accessed February 6, 2023.
60. Bickle I. Color flow doppler (ultrasound). Radiopaedia Blog RSS. <https://radiopaedia.org/articles/color-flow-doppler-ultrasound>. Published April 2, 2022. Accessed January 26, 2023.
61. Dytham C. Chapters 4, 5, 8. In: *Choosing and Using Statistics: A Biologist's Guide*. Oxford, England: Blackwell; 2003:22-29, 30-42, 147-176.

62. Micheaux PLde. *The R Software: Fundamentals of Programming and Statistical Analysis*. New York, NY: Springer; 2014.
63. Stoltzfus JC. Logistic regression: a brief primer. *Acad Emerg Med*. 2011;18(10):1099-1104. doi:10.1111/j.1553-2712.2011.01185.x
64. CDC. Facts about hypertension. Centers for Disease Control and Prevention. <https://www.cdc.gov/bloodpressure/facts.htm>. Published January 5, 2023. Accessed January 31, 2023.
65. CDC. National Diabetes Statistics Report. Centers for Disease Control and Prevention. <https://www.cdc.gov/diabetes/data/statistics-report/index.html>. Published June 29, 2022. Accessed January 31, 2023.
66. CDC. High cholesterol facts. Centers for Disease Control and Prevention. <https://www.cdc.gov/cholesterol/facts.htm>. Published October 24, 2022. Accessed January 31, 2023.
67. CDC. Adult obesity facts. Centers for Disease Control and Prevention. <https://www.cdc.gov/obesity/data/adult.html>. Published May 17, 2022. Accessed January 31, 2023.
68. CDC. National Diabetes Statistics Report 2020. estimates of diabetes and its ... National Diabetes Statistics Report. <https://www.cdc.gov/diabetes/pdfs/data/statistics/national-diabetes-statistics-report.pdf>. Published 2020. Accessed February 1, 2023.
69. CDC. Overweight & Obesity Statistics. National Institute of Diabetes and Digestive and Kidney Diseases. <https://www.niddk.nih.gov/health-information/health-statistics/overweight-obesity>. Published 2021. Accessed January 31, 2023.
70. Eberhardt R, Raffetto J. Chronic venous insufficiency | circulation. *Chronic Venous Insufficiency*. <https://www.ahajournals.org/doi/10.1161/CIRCULATIONAHA.113.006898>. Published 2014. Accessed February 1, 2023.
71. Lohr J, Bush R. Venous disease in women: Epidemiology, manifestations, and treatment. *Journal of Vascular Surgery*. <https://www.sciencedirect.com/science/article/pii/S0741521412023968>. Published March 20, 2013. Accessed January 31, 2023.
72. Needleman L. Ultrasound for lower extremity deep venous thrombosis. ? <https://www.ahajournals.org/doi/pdf/10.1161/CIRCULATIONAHA.117.030687>. Published 2018. Accessed February 1, 2023.
73. Sanford D. Importance of phasicity in detection of proximal iliac vein thrombosis ... *Sage Journals*. <https://journals.sagepub.com/doi/abs/10.1177/154431671103500305>. Published

2018. Accessed February 1, 2023.

74. Kim E. Interpretation of peripheral arterial and venous Doppler waveforms. Portail Vasculaire.
https://www.portailvasculaire.fr/sites/default/files/docs/interpretation_of_peripheral_arterial_and_venous_doppler_waveforms-_a_consensus_statement_vm2020.pdf. Published 2020. Accessed February 1, 2023.
75. Hedrick W, Hykes D. A simplified explanation of Fourier analysis. Sagepub.com.
<https://journals.sagepub.com/doi/10.1177/875647939200800602>. Published 1992. Accessed February 1, 2023.
76. Necas M. Duplex ultrasound in the assessment of lower extremity venous insufficiency. *Australas J Ultrasound Med.* 2010;13(4):37-45. doi:10.1002/j.2205-0140.2010.tb00178.x
77. Selis J, Kadakia S. Venous doppler sonography of the extremities: A window to ... - home (AJR). *Ajronline.org*. <https://www.ajronline.org/doi/10.2214/AJR.09.2640>. Published 2009. Accessed February 1, 2023.
78. Grotberg JB, Jensen OE. Biofluid mechanics in flexible tubes. *Annu Rev Fluid Mech.* 2004;36:121-147.
http://library.tcu.edu/PURL/EZproxy_link.asp?login?url=https://www.proquest.com/scholarly-journals/biofluid-mechanics-flexible-tubes/docview/220774694/se-2.
79. Baker R. Chapter 5. In: *Introductory Guide to Flow Measurement*. New York, NY: ASME Press; 2004:105-113.
80. Berthier J. 1. In: *Microfluidics for Biotechnology*. Norwood, MA: Artech House; 2009:1-16.
81. Munson BR, Young DF, Okiishi TH. 2,3,6,8,9. In: *Fundamentals of Fluid Mechanics*. John Wiley; 2002: 41-44,102-105, 300-306, 444-454, 534-539.
82. Grene MG, Depew DJ. 10,12. In: *The Philosophy of Biology: An Episodic History*. New York, NY: Cambridge University Press; 2014:306-313, 348-361
83. Zar JH. 2,3,4,6,7,20. In: *Biostatistical Analysis*. Upper Saddle River, NJ: Prentice Hall; 1999:16-46,65-119,413-459.
84. Pelham BGE, Hunter WG, Hunter JS. 1,2,3. In: *Statistics for Experimenters: Design, Innovation, and Discovery*. Hoboken, NJ: Wiley-Interscience; 2005:6-132.
85. Myers JL, Well AD. 2,3,4,5,10,21. In: *Research Design and Statistical Analysis*. Mahwah, NJ: L. Erlbaum Associates; 2003:START-END. 10-131,267-281,614-637

86. Novikov AM, Novikov DA. *Research Methodology: From Philosophy of Science to Research Design*. Boca Raton, FL: CRC Press; 2013.
87. Hartvigsen G. *A Primer in Biological Data Analysis Using R*. Columbia, NY: Columbia University Press; 2014.
88. Dubaj. File:Tokyo.png – Wikimedia Commons.
<https://commons.wikimedia.org/wiki/File:Tokyo.png> (accessed Feb 13th, 2023).
89. Platz R. Types of ionising radiation. Types of ionising radiation | Portal on Nuclear Safety. <https://www.nuklearesicherheit.de/en/science/physics/ionising-radiation/types-of-ionising-radiation/>. Published 2018. Accessed February 8, 2023.
90. Johnston A. New angiography suite nearing completion. Thompson Health. <https://www.thompsonhealth.com/About-Us/News-Room/New-Press-Releases/new-angiography-suite-nearing-completion>. Published 2020. Accessed February 8, 2023.
91. Betts JG, Wise J, Young KA, et al. 20.1. In: *Anatomy and Physiology*. Acton, MA: XanEdu; 2017:887-889. Access for free at <https://openstax.org/books/anatomy-and-physiology/pages/1-introduction>
92. Kraaiennest. File:Sine wave amplitude.svg – Wikimedia Commons.
https://commons.wikimedia.org/wiki/File:Sine_wave_amplitude.svg. (accessed Feb 13th, 2023).
93. Jhelebrant. File:Illustration of Crookes X-ray tube.svg – Wikimedia Commons.
https://commons.wikimedia.org/wiki/File:Illustration_of_Crookes_X-ray_tube.svg. (accessed Feb 13th, 2023).
94. Housecroft CE, Sharpe AG. 1,2. In: *Inorganic Chemistry*. Harlow, England: Pearson; 2012:1-47.
95. Alberts B. 2,10,22. In: *Molecular Biology of the Cell*. New York, NY: Garland Science; 2015:43-88, 566-594,1235-1238.
96. Ammendolia, D.A., Bement, W.M. & Brumell, J.H. Plasma membrane integrity: implications for health and disease. *BMC Biol* **19**, 71 (2021).
<https://doi.org/10.1186/s12915-021-00972-y>
97. Zain MA, Jamil RT, Siddiqui WJ. Neointimal Hyperplasia. [Updated 2022 Oct 25]. In: StatPearls [Internet]. Treasure Island (FL): StatPearls Publishing; 2022 Jan-. Available <https://www.ncbi.nlm.nih.gov/books/NBK499893/>
98. Blazek AD, Paleo BJ, Weisleder N. Plasma Membrane Repair: A Central Process for Maintaining Cellular Homeostasis. *Physiology (Bethesda)*. 2015;30(6):438-448.
doi:10.1152/physiol.00019.2015

99. Tabouillot T, Muddana HS, Butler PJ. Endothelial Cell Membrane Sensitivity to Shear Stress is Lipid Domain Dependent. *Cell Mol Bioeng.* 2011;4(2):169-181. doi:10.1007/s12195-010-0136-9
100. Atkins, P. W., & Paula, J.D. (2011). 2,11. In *Physical Chemistry for the life sciences* (pp. 69-88, 449-450). Essay, W.H. Freeman & Company.
101. Ashrafuzzaman M, Tuszynski J. 2,3. In: *Membrane Biophysics*. Berlin, Germany: Springer Berlin Heidelberg; 2013:9-33.
102. Alberts B, Johnson A, Lewis J, et al. *Molecular Biology of the Cell*. 4th edition. New York: Garland Science; 2002. The Lipid Bilayer. Available from: <https://www.ncbi.nlm.nih.gov/books/NBK26871/>
103. Fleck D, Albadawi H, Shamoun F, Knuttinen G, Naidu S, Oklu R. Catheter-directed thrombolysis of deep vein thrombosis: literature review and practice considerations. *Cardiovasc Diagn Ther.* 2017;7(Suppl 3):S228-S237. doi:10.21037/cdt.2017.09.15
104. Stolfi. File: Vorticity Figure 01 c.png – Wikimedia commons. https://commons.wikimedia.org/wiki/File:Vorticity_Figure_01_c.png (accessed February 21st, 2023).
105. Stolfi, File: Vorticity Figure 01 b.png – Wikimedia commons. https://en.wikipedia.org/wiki/File:Vorticity_Figure_01_b.png (accessed February 21st, 2023).

VITA

Kevin Rivera attended the University of North Texas in Denton, Texas, and graduated with a Bachelor of Arts degree with a major in Biology and Bachelor of Arts degree with a major in Psychology in May of 2018. He then enrolled at the University of North Texas Health Science Center in Fort Worth, Texas, and graduated in 2019 with a Master of Science in Medical Science. That same year he enrolled in the Burnett School of Medicine at Texas Christian University for work towards a Doctorate of Medicine. Upon graduation, Kevin will continue his education as a resident physician in emergency medicine.

ABSTRACT

MAY-THURNER SYNDROME AND OTHER PELVIC VEIN COMPRESSION SYNDROMES: EARLY DETECTION WITH DUPLEX ULTRASOUND AND VENOGRAPHY

By Kevin Joel Rivera, M.D., 2023

Anne Burnett Marion School of Medicine

Texas Christian University

Major Professor: Sam Ahn M.D., Professor of Medicine

Research Question

This study aims to identify duplex ultrasound and venography imaging findings that can identify May-Thurner Syndrome (MTS) and other pelvic vein compression syndromes at an earlier stage of disease for adults with lower extremity leg pain and edema. This aim is achieved by investigating if reflux, abnormal flow patterns, spontaneity, phasicity, or competency on duplex ultrasound predicts venous compression on intravascular ultrasound (IVUS). Spontaneity, compressibility, and competency on duplex ultrasound at the common femoral vein are also researched for predictability of venous compression on IVUS. Compression on venography is also evaluated for its predictability of venous compression on IVUS.

Background, Significance, and Rationale

May-Thurner Syndrome (MTS) and other pelvic vein compression syndromes are usually diagnosed late in the disease course given the absence of reliable non-invasive diagnostic imaging. This leads to worse clinical outcomes which is on a spectrum of venous ulcers to recurrent thromboses or amputation. Additionally, this contributes to the economic impact of chronic venous diseases that is estimated to cost \$5 billion in the United States. Research in biofluid mechanics and vascular pathology have demonstrated that alterations in intravascular hemodynamics contribute to pathophysiological changes and adaptations. A small study demonstrated that MTS might be detected earlier than is currently practiced by focusing on specific duplex ultrasound findings. The present investigation builds on both the small study and established physical principles of fluids and sound to shape its theoretical basis and clinical application to the imaging modalities of interest.

Materials and Methods

This study selected 237 patients over a 7-year period that presented with lower extremity pain and edema who were also found to have venous compression. This study occurred at a single center that contained an endovascular AngioSuite in Dallas, Texas and patient data was obtained from the electronic medical record, duplex ultrasound studies, venography studies, and IVUS studies. Since most variables of interest were categorical, data was analyzed using logistic regression on the R statistical software and the criteria to reject the null hypotheses was set to an alpha level of $p < 0.05$.

Results

Statistical measures between males and females show nearly symmetric and platykurtic distributions with similar risk factors. Data from Venography and IVUS showed high relative frequencies of $\geq 50\%$ stenosis for multiple vessels. Data analysis identified that spontaneity that is either reduced, absent, or pulsatile, compressibility that is reduced, and the presence of thrombosis predict compression on venography. Analysis also indicated that the absence of reflux and normal competency on duplex ultrasound predict compression on IVUS.

Conclusions

In conclusion, MTS and other pelvic vein compression syndromes are often diagnosed late which causes poor clinical outcomes and increases healthcare expenditures. This single center study investigated imaging modalities on the basis of a small previous study and principles of physics, and suggests predictors of $\geq 50\%$ stenosis on IVUS.

Appendix A: R Data Output

```
knitr::opts_chunk$set(echo = TRUE)
```

```
library(dplyr)
```

```
##  
## Attaching package: 'dplyr'
```

```
## The following objects are masked from 'package:stats':  
##  
##   filter, lag
```

```
## The following objects are masked from 'package:base':  
##  
##   intersect, setdiff, setequal, union
```

```

library(stats)

dfw <- read.csv("KevinData2.csv")
dfw <- dfw %>% mutate(RLE_US_CFV_Overall=RLE_US_CFV_Overall-1,RLE_Venogram_CFV_Percent_Stenosis=RLE_Venogram_CFV_Percent_Stenosis-12)
dfw <- dfw %>% mutate(RLE_Venogram_CFV_Compression=RLE_Venogram_CFV_Compression-1, RLE_Venogram_CFV_Vessel_Patency=RLE_Venogram_CFV_Vessel_Patency-1)

dfw <- dfw %>% mutate(RLE_IVUS_CFV_percent_stenosis=RLE_IVUS_CFV_percent_stenosis-12)
dfw <- dfw %>% mutate(RLE_US_CFV_Reflux_With_Inspiration=RLE_US_CFV_Reflux_With_Inspiration-1)

dfw <- dfw %>% mutate(LLE_US_CFV_Overall=LLE_US_CFV_Overall-1,LLE_Venogram_CFV_Percent_Stenosis=LLE_Venogram_CFV_Percent_Stenosis-12)
dfw <- dfw %>% mutate(LLE_Venogram_CFV_Compression=LLE_Venogram_CFV_Compression-1, LLE_Venogram_CFV_Vessel_Patency=LLE_Venogram_CFV_Vessel_Patency-1)
dfw <- dfw %>% mutate(LLE_IVUS_CFV_percent_stenosis=LLE_IVUS_CFV_percent_stenosis-12)
dfw <- dfw %>% mutate(LLE_US_CFV_Reflux_with_inspiration=LLE_US_CFV_Reflux_with_inspiration-1)

RefluxIVUS <- glm(RLE_IVUS_CFV_percent_stenosis~RLE_US_CFV_Reflux_With_Inspiration,family="binomial",data=dfw)
R1 <- dplyr::select(dfw,c(RLE_US_CFV_Reflux_With_Inspiration,RLE_IVUS_CFV_percent_stenosis))
R1 <- R1 %>% filter(!is.na(RLE_US_CFV_Reflux_With_Inspiration)) %>% filter(!is.na(RLE_IVUS_CFV_percent_stenosis))

RefluxIVUS <- glm(LLE_IVUS_CFV_percent_stenosis~LLE_US_CFV_Reflux_with_inspiration,family="binomial",data=dfw)
R1 <- dplyr::select(dfw,c(LLE_US_CFV_Reflux_with_inspiration,LLE_IVUS_CFV_percent_stenosis))
R1 <- R1 %>% filter(!is.na(LLE_US_CFV_Reflux_with_inspiration)) %>% filter(!is.na(LLE_IVUS_CFV_percent_stenosis))

Flow <- glm(RLE_IVUS_CFV_percent_stenosis~as.factor(RLE_US_CFV_Flow),family="binomial",data=dfw)
flow2 <- glm(RLE_IVUS_CFV_percent_stenosis~(RLE_US_CFV_Flow>1),family="binomial",data=dfw)
Flow <- glm(LLE_IVUS_CFV_percent_stenosis~as.factor(LLE_US_CFV_Flow),family="binomial",data=dfw)
flow2 <- glm(LLE_IVUS_CFV_percent_stenosis~(LLE_US_CFV_Flow!=4),family="binomial",data=dfw)
# IVUSsten <- glm(RLE_IVUS_CFV_percent_stenosis~RLE_US_CFV_Overall,family="binomial",data=dfw)

Compress <- glm(RLE_IVUS_CFV_percent_stenosis~as.factor(RLE_US_CFV_Compressibility),family="binomial",data=dfw)
Compress2 <- glm(RLE_IVUS_CFV_percent_stenosis~(RLE_US_CFV_Compressibility>1),family="binomial",data=dfw)
Compress <- glm(LLE_IVUS_CFV_percent_stenosis~as.factor(LLE_US_CFV_Compressibility),family="binomial",data=dfw)

Th <- glm(RLE_IVUS_CFV_percent_stenosis~as.factor(RLE_US_CFV_Thrombosis),family="binomial",data=dfw)
Th2 <- glm(RLE_IVUS_CFV_percent_stenosis~(RLE_US_CFV_Thrombosis>1),family="binomial",data=dfw)
Th <- glm(LLE_IVUS_CFV_percent_stenosis~as.factor(LLE_US_CFV_Thrombosis),family="binomial",data=dfw)

Sp <- glm(RLE_IVUS_CFV_percent_stenosis~as.factor(RLE_US_CFV_Spontaneity),family="binomial",data=dfw)
Sp2 <- glm(RLE_IVUS_CFV_percent_stenosis~(RLE_US_CFV_Spontaneity>1),family="binomial",data=dfw)
Sp <- glm(LLE_IVUS_CFV_percent_stenosis~as.factor(LLE_US_CFV_Spontaneity),family="binomial",data=dfw)
Sp2 <- glm(LLE_IVUS_CFV_percent_stenosis~(LLE_US_CFV_Spontaneity>1),family="binomial",data=dfw)

Ph <- glm(RLE_IVUS_CFV_percent_stenosis~as.factor(RLE_US_CFV_Phasicity),family="binomial",data=dfw)
Ph2 <- glm(RLE_IVUS_CFV_percent_stenosis~(RLE_US_CFV_Phasicity>1),family="binomial",data=dfw)
Ph <- glm(LLE_IVUS_CFV_percent_stenosis~as.factor(LLE_US_CFV_Phasicity),family="binomial",data=dfw)
Ph2 <- glm(LLE_IVUS_CFV_percent_stenosis~(LLE_US_CFV_Phasicity>1),family="binomial",data=dfw)
Ph2 <- glm(LLE_IVUS_CFV_percent_stenosis~(LLE_US_CFV_Phasicity!=11),family="binomial",data=dfw)

Aug <- glm(RLE_IVUS_CFV_percent_stenosis~as.factor(RLE_US_CFV_Augmentation),family="binomial",data=dfw)
Aug2 <- glm(RLE_IVUS_CFV_percent_stenosis~(RLE_US_CFV_Augmentation>1),family="binomial",data=dfw)
Aug <- glm(LLE_IVUS_CFV_percent_stenosis~as.factor(LLE_US_CFV_Augmentation),family="binomial",data=dfw)
Aug2 <- glm(LLE_IVUS_CFV_percent_stenosis~(LLE_US_CFV_Augmentation>1),family="binomial",data=dfw)

```



```

Comp <- glm(RLE_IVUS_CFV_percent_stenosis~as.factor(RLE_US_CFV_Competency),family="binomial",data=dfw)
Comp <- glm(LLE_IVUS_CFV_percent_stenosis~as.factor(LLE_US_CFV_Competency),family="binomial",data=dfw)

#RLE CFV US Overall vs. Venogram Stenosis
# R1 <- dplyr::select(dfw,c(RLE_US_CFV_Overall,RLE_Venogram_CFV_Percent_Stenosis))
# R1 <- R1 %>% filter(!is.na(RLE_US_CFV_Overall)) %>% filter(!is.na(RLE_Venogram_CFV_Percent_Stenosis))
# Rtable <- table(R1$RLE_US_CFV_Overall,R1$RLE_Venogram_CFV_Percent_Stenosis)
# chisq.test(Rtable)

#RLE CFV US Overall vs. Venogram Compression
# R1 <- dplyr::select(dfw,c(RLE_US_CFV_Overall,RLE_Venogram_CFV_Compression))
# R1 <- R1 %>% filter(!is.na(RLE_US_CFV_Overall)) %>% filter(!is.na(RLE_Venogram_CFV_Compression))
# Rtable <- table(R1$RLE_US_CFV_Overall,R1$RLE_Venogram_CFV_Compression)
# Rtable
# chisq.test(Rtable)

stenUS <- glm(RLE_Venogram_CFV_Percent_Stenosis~as.factor(RLE_US_CFV_Overall),family="binomial",data=dfw)
# CompUS <- glm(RLE_Venogram_CFV_Compression~RLE_US_CFV_Overall,family="binomial",data=dfw)
# PatUS <- glm(RLE_Venogram_CFV_Vessel_Patency~RLE_US_CFV_Overall,family="binomial",data=dfw)

IVUSsten <- glm(LLE_IVUS_CFV_percent_stenosis~as.factor(LLE_US_CFV_Overall),family="binomial",data=dfw)

#
# stenUS <- glm(LLE_Venogram_CFV_Percent_Stenosis~LLE_US_CFV_Overall,family="binomial",data=dfw)
# CompUS <- glm(LLE_Venogram_CFV_Compression~LLE_US_CFV_Overall,family="binomial",data=dfw)
# PatUS <- glm(LLE_Venogram_CFV_Vessel_Patency~LLE_US_CFV_Overall,family="binomial",data=dfw)
RefluxVen <- glm(RLE_Venogram_CFV_Percent_Stenosis~as.factor(RLE_US_CFV_Reflux_With_Inspiration),family="binomial",data=dfw)
summary(RefluxVen)

```

```

##
## Call:
## glm(formula = RLE_Venogram_CFV_Percent_Stenosis ~ as.factor(RLE_US_CFV_Reflux_With_Inspiration),
##      family = "binomial", data = dfw)
##
## Deviance Residuals:
##      Min       1Q   Median       3Q      Max
## -1.051  -1.051  -1.032   1.310   1.330
##
## Coefficients:
##              Estimate Std. Error z value
## (Intercept)      -0.30538     0.20336  -1.502
## as.factor(RLE_US_CFV_Reflux_With_Inspiration)1 -0.04602     0.36197  -0.127
##
##              Pr(>|z|)
## (Intercept)           0.133
## as.factor(RLE_US_CFV_Reflux_With_Inspiration)1    0.899
##
## (Dispersion parameter for binomial family taken to be 1)
##
## Null deviance: 197.35  on 144  degrees of freedom
## Residual deviance: 197.33  on 143  degrees of freedom
## (97 observations deleted due to missingness)
## AIC: 201.33
##
## Number of Fisher Scoring iterations: 4

```

```

RefluxVen <- glm(LLE_Venogram_CFV_Percent_Stenosis~LLE_US_CFV_Reflux_with_inspiration,family="binomial",data=dfw)
summary(RefluxVen)

```

```
##
## Call:
## glm(formula = LLE_Venogram_CFV_Percent_Stenosis ~ LLE_US_CFV_Reflux_with_inspiration,
##      family = "binomial", data = dfw)
##
## Deviance Residuals:
##      Min       1Q   Median       3Q      Max
## -1.0727  -1.0727  -0.8157   1.2858   1.5889
##
## Coefficients:
##              Estimate Std. Error z value Pr(>|z|)
## (Intercept)      -0.2513     0.1905  -1.319   0.1870
## LLE_US_CFV_Reflux_with_inspiration -0.6782     0.3595  -1.886   0.0592 .
## ---
## Signif. codes:  0 '***' 0.001 '**' 0.01 '*' 0.05 '.' 0.1 ' ' 1
##
## (Dispersion parameter for binomial family taken to be 1)
##
##      Null deviance: 220.37  on 164  degrees of freedom
## Residual deviance: 216.66  on 163  degrees of freedom
## (77 observations deleted due to missingness)
## AIC: 220.66
##
## Number of Fisher Scoring iterations: 4
```

```
Flow <- glm(RLE_Venogram_CFV_Percent_Stenosis~as.factor(RLE_US_CFV_Flow),family="binomial",data=dfw)
summary(Flow)
```

```
##
## Call:
## glm(formula = RLE_Venogram_CFV_Percent_Stenosis ~ as.factor(RLE_US_CFV_Flow),
##      family = "binomial", data = dfw)
##
## Deviance Residuals:
##      Min       1Q   Median       3Q      Max
## -1.1501  -1.0466  -0.8855   1.3141   1.5829
##
## Coefficients:
##              Estimate Std. Error z value Pr(>|z|)
## (Intercept)      -0.3159     0.2223  -1.421   0.155
## as.factor(RLE_US_CFV_Flow)3  0.2513     0.4226   0.595   0.552
## as.factor(RLE_US_CFV_Flow)4 -0.6004     0.6320  -0.950   0.342
## as.factor(RLE_US_CFV_Flow)5 -0.2438     0.6650  -0.367   0.714
## as.factor(RLE_US_CFV_Flow)6 15.8819    840.2742   0.019   0.985
##
## (Dispersion parameter for binomial family taken to be 1)
##
##      Null deviance: 194.03  on 141  degrees of freedom
## Residual deviance: 187.13  on 137  degrees of freedom
## (100 observations deleted due to missingness)
## AIC: 197.13
##
## Number of Fisher Scoring iterations: 14
```

```
flow2 <- glm(RLE_Venogram_CFV_Percent_Stenosis~(RLE_US_CFV_Flow>1),family="binomial",data=dfw)
summary(flow2)
```

```
##
## Call:
## glm(formula = RLE_Venogram_CFV_Percent_Stenosis ~ (RLE_US_CFV_Flow >
## 1), family = "binomial", data = dfw)
##
## Deviance Residuals:
##   Min       1Q   Median       3Q      Max
## -1.078  -1.047  -1.047   1.280   1.314
##
## Coefficients:
##              Estimate Std. Error z value Pr(>|z|)
## (Intercept)      -0.31585    0.22227  -1.421   0.155
## RLE_US_CFV_Flow > 1TRUE  0.07744    0.34376   0.225   0.822
##
## (Dispersion parameter for binomial family taken to be 1)
##
##   Null deviance: 194.03  on 141  degrees of freedom
## Residual deviance: 193.98  on 140  degrees of freedom
## (100 observations deleted due to missingness)
## AIC: 197.98
##
## Number of Fisher Scoring iterations: 4
```

```
Flow <- glm(LLE_Venogram_CFV_Percent_Stenosis~as.factor(LLE_US_CFV_Flow),family="binomial",data=dfw)
summary(Flow)
```

```
##
## Call:
## glm(formula = LLE_Venogram_CFV_Percent_Stenosis ~ as.factor(LLE_US_CFV_Flow),
## family = "binomial", data = dfw)
##
## Deviance Residuals:
##   Min       1Q   Median       3Q      Max
## -1.0108  -0.9914  -0.9005   1.3756   1.5252
##
## Coefficients:
##              Estimate Std. Error z value Pr(>|z|)
## (Intercept)      -0.45474    0.22256  -2.043   0.041 *
## as.factor(LLE_US_CFV_Flow)3  0.04927    0.37700   0.131   0.896
## as.factor(LLE_US_CFV_Flow)4 -0.23841    0.54730  -0.436   0.663
## as.factor(LLE_US_CFV_Flow)5 -0.33372    0.58347  -0.572   0.567
## as.factor(LLE_US_CFV_Flow)6  16.02080  1029.12149   0.016   0.988
## ---
## Signif. codes:  0 '***' 0.001 '**' 0.01 '*' 0.05 '.' 0.1 ' ' 1
##
## (Dispersion parameter for binomial family taken to be 1)
##
##   Null deviance: 221.35  on 165  degrees of freedom
## Residual deviance: 216.91  on 161  degrees of freedom
## (76 observations deleted due to missingness)
## AIC: 226.91
##
## Number of Fisher Scoring iterations: 14
```

```
flow2 <- glm(LLE_Venogram_CFV_Percent_Stenosis~(LLE_US_CFV_Flow!=4),family="binomial",data=dfw)
summary(flow2)
```

```
##
## Call:
## glm(formula = LLE_Venogram_CFV_Percent_Stenosis ~ (LLE_US_CFV_Flow !=
## 4), family = "binomial", data = dfw)
##
## Deviance Residuals:
##   Min       1Q   Median       3Q      Max
## -0.9974 -0.9974 -0.9974  1.3688  1.4823
##
## Coefficients:
##              Estimate Std. Error z value Pr(>|z|)
## (Intercept)      -0.6931    0.5000  -1.386   0.166
## LLE_US_CFV_Flow != 4TRUE  0.2538    0.5276   0.481   0.631
##
## (Dispersion parameter for binomial family taken to be 1)
##
## Null deviance: 221.35  on 165  degrees of freedom
## Residual deviance: 221.11  on 164  degrees of freedom
## (76 observations deleted due to missingness)
## AIC: 225.11
##
## Number of Fisher Scoring iterations: 4
```

```
Compress <- glm(RLE_Venogram_CFV_Percent_Stenosis~as.factor(RLE_US_CFV_Compressibility),family="binomial",data=dfw)
summary(Compress)
```

```
##
## Call:
## glm(formula = RLE_Venogram_CFV_Percent_Stenosis ~ as.factor(RLE_US_CFV_Compressibility),
## family = "binomial", data = dfw)
##
## Deviance Residuals:
##   Min       1Q   Median       3Q      Max
## -2.0393 -0.9959 -0.9959  1.3705  1.3705
##
## Coefficients:
##              Estimate Std. Error z value Pr(>|z|)
## (Intercept)      -0.4432    0.1777  -2.494   0.0126 *
## as.factor(RLE_US_CFV_Compressibility)7  2.3891    1.0837   2.205   0.0275 *
## as.factor(RLE_US_CFV_Compressibility)8  16.0093  1029.1215   0.016   0.9876
## ---
## Signif. codes:  0 '***' 0.001 '**' 0.01 '*' 0.05 '.' 0.1 ' ' 1
##
## (Dispersion parameter for binomial family taken to be 1)
##
## Null deviance: 195.14  on 142  degrees of freedom
## Residual deviance: 184.03  on 140  degrees of freedom
## (99 observations deleted due to missingness)
## AIC: 190.03
##
## Number of Fisher Scoring iterations: 14
```

```
Compress2 <- glm(RLE_Venogram_CFV_Percent_Stenosis~(RLE_US_CFV_Compressibility>1),family="binomial",data=dfw)
summary(Compress2)
```

```
##
## Call:
## glm(formula = RLE_Venogram_CFV_Percent_Stenosis ~ (RLE_US_CFV_Compressibility >
## 1), family = "binomial", data = dfw)
##
## Deviance Residuals:
##   Min       1Q   Median       3Q      Max
## -2.1460  -0.9959  -0.9959   1.3705   1.3705
##
## Coefficients:
##              Estimate Std. Error z value Pr(>|z|)
## (Intercept)      -0.4432     0.1777  -2.494  0.0126 *
## RLE_US_CFV_Compressibility > 1TRUE  2.6404     1.0689   2.470  0.0135 *
## ---
## Signif. codes:  0 '***' 0.001 '**' 0.01 '*' 0.05 '.' 0.1 ' ' 1
##
## (Dispersion parameter for binomial family taken to be 1)
##
##   Null deviance: 195.14  on 142  degrees of freedom
## Residual deviance: 184.50  on 141  degrees of freedom
## (99 observations deleted due to missingness)
## AIC: 188.5
##
## Number of Fisher Scoring iterations: 4
```

```
Compress <- glm(LLE_Venogram_CFV_Percent_Stenosis~as.factor(LLE_US_CFV_Compressibility),family="binomial",data=dfw)
summary(Compress)
```

```
##
## Call:
## glm(formula = LLE_Venogram_CFV_Percent_Stenosis ~ as.factor(LLE_US_CFV_Compressibility),
##   family = "binomial", data = dfw)
##
## Deviance Residuals:
##   Min       1Q   Median       3Q      Max
## -1.7344  -0.9393  -0.9393   1.4359   1.4359
##
## Coefficients:
##              Estimate Std. Error z value Pr(>|z|)
## (Intercept)      -0.5898     0.1666  -3.54  0.0004 ***
## as.factor(LLE_US_CFV_Compressibility)7  1.8425     0.8189   2.25  0.0245 *
## ---
## Signif. codes:  0 '***' 0.001 '**' 0.01 '*' 0.05 '.' 0.1 ' ' 1
##
## (Dispersion parameter for binomial family taken to be 1)
##
##   Null deviance: 220.39  on 165  degrees of freedom
## Residual deviance: 214.10  on 164  degrees of freedom
## (76 observations deleted due to missingness)
## AIC: 218.1
##
## Number of Fisher Scoring iterations: 4
```

```
table(dfw$RLE_Venogram_CFV_Percent_Stenosis,dfw$RLE_US_CFV_Compressibility)
```

```
##
##   1 7 8
## 0 81 1 0
## 1 52 7 2
```

```
table(dfw$LLE_Venogram_CFV_Percent_Stenosis,dfw$LLE_US_CFV_Compressibility)
```

```
##
##      1  7  8
##    0 101  2  0
##    1  56  7  0
```

```
Th <- glm(RLE_Venogram_CFV_Percent_Stenosis~as.factor(RLE_US_CFV_Thrombosis),family="binomial",data=dfw)
summary(Th)
```

```
##
## Call:
## glm(formula = RLE_Venogram_CFV_Percent_Stenosis ~ as.factor(RLE_US_CFV_Thrombosis),
##      family = "binomial", data = dfw)
##
## Deviance Residuals:
##      Min       1Q   Median       3Q      Max
## -2.1899  -0.9883  -0.9883   1.3791   1.3791
##
## Coefficients:
##              Estimate Std. Error z value Pr(>|z|)
## (Intercept)    -0.4626    0.1788  -2.588  0.00965 **
## as.factor(RLE_US_CFV_Thrombosis)9  2.7652    1.0637   2.600  0.00933 **
## ---
## Signif. codes:  0 '***' 0.001 '**' 0.01 '*' 0.05 '.' 0.1 ' ' 1
##
## (Dispersion parameter for binomial family taken to be 1)
##
## Null deviance: 195.14 on 142 degrees of freedom
## Residual deviance: 182.81 on 141 degrees of freedom
## (99 observations deleted due to missingness)
## AIC: 186.81
##
## Number of Fisher Scoring iterations: 4
```

```
Th2 <- glm(RLE_Venogram_CFV_Percent_Stenosis~(RLE_US_CFV_Thrombosis>1),family="binomial",data=dfw)
summary(Th2)
```

```
##
## Call:
## glm(formula = RLE_Venogram_CFV_Percent_Stenosis ~ (RLE_US_CFV_Thrombosis >
##      1), family = "binomial", data = dfw)
##
## Deviance Residuals:
##      Min       1Q   Median       3Q      Max
## -2.1899  -0.9883  -0.9883   1.3791   1.3791
##
## Coefficients:
##              Estimate Std. Error z value Pr(>|z|)
## (Intercept)    -0.4626    0.1788  -2.588  0.00965 **
## RLE_US_CFV_Thrombosis > 1TRUE  2.7652    1.0637   2.600  0.00933 **
## ---
## Signif. codes:  0 '***' 0.001 '**' 0.01 '*' 0.05 '.' 0.1 ' ' 1
##
## (Dispersion parameter for binomial family taken to be 1)
##
## Null deviance: 195.14 on 142 degrees of freedom
## Residual deviance: 182.81 on 141 degrees of freedom
## (99 observations deleted due to missingness)
## AIC: 186.81
##
## Number of Fisher Scoring iterations: 4
```

```
Th <- glm(LLE_Venogram_CFV_Percent_Stenosis~as.factor(LLE_US_CFV_Thrombosis),family="binomial",data=dfw)
summary(Th)
```

```
##
## Call:
## glm(formula = LLE_Venogram_CFV_Percent_Stenosis ~ as.factor(LLE_US_CFV_Thrombosis),
##      family = "binomial", data = dfw)
##
## Deviance Residuals:
##      Min       1Q   Median       3Q      Max
## -1.7941  -0.9393  -0.9393   1.4359   1.4359
##
## Coefficients:
##              Estimate Std. Error z value Pr(>|z|)
## (Intercept)      -0.5898    0.1666  -3.540  0.0004 ***
## as.factor(LLE_US_CFV_Thrombosis)9  1.9761    0.8079   2.446  0.0145 *
## ---
## Signif. codes:  0 '***' 0.001 '**' 0.01 '*' 0.05 '.' 0.1 ' ' 1
##
## (Dispersion parameter for binomial family taken to be 1)
##
##      Null deviance: 222.32 on 166 degrees of freedom
## Residual deviance: 214.58 on 165 degrees of freedom
## (75 observations deleted due to missingness)
## AIC: 218.58
##
## Number of Fisher Scoring iterations: 4
```

```
table(dfw$RLE_Venogram_CFV_Percent_Stenosis,dfw$RLE_US_CFV_Thrombosis)
```

```
##
##      1  9
## 0 81  1
## 1 51 10
```

```
table(dfw$LLE_Venogram_CFV_Percent_Stenosis,dfw$LLE_US_CFV_Thrombosis)
```

```
##
##      1  9
## 0 101  2
## 1  56  8
```

```
Sp <- glm(RLE_Venogram_CFV_Percent_Stenosis~as.factor(RLE_US_CFV_Spontaneity),family="binomial",data=dfw)
summary(Sp)
```

```
##
## Call:
## glm(formula = RLE_Venogram_CFV_Percent_Stenosis ~ as.factor(RLE_US_CFV_Spontaneity),
##      family = "binomial", data = dfw)
##
## Deviance Residuals:
##      Min       1Q   Median       3Q      Max
## -1.3018  -0.9751  -0.9751   1.3942   1.3942
##
## Coefficients:
##              Estimate Std. Error z value Pr(>|z|)
## (Intercept)      -0.4964    0.1957  -2.537  0.0112 *
## as.factor(RLE_US_CFV_Spontaneity)7    0.7841    0.4291   1.827  0.0677 .
## as.factor(RLE_US_CFV_Spontaneity)8   17.0625  1385.3778   0.012  0.9902
## as.factor(RLE_US_CFV_Spontaneity)10 -16.0696  2399.5447  -0.007  0.9947
## ---
## Signif. codes:  0 '***' 0.001 '**' 0.01 '*' 0.05 '.' 0.1 ' ' 1
##
## (Dispersion parameter for binomial family taken to be 1)
##
##      Null deviance: 195.14 on 142 degrees of freedom
## Residual deviance: 185.49 on 139 degrees of freedom
## (99 observations deleted due to missingness)
## AIC: 193.49
##
## Number of Fisher Scoring iterations: 15
```

```
Sp2 <- glm(RLE_Venogram_CFV_Percent_Stenosis~(RLE_US_CFV_Spontaneity>1),family="binomial",data=dfw)
summary(Sp2)
```

```
##
## Call:
## glm(formula = RLE_Venogram_CFV_Percent_Stenosis ~ (RLE_US_CFV_Spontaneity >
##      1), family = "binomial", data = dfw)
##
## Deviance Residuals:
##      Min       1Q   Median       3Q      Max
## -1.3422  -0.9751  -0.9751   1.3942   1.3942
##
## Coefficients:
##              Estimate Std. Error z value Pr(>|z|)
## (Intercept)      -0.4964    0.1957  -2.537  0.0112 *
## RLE_US_CFV_Spontaneity > 1TRUE  0.8759    0.4097   2.138  0.0325 *
## ---
## Signif. codes:  0 '***' 0.001 '**' 0.01 '*' 0.05 '.' 0.1 ' ' 1
##
## (Dispersion parameter for binomial family taken to be 1)
##
##      Null deviance: 195.14 on 142 degrees of freedom
## Residual deviance: 190.47 on 141 degrees of freedom
## (99 observations deleted due to missingness)
## AIC: 194.47
##
## Number of Fisher Scoring iterations: 4
```

```
Sp <- glm(LLE_Venogram_CFV_Percent_Stenosis~as.factor(LLE_US_CFV_Spontaneity),family="binomial",data=dfw)
summary(Sp)
```



```
##
## Call:
## glm(formula = LLE_Venogram_CFV_Percent_Stenosis ~ as.factor(LLE_US_CFV_Spontaneity),
##      family = "binomial", data = dfw)
##
## Deviance Residuals:
##      Min       1Q   Median       3Q      Max
## -1.0021  -0.9448  -0.9448   1.4294   1.4294
##
## Coefficients:
##              Estimate Std. Error z value Pr(>|z|)
## (Intercept)      -0.5754    0.1863  -3.088  0.00202 **
## as.factor(LLE_US_CFV_Spontaneity)7    0.1479    0.3806   0.389  0.69755
## as.factor(LLE_US_CFV_Spontaneity)8   17.1414  1696.7344   0.010  0.99194
## as.factor(LLE_US_CFV_Spontaneity)10  17.1414  1696.7344   0.010  0.99194
## ---
## Signif. codes:  0 '***' 0.001 '**' 0.01 '*' 0.05 '.' 0.1 ' ' 1
##
## (Dispersion parameter for binomial family taken to be 1)
##
##      Null deviance: 222.32  on 166  degrees of freedom
## Residual deviance: 214.34  on 163  degrees of freedom
## (75 observations deleted due to missingness)
## AIC: 222.34
##
## Number of Fisher Scoring iterations: 15
```

```
Sp2 <- glm(LLE_Venogram_CFV_Percent_Stenosis~(LLE_US_CFV_Spontaneity>1),family="binomial",data=dfw)
summary(Sp2)
```

```
##
## Call:
## glm(formula = LLE_Venogram_CFV_Percent_Stenosis ~ (LLE_US_CFV_Spontaneity >
##      1), family = "binomial", data = dfw)
##
## Deviance Residuals:
##      Min       1Q   Median       3Q      Max
## -1.0974  -0.9448  -0.9448   1.4294   1.4294
##
## Coefficients:
##              Estimate Std. Error z value Pr(>|z|)
## (Intercept)      -0.5754    0.1863  -3.088  0.00202 **
## LLE_US_CFV_Spontaneity > 1TRUE    0.3843    0.3617   1.062  0.28801
## ---
## Signif. codes:  0 '***' 0.001 '**' 0.01 '*' 0.05 '.' 0.1 ' ' 1
##
## (Dispersion parameter for binomial family taken to be 1)
##
##      Null deviance: 222.32  on 166  degrees of freedom
## Residual deviance: 221.20  on 165  degrees of freedom
## (75 observations deleted due to missingness)
## AIC: 225.2
##
## Number of Fisher Scoring iterations: 4
```

```
table(dfw$RLE_Venogram_CFV_Percent_Stenosis,dfw$RLE_US_CFV_Spontaneity)
```

```
##
##      1  7  8 10
## 0 69 12 0  1
## 1 42 16 3  0
```

```
Ph <- glm(RLE_Venogram_CFV_Percent_Stenosis~as.factor(RLE_US_CFV_Phasicity),family="binomial",data=dfw)
summary(Ph)
```

```
##
## Call:
## glm(formula = RLE_Venogram_CFV_Percent_Stenosis ~ as.factor(RLE_US_CFV_Phasicity),
##      family = "binomial", data = dfw)
##
## Deviance Residuals:
##      Min       1Q   Median       3Q      Max
## -1.2735  -1.0068  -0.8657   1.3582   1.5252
##
## Coefficients:
##              Estimate Std. Error z value Pr(>|z|)
## (Intercept)      -0.4155     0.2243  -1.853  0.0639 .
## as.factor(RLE_US_CFV_Phasicity)7    0.6387     0.7073   0.903  0.3666
## as.factor(RLE_US_CFV_Phasicity)8   15.9816    1029.1215   0.016  0.9876
## as.factor(RLE_US_CFV_Phasicity)10   0.3549     0.4143   0.857  0.3916
## as.factor(RLE_US_CFV_Phasicity)11  -0.3729     0.5841  -0.638  0.5232
## ---
## Signif. codes:  0 '***' 0.001 '**' 0.01 '*' 0.05 '.' 0.1 ' ' 1
##
## (Dispersion parameter for binomial family taken to be 1)
##
## Null deviance: 195.14  on 142  degrees of freedom
## Residual deviance: 189.51  on 138  degrees of freedom
## (99 observations deleted due to missingness)
## AIC: 199.51
##
## Number of Fisher Scoring iterations: 14
```

```
Ph2 <- glm(RLE_Venogram_CFV_Percent_Stenosis~(RLE_US_CFV_Phasicity>1),family="binomial",data=dfw)
summary(Ph2)
```

```
##
## Call:
## glm(formula = RLE_Venogram_CFV_Percent_Stenosis ~ (RLE_US_CFV_Phasicity >
##      1), family = "binomial", data = dfw)
##
## Deviance Residuals:
##      Min       1Q   Median       3Q      Max
## -1.121  -1.007  -1.007   1.235   1.358
##
## Coefficients:
##              Estimate Std. Error z value Pr(>|z|)
## (Intercept)      -0.4155     0.2243  -1.853  0.0639 .
## RLE_US_CFV_Phasicity > 1TRUE   0.2820     0.3424   0.823  0.4103
## ---
## Signif. codes:  0 '***' 0.001 '**' 0.01 '*' 0.05 '.' 0.1 ' ' 1
##
## (Dispersion parameter for binomial family taken to be 1)
##
## Null deviance: 195.14  on 142  degrees of freedom
## Residual deviance: 194.47  on 141  degrees of freedom
## (99 observations deleted due to missingness)
## AIC: 198.47
##
## Number of Fisher Scoring iterations: 4
```

```
Ph <- glm(LLE_Venogram_CFV_Percent_Stenosis~as.factor(LLE_US_CFV_Phasicity),family="binomial",data=dfw)
summary(Ph)
```

```
##
## Call:
## glm(formula = LLE_Venogram_CFV_Percent_Stenosis ~ as.factor(LLE_US_CFV_Phasicity),
##      family = "binomial", data = dfw)
##
## Deviance Residuals:
##      Min       1Q   Median       3Q      Max
## -1.0769  -0.9914  -0.9123   1.3756   1.4680
##
## Coefficients:
##              Estimate Std. Error z value Pr(>|z|)
## (Intercept)      -0.45474    0.22256  -2.043   0.041 *
## as.factor(LLE_US_CFV_Phasicity)7  0.04927    0.68279   0.072   0.942
## as.factor(LLE_US_CFV_Phasicity)10 -0.20666    0.37986  -0.544   0.586
## as.factor(LLE_US_CFV_Phasicity)11  0.21357    0.46029   0.464   0.643
## ---
## Signif. codes:  0 '***' 0.001 '**' 0.01 '*' 0.05 '.' 0.1 ' ' 1
##
## (Dispersion parameter for binomial family taken to be 1)
##
##      Null deviance: 222.32  on 166  degrees of freedom
## Residual deviance: 221.59  on 163  degrees of freedom
## (75 observations deleted due to missingness)
## AIC: 229.59
##
## Number of Fisher Scoring iterations: 4
```

```
Ph2 <- glm(LLE_Venogram_CFV_Percent_Stenosis~(LLE_US_CFV_Phasicity>1),family="binomial",data=dfw)
summary(Ph2)
```

```
##
## Call:
## glm(formula = LLE_Venogram_CFV_Percent_Stenosis ~ (LLE_US_CFV_Phasicity >
##      1), family = "binomial", data = dfw)
##
## Deviance Residuals:
##      Min       1Q   Median       3Q      Max
## -0.9914  -0.9914  -0.9746   1.3756   1.3948
##
## Coefficients:
##              Estimate Std. Error z value Pr(>|z|)
## (Intercept)      -0.4547    0.2226  -2.043   0.041 *
## LLE_US_CFV_Phasicity > 1TRUE  -0.0431    0.3184  -0.135   0.892
## ---
## Signif. codes:  0 '***' 0.001 '**' 0.01 '*' 0.05 '.' 0.1 ' ' 1
##
## (Dispersion parameter for binomial family taken to be 1)
##
##      Null deviance: 222.32  on 166  degrees of freedom
## Residual deviance: 222.30  on 165  degrees of freedom
## (75 observations deleted due to missingness)
## AIC: 226.3
##
## Number of Fisher Scoring iterations: 4
```

```
Ph2 <- glm(LLE_Venogram_CFV_Percent_Stenosis~(LLE_US_CFV_Phasicity!=11),family="binomial",data=dfw)
summary(Ph2)
```

```
##
## Call:
## glm(formula = LLE_Venogram_CFV_Percent_Stenosis ~ (LLE_US_CFV_Phasicity !=
## 11), family = "binomial", data = dfw)
##
## Deviance Residuals:
##   Min       1Q   Median       3Q      Max
## -1.0769  -0.9666  -0.9666   1.4040   1.4040
##
## Coefficients:
##                Estimate Std. Error z value Pr(>|z|)
## (Intercept)          -0.2412    0.4029  -0.599   0.549
## LLE_US_CFV_Phasicity != 11TRUE -0.2772    0.4387  -0.632   0.527
##
## (Dispersion parameter for binomial family taken to be 1)
##
##   Null deviance: 222.32  on 166  degrees of freedom
## Residual deviance: 221.92  on 165  degrees of freedom
## (75 observations deleted due to missingness)
## AIC: 225.92
##
## Number of Fisher Scoring iterations: 4
```

```
Aug <- glm(RLE_Venogram_CFV_Percent_Stenosis~as.factor(RLE_US_CFV_Augmentation),family="binomial",data=dfw)
summary(Aug)
```

```
##
## Call:
## glm(formula = RLE_Venogram_CFV_Percent_Stenosis ~ as.factor(RLE_US_CFV_Augmentation),
## family = "binomial", data = dfw)
##
## Deviance Residuals:
##   Min       1Q   Median       3Q      Max
## -1.039  -1.039  -1.039   1.322   1.322
##
## Coefficients:
##                Estimate Std. Error z value Pr(>|z|)
## (Intercept)          -0.334    0.172  -1.942   0.0522 .
## as.factor(RLE_US_CFV_Augmentation)7  15.900  1029.121   0.015   0.9877
## as.factor(RLE_US_CFV_Augmentation)8  15.900  1455.398   0.011   0.9913
## ---
## Signif. codes:  0 '***' 0.001 '**' 0.01 '*' 0.05 '.' 0.1 ' ' 1
##
## (Dispersion parameter for binomial family taken to be 1)
##
##   Null deviance: 194.03  on 141  degrees of freedom
## Residual deviance: 188.87  on 139  degrees of freedom
## (100 observations deleted due to missingness)
## AIC: 194.87
##
## Number of Fisher Scoring iterations: 14
```

```
Aug2 <- glm(RLE_Venogram_CFV_Percent_Stenosis~(RLE_US_CFV_Augmentation>1),family="binomial",data=dfw)
summary(Aug2)
```

```
##
## Call:
## glm(formula = RLE_Venogram_CFV_Percent_Stenosis ~ (RLE_US_CFV_Augmentation >
## 1), family = "binomial", data = dfw)
##
## Deviance Residuals:
##   Min       1Q   Median       3Q      Max
## -1.039 -1.039 -1.039  1.322  1.322
##
## Coefficients:
##              Estimate Std. Error z value Pr(>|z|)
## (Intercept)          -0.334     0.172  -1.942  0.0522 .
## RLE_US_CFV_Augmentation > 1TRUE  15.900   840.274  0.019  0.9849
## ---
## Signif. codes:  0 '***' 0.001 '**' 0.01 '*' 0.05 '.' 0.1 ' ' 1
##
## (Dispersion parameter for binomial family taken to be 1)
##
##   Null deviance: 194.03  on 141  degrees of freedom
## Residual deviance: 188.87  on 140  degrees of freedom
## (100 observations deleted due to missingness)
## AIC: 192.87
##
## Number of Fisher Scoring iterations: 14
```

```
Aug <- glm(LLE_Venogram_CFV_Percent_Stenosis~as.factor(LLE_US_CFV_Augmentation),family="binomial",data=dfw)
summary(Aug)
```

```
##
## Call:
## glm(formula = LLE_Venogram_CFV_Percent_Stenosis ~ as.factor(LLE_US_CFV_Augmentation),
## family = "binomial", data = dfw)
##
## Deviance Residuals:
##   Min       1Q   Median       3Q      Max
## -0.9683 -0.9683 -0.9683  1.4021  1.4021
##
## Coefficients:
##              Estimate Std. Error z value Pr(>|z|)
## (Intercept)          -0.5141     0.1619  -3.176  0.00149 **
## as.factor(LLE_US_CFV_Augmentation)7  16.0802  1029.1215  0.016  0.98753
## as.factor(LLE_US_CFV_Augmentation)8  16.0802  1455.3975  0.011  0.99118
## ---
## Signif. codes:  0 '***' 0.001 '**' 0.01 '*' 0.05 '.' 0.1 ' ' 1
##
## (Dispersion parameter for binomial family taken to be 1)
##
##   Null deviance: 221.35  on 165  degrees of freedom
## Residual deviance: 215.54  on 163  degrees of freedom
## (76 observations deleted due to missingness)
## AIC: 221.54
##
## Number of Fisher Scoring iterations: 14
```

```
Aug2 <- glm(LLE_Venogram_CFV_Percent_Stenosis~(LLE_US_CFV_Augmentation>1),family="binomial",data=dfw)
summary(Aug2)
```

```
##
## Call:
## glm(formula = LLE_Venogram_CFV_Percent_Stenosis ~ (LLE_US_CFV_Augmentation >
## 1), family = "binomial", data = dfw)
##
## Deviance Residuals:
##   Min       1Q   Median       3Q      Max
## -0.9683 -0.9683 -0.9683  1.4021  1.4021
##
## Coefficients:
##                Estimate Std. Error z value Pr(>|z|)
## (Intercept)        -0.5141    0.1619  -3.176  0.00149 **
## LLE_US_CFV_Augmentation > 1TRUE  16.0802   840.2742   0.019  0.98473
## ---
## Signif. codes:  0 '***' 0.001 '**' 0.01 '*' 0.05 '.' 0.1 ' ' 1
##
## (Dispersion parameter for binomial family taken to be 1)
##
##   Null deviance: 221.35  on 165  degrees of freedom
## Residual deviance: 215.54  on 164  degrees of freedom
## (76 observations deleted due to missingness)
## AIC: 219.54
##
## Number of Fisher Scoring iterations: 14
```

```
Comp <- glm(RLE_Venogram_CFV_Percent_Stenosis~as.factor(RLE_US_CFV_Competency),family="binomial",data=dfw)
summary(Comp)
```

```
##
## Call:
## glm(formula = RLE_Venogram_CFV_Percent_Stenosis ~ as.factor(RLE_US_CFV_Competency),
##   family = "binomial", data = dfw)
##
## Deviance Residuals:
##   Min       1Q   Median       3Q      Max
## -1.053  -1.046  -1.046   1.315   1.315
##
## Coefficients:
##                Estimate Std. Error z value Pr(>|z|)
## (Intercept)        -0.31845    0.20780  -1.532   0.125
## as.factor(RLE_US_CFV_Competency)7  0.01835    0.36086   0.051   0.959
##
## (Dispersion parameter for binomial family taken to be 1)
##
##   Null deviance: 193.43  on 141  degrees of freedom
## Residual deviance: 193.43  on 140  degrees of freedom
## (100 observations deleted due to missingness)
## AIC: 197.43
##
## Number of Fisher Scoring iterations: 4
```

```
Comp <- glm(LLE_Venogram_CFV_Percent_Stenosis~as.factor(LLE_US_CFV_Competency),family="binomial",data=dfw)
summary(Comp)
```

```

##
## Call:
## glm(formula = LLE_Venogram_CFV_Percent_Stenosis ~ as.factor(LLE_US_CFV_Competency),
##      family = "binomial", data = dfw)
##
## Deviance Residuals:
##      Min       1Q   Median       3Q      Max
## -1.0517  -1.0517  -0.8157   1.3086   1.5889
##
## Coefficients:
##              Estimate Std. Error z value Pr(>|z|)
## (Intercept)      -0.3032     0.1903  -1.593   0.1111
## as.factor(LLE_US_CFV_Competency)7 -0.6263     0.3594  -1.743   0.0814 .
## ---
## Signif. codes:  0 '***' 0.001 '**' 0.01 '*' 0.05 '.' 0.1 ' ' 1
##
## (Dispersion parameter for binomial family taken to be 1)
##
##      Null deviance: 220.39  on 165  degrees of freedom
## Residual deviance: 217.24  on 164  degrees of freedom
## (76 observations deleted due to missingness)
## AIC: 221.24
##
## Number of Fisher Scoring iterations: 4

```